by

Shawnta Y. Chaney

August 2013

RETINAL DEVELOPMENT AND AGE-RELATED DEGENERATION FOLLOWING GESTATIONAL LEAD EXPOSURE

A Dissertation

Presented to

the Faculty of the Department of Biology and Biochemistry

University of Houston

In Partial Fulfillment

of the Requirements for the Degree

Doctor of Philosophy

by

Shawnta Yvonne Chaney

August 2013

RETINAL DEVELOPMENT AND AGE-RELATED DEGENERATION FOLLOWING GESTATIONAL LEAD EXPOSURE

_____

Shawnta Yvonne Chaney

APPROVED:

_____

Dr. Donald A. Fox, Chair

_____

Dr. Joseph Eichberg

_____

Dr. Preethi Gunaratne

_____

Dr. Jerry E. Johnson, Jr.

_____

Dean, College of Natural Science and Mathematics

ACKNOWLEDGEMENTS

I am extremely thankful to Dr. Donald A Fox who allowed me to work under his guidance and tutelage. Over the past few years, he has taught me to be a thorough scientist and he has done his best to give me the proper foundation for future success. Above all, he has become a trusted mentor and friend. I could not have accomplished my academic goals without him and there truly are no words to describe how grateful I am to have met him when I was an undergraduate.

I am thankful to my committee members Drs. Jerry E. Johnson, Preethi Gunaratne, and Joseph Eichberg. Throughout this process, they willingly offered their time, guidance, support, and suggestions with the aim of making me a competent colleague. I am also appreciative to Drs. Christina Chan and Laura Frishman who provided mentorship and funding throughout this process.

It was my privilege to have worked with a host of other talented researchers and students in Dr. Fox's lab. These include Anand Giddabasappa, Weimin Xiao, Ryan Hamilton, Shradha Mukherjee, Bin Xu, Elda Rueda, Jaime Carrillo, and Julia Miao. There were many times when the community they provided meant much more than the science; however, that community was also the catalyst for the science.

I had a larger than average support network of friends and spiritual brothers and sisters to help me along this road. Although I cannot list each one

by name, I am thankful for the intangible gifts that each individual person contributed.

I dedicate this dissertation to all the members of my family. My parents, grandparents, aunts, and uncles all contributed to the person I am today – it really took a village. I am especially grateful to my husband, Darwin James Gibson, whose unconditional love and support will foster all of my future endeavors. I am also grateful to my parents, John Daniel Chaney Jr. and Jacquelyn Chaney. Specifically, my mother sacrificed so much to see me succeed. It is sad to think I could never fully repay her. However, it is extremely rewarding to see how proud she is of me. In the future, if I am half of the mother that she is, I will be exceptional.

Most of all, I am thankful to Jehovah God for blessing me with the patience, determination, and intellect to accomplish this major goal. While nothing can compare to living by his standards, it is truly humbling when doing so results in success in other areas of my life.

This work was supported by NIH Grants (ES03183, ES012482, EY07551, and EY07024), the Department of Biology and Biochemistry, and the Department of Optometry at the University of Houston.

RETINAL DEVELOPMENT AND AGE-RELATED DEGENERATION FOLLOWING GESTATION LEAD EXPOSURE

An Abstract of a Dissertation

Presented to

the Faculty of the Department of Biology and Biochemistry

University of Houston

In Partial Fulfillment

of the Requirements for the Degree

Doctor of Philosophy

by

Shawnta Yvonne Chaney

August 2013

ABSTRACT

PURPOSE: Gestational lead exposure (GLE) increased and prolonged retinal progenitor cell proliferation in mice, resulting in a dose-dependent increase in two late-born retinal neurons: rod photoreceptors and bipolar cells. The present goals were to examine: 1) the spatiotemporal differentiation and functional development of these two cell types, 2) the profile of glutamatergic responses in developing retina prior to canonical synaptic function, and 3) the structural integrity of aging retinas after GLE. **METHODS:** RT-qPCR, immunohistochemistry, confocal microscopy, agmatine probe labeling, and pharmacological assays. **RESULTS:** GLE decreased the relative expression of rod specific genes at PN2; delayed the differentiation and functional development of rod photoreceptors and bipolar cells by 2-3 days; increased and prolonged the glutamatergic response of post-mitotic rod and bipolar precursors in the ventricular zone of developing retina; and increased and accelerated the age-related degeneration of rod photoreceptors and bipolar cells. **CONCLUSIONS:** Gestational exposure to environmental toxicants such as lead can produce differential age-dependent effects on the developing and aging retina. Furthermore, the lifespan effect of increased proliferation can result in degeneration later in life.

TABLE OF CONTENTS

FIGURES AND TABLES

ABBREVIATIONS

ACH, acetyl choline; **AGB,** agmatine; **AMPA,** alpha-amino-3-hydroxy-5-methyl-4-isoxazole propionic acid; **ATP,** adenosine triphosphate; **BC,** bipolar cell; **[BPb],** blood lead concentration; **BrdU,** 5'-bromo-2'-deoxyuridine; **CCND1,** cyclin D1; **cDNA,** complementary DNA; **CDC,** center for disease control; **CHX10,** ceh-10 homeodomain containing homolog; **CNTF,** ciliary neurotrophic factor; **CNS,** central nervous system; **CRX,** cone-rod homeobox protein; **DEPC,** diethylpurocarbonate; **DMPP,** 1-dimethyl-4-phenylpiperazinium**;** **DNA,** deoxyribonucleic acid; **DNQX,** 6,7-dinitroquinoxaline-2,3-dione; **E,** embryonic; **ERG,** electroretinogram; **GCL,** ganglion cell layer; **GFP,** green fluorescent protein; **GLE,** gestational lead exposure; **GLU,** glutamate; **HM,** hexamethonium; **IHC,** immunohistochemistry; **IGLUR,** ionotropic glutamate receptor; **INL,** inner nuclear layer; **IPL,** inner plexiform layer; **IR,** immunoreactive; **IS,** inner segments; **KA,** kainite; **KCL,** potassium chloride; **LSCM,** laser scanning confocal microscopy; **MCAR,** m-cone arrestin; **MCM6,** minichromosome maintenance complex component 6; **NBL,** neuroblastic layer; **NMDA,** N-methyl-D-aspartic acid; **NR,** NMDA receptor; **NRL,** neural retina-specific leucine zipper; **NR2E3,** nuclear receptor subfamily 2 group E member 3; **ONL,** outer nuclear layer; **OPL,** outer plexiform layer; **OS,** outer segments; **OTX2,** orthodenticle homeobox 2; **PB,** lead; **PBS,** phosphate buffered saline; **PCNA,** proliferating cell nuclear antigen; **PCR,** polymerase chain reaction; **PKCα,** protein kinase c alpha; **PMCA,** plasma membrane calcium ATPase; **PN,** postnatal day; **RGC,** retinal ganglion cells; **RHO,** rhodopsin; **RNA,** ribonucleic acid; **RPC,** retinal progenitor cell; **RPE,** retinal

pigment epithelium; **RPM,** revolutions per minute; **RT-qPCR,** real-time quantitative polymerase chain reaction; **SCGN,** secretagogin; **SEM,** standard error of mean; **SV2B,** synaptic vesicle protein 2B; **TRPM1-L,** transient receptor potential melastatin 1-long isoform; **VGluT1**, vesicular glutamate transporter 1; **VSX2,** visual system homeobox 2; **VZ,** ventricular zone

CHAPTER 1:

INTRODUCTION TO RETINAL STRUCTURE, FUNCTION, DEVELOPMENT, AND LEAD NEUROTOXICITY

1.1 Introduction

1.1.1 Retinal structure and function

The retina is a thin neural tissue located at the back of the eye that functions to sense and process light by converting physical stimuli into a biochemical and then an electrical response (Figure 1.1A). The mature retina is composed of six different neuronal cell types and one glial cell type. Each of these major cell types is characterized further by its morphology, location, size, neurotransmitter signature, connectivity to other cells, and response to light (Figures 1.1B and 1.2). The retina is composed of three distinct nuclear cell layers, the outer and inner nuclear layers (ONL and INL) and the ganglion cell layer (GCL), and two synaptic layers, the outer and inner plexiform layers (OPL and IPL) (Figure 1.1B). Retinal rod and cone photoreceptor nuclei are located in the ONL. They comprise 70-75% of all the retinal cells (Jeon et al., 1998). Rods and cones make up 97% and 3%, respectively, of the photoreceptor population (Carter-Dawson and LaVail, 1979; Jeon et al., 1998). The INL of the mouse retina has approximately 41%, 40%, 15% and 3% amacrine cells, bipolar cells (BC), Müller glial cells (MGC) and horizontal cells (HC), respectively (Jeon at al., 1998). MGCs in the INL provide structural and functional support to the retinal cells as they buffer extracellular potassium and uptake glutamate for conversion into glutamine, which is provided to photoreceptors for conversion into glutamate (Kofuji and Newman, 2004).

Figure 1.1. Retinal location in the eye and structural layout. (A) The retina is a thin piece of neural tissue located at the back of the eye that gathers and processes light information (adapted from Webvision: http://webvision.med.utah.edu). **(B)** Schematic illustration of laminar network of the retina cells. Rod and cone photoreceptors (PR) are located in the outer nuclear layer (ONL). Bipolar cells, horizontal cells, amacrine cells and Müller glial cells are located in the inner nuclear layer (INL). Ganglion cells and displaced amacrine cells are located in the ganglion cell layer (GCL). The bipolar cells consist of the rod (depolarizing: ON) and cone (depolarizing and hyperpolarizing: ON and OFF) bipolar cells. Several types of amacrine cells include GABAergic, cholinergic, dopaminergic and glycinergic amacrine cells. The ganglion cells consist of ON- and OFF-ganglion cells. The synaptic connections between the first order neurons (PRs) and the second order neurons (horizontal and bipolar cells) occur in the outer plexiform layer (OPL), whereas the synaptic connections between the second order neurons and third order neurons (amacrine and ganglion cells) occur in the inner plexiform layer (IPL). HC: horizontal cell; HCB: hyperpolarizing cone bipolar cells; RBC: Rod-bipolar cells; DCB: Depolarizing cone bipolar cells; DA: Dopamine; ChAT: Choline acetyl transferase; GABA: Gamma amino butyric acid; RGC: Retinal ganglion cells (Adapted from Contini and Raviola, 2003).

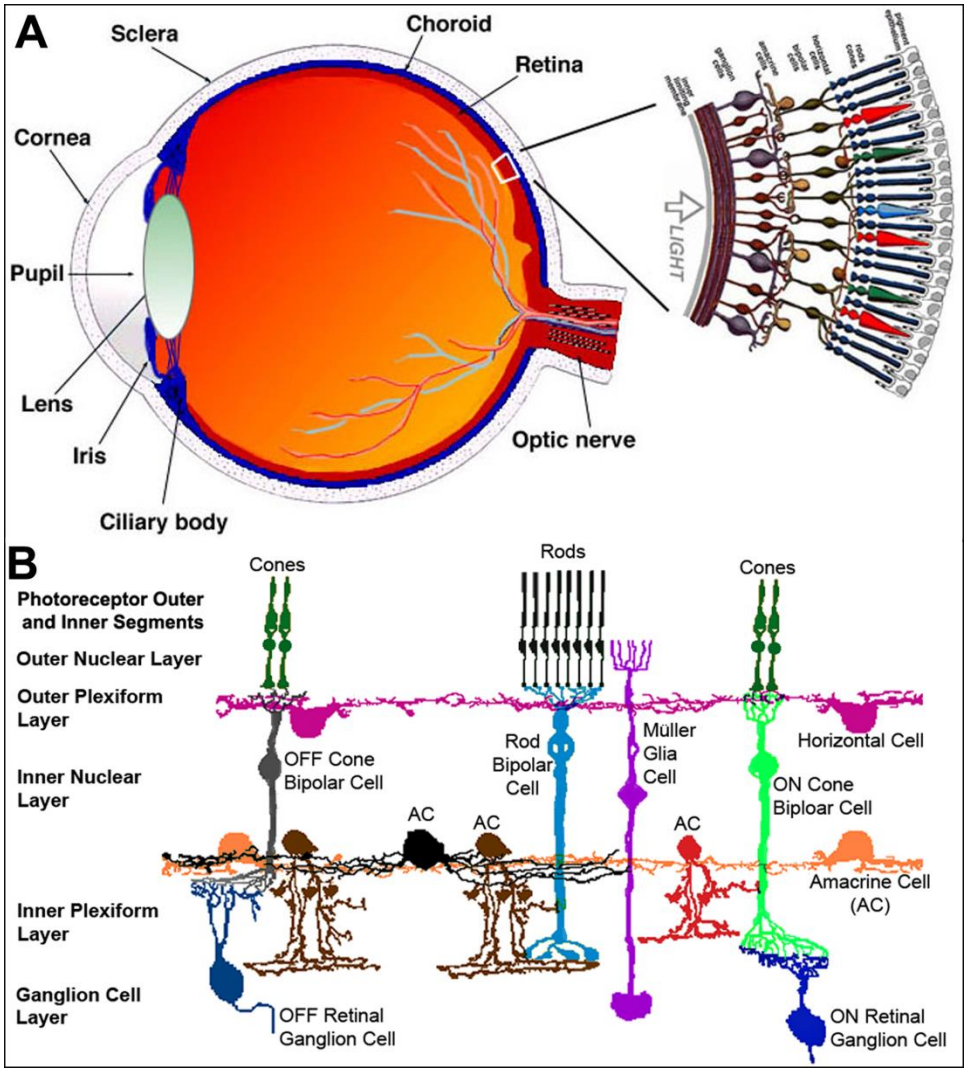
A
Sclera
Choroid
Retina
Cornea
Pupil
Lens
Iris
Ciliary body
Optic nerve
LIGHT
B
Photoreceptor Outer and Inner Segments
Outer Nuclear Layer
Outer Plexiform Layer
Inner Nuclear Layer
Inner Plexiform Layer
Ganglion Cell Layer
Cones
Rods
Cones
OFF Cone Bipolar Cell
Rod Bipolar Cell
Müller Glia Cell
Horizontal Cell
ON Cone Biploar Cell
AC
AC
AC
Amacrine Cell (AC)
OFF Retinal Ganglion Cell
ON Retinal Ganglion Cell

Light activation of photoreceptors leads to their hyperpolarization and a decrease in synaptic glutamate release, which signals the rod bipolar cells (RBC) and ON cone BCs to depolarize and the OFF cone bipolar cells to hyperpolarize (Sharpe and Stockman, 1999). Rod photoreceptors mediate low-light light (scotopic) vision while cone photoreceptors mediate bright-light (photopic) and color vision. Cone photoreceptors contact either OFF cone BCs or ON cone BCs in INL sublamina a and b, respectively, which directly contact ON and OFF ganglion cell (GC) dendrites in these respective sublamina (Figure 1.2) (Sharpe and Stockman, 1999). The separate ON and OFF pathways of the retinal cone system creates the receptive field and center-surround vision. In contrast, rod photoreceptors contact RBCs, which contact AII glycinergic amacrine cells through a glutamatergic synapse. AII amacrine cells then pass RBC information onto either ON or OFF cone BCs through a connexin 36 (Cx36) gap junction hemi-channel or an inhibitory glycinergic synapse, respectively, which connect with ON and OFF GCs (Figure 1.2) (Sharpe and Stockman, 1999; Wassle, 2004). AII amacrine cells form a homogeneous network of cells connected through Cx36 gap junctions. The extent of AII amacrine cell networking and, by extension, the ability of rod photoreceptor signal to reach the RGCs, depends on the amount of light stimulation onto the retina. Photoreceptors make use of the cone pathway since rods and cones operate over different ranges of light intensity (Figure 1.2). As the light intensity increases from absolute darkness, the rod pathway signaling increases. Retinal single photon sensitivity is due to a high

level of convergence of the rods (Baylor, 1987; Sterling et al., 1988). In the mammalian rod system, 1500 rod photoreceptors converge onto 100 RBCs, which converge onto 5 AII amacrine cells and these AII amacrine cells signal onto 4 cone BCs and onto a single ON RGC (Sterling et al., 1988). Several minor alternate pathways exist for the rod photoreceptor signal to reach the GCs. Rods and cones interconnect through gap junctions near the synaptic terminals in the OPL (Raviola and Gilula, 1975; Nelson et al., 1985; Güldenagel et al., 2000; Söhl et al., 2000). Also, a very small percentage of rod photoreceptors connect directly to OFF cone BCs (Hack et al., 1999).

Figure 1.2. Schematic illustration of retinal signal flow. (1) Rod PRs transmit information onto rod BCs through a sign-inverting glutamatergic synapse, **(2)** then to an AII amacrine through a sign-conserving glutamatergic synapse. AII amacrine cells are electrically coupled to each other as well as to ON cone BCs **(3)**, which take rod signal ON signals and pass them directly to ON GCs. AII ACs are also presynaptic to OFF cone BCs **(4)** through a sign-inverting glycinergic synapse. This pathway carries rod OFF signal to the OFF GCs. **(5)** Rod and cone PRs are coupled to each other through gap junctions to facilitate an alternate pathway for rods to reach the GC layer. **(6)** Rarely, rod PRs will directly connect to OFF cone BCs through an ionotropic glutamatergic synapse (Adapted from Sharpe and Stockman, 1999).

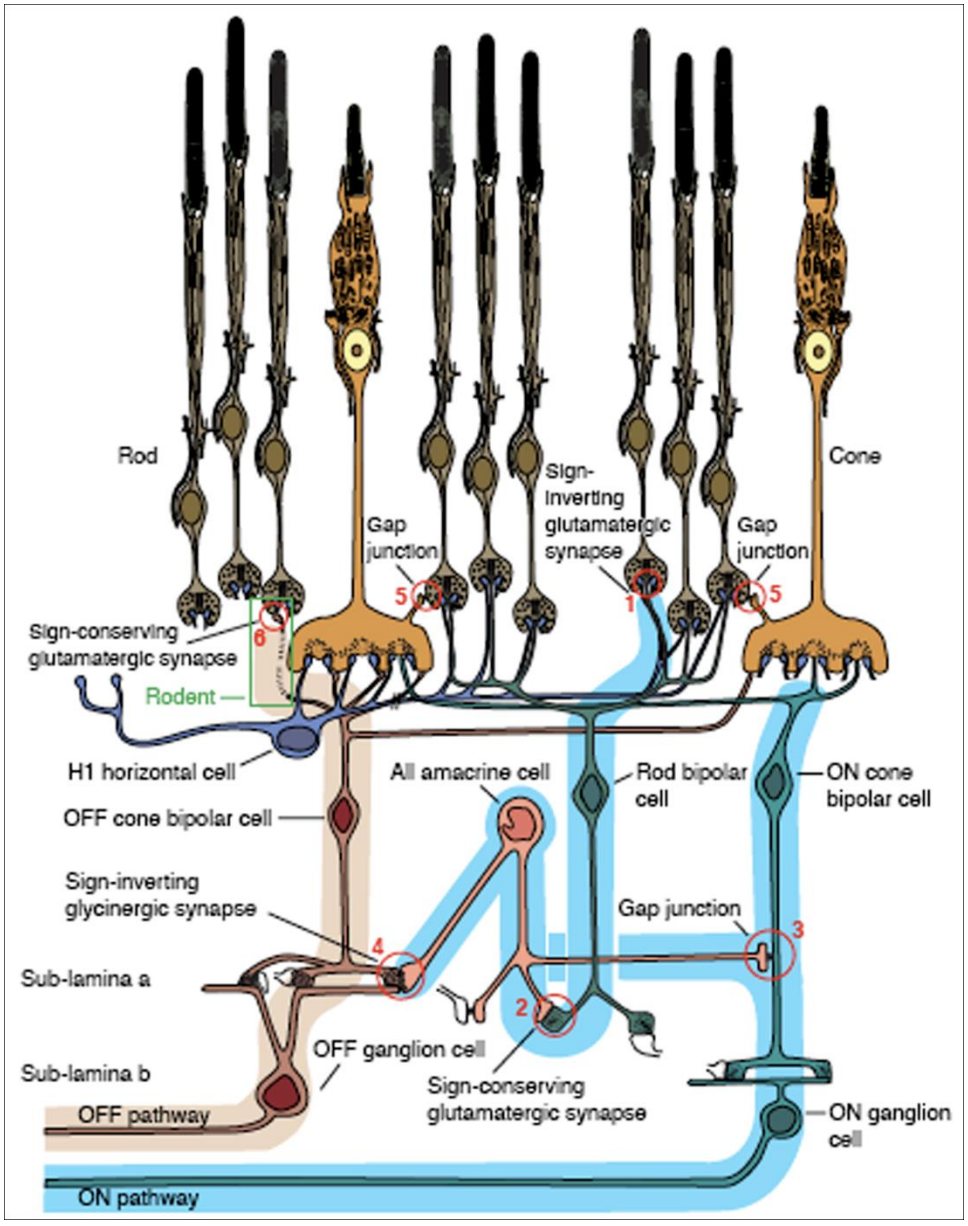
Rod
Cone
Gap junction
Sign-inverting glutamatergic synapse
Gap junction
Sign-conserving glutamatergic synapse
Rodent
H1 horizontal cell
AII amacrine cell
Rod bipolar cell
ON cone bipolar cell
OFF cone bipolar cell
Sign-inverting glycinergic synapse
Gap junction
Sub-lamina a
Sub-lamina b
OFF ganglion cell
Sign-conserving glutamatergic synapse
OFF pathway
ON ganglion cell
ON pathway
1
2
3
4
5
5
6

1.1.2 Retinal histogenesis

The neuronal and glial cells of the central nervous system (CNS) are born in a highly ordered sequence and regulated by extrinsic and intrinsic cues. Likewise, in the retina, the neuronal and glial cell types are born in a fixed chronological sequence (Figure 1.3) (Young, 1985; Rapaport et al., 2004). This histogenic order of cell birth exists in the retina due to a strong correlation between the day a progenitor cell undergoes its last cell division to exit cell cycle, and the type of cell it becomes (Cepko, 1993). For example, a progenitor cell that exits cell cycle prenatally around embryonic age 16.5 (E16.5), can only differentiate into a ganglion cell, an amacrine cell, a cone photoreceptor or a horizontal cell. On the other hand, a retinal progenitor cell (RPC) that exits the cell cycle after birth in mice, only differentiates into a rod photoreceptor cell, a bipolar cell or a Müller glial cell (Figure. 1.3) (Young, 1985; Marquardt and Gruss, 2002).

The seven cell types in the murine retina are generated from a common pool of multipotent RPCs during a two-week period of development (Turner and Cepko, 1987). Proliferation of the RPCs as well as their differentiation into the various retinal cells occurs simultaneously. After undergoing M phase, the RPCseither enter or exit the cell cycle to become postmitotic and then differentiate into various cell types (Turner and Cepko, 1987; Levine and Green, 2004). In addition, some of the newly generated differentiated neurons differentially undergo apoptosis (Young, 1984; Giddabasappa et al., 2011). The net result of proliferation, differentiation and apoptosis defines the final number of differentiated cells of each cell type in the retina. Rods, bipolar cells, and Müller

Figure 1.3. Retinogenesis of the mouse retina. The birth of retinal cells in the mouse occurs from embryonic day 9.5 (E9.5) until postnatal day 10 (PN10). All seven types of retinal cells arise from a multipotent retinal progenitor cell (RPC). Early-born retinal cell types include ganglion cells, cone photoreceptors, horizontal cells and amacrine cells, whereas late-born retinal cell types include rod photoreceptors, rod and cone bipolar cells, and Müller glial cells. Approximately 50% of all cells in the rodent retina are born after birth (Rapaport et al., 2004) Rods constitute the major population (70-75%) of all the retinal cells. Horizontal cells, bipolar cells, amacrine cells and Müller glial cells constitute ~3%, 40%, 40% and 12% of the INL, respectively (Jeon et al., 1998). (Figure adapted from Young, 1985 and Marquardt and Gruss, 2002).

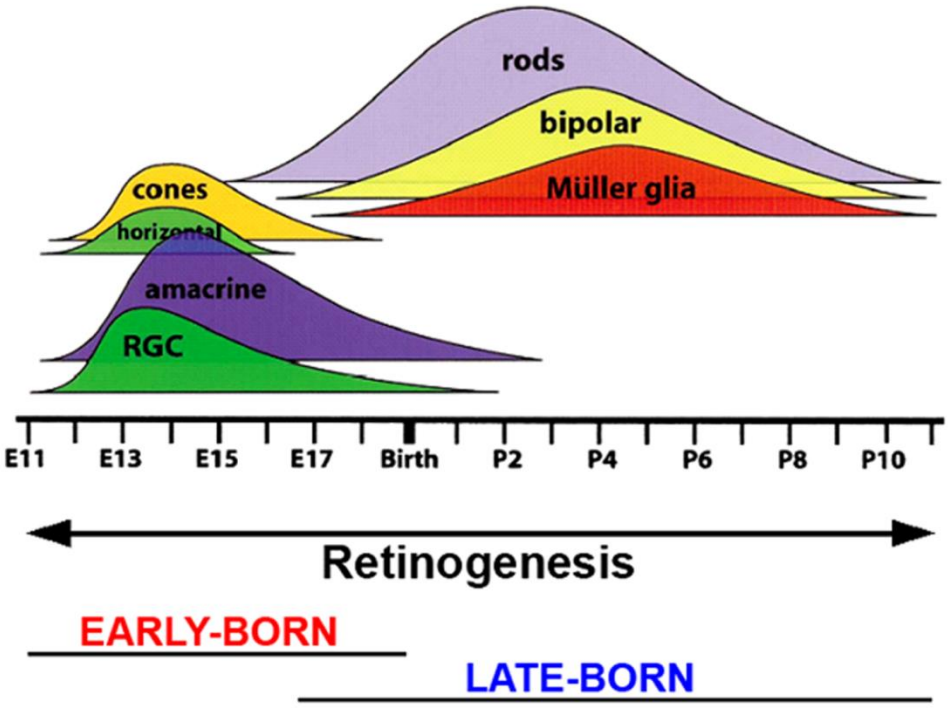
rods
bipolar
Müller glia
cones
horizontal
amacrine
RGC
E11
E13
E15
E17
Birth
P2
P4
P6
P8
P10
Retinogenesis
EARLY-BORN
LATE-BORN

glial cells together comprise ~80% of the total retinal cells (Jeon et al., 1998; Rapaport et al., 2004). Thus to achieve this number, the progenitor cell pool has the highest number of mitotic cells postnatally relative to embryonic retina (Alexiades and Cepko, 1996).As development progresses these progenitor cells repeatedly undergo cell division to maintain the progenitor pool and exit cell cycle to give rise to differentiated cells in appropriate numbers (Dyer and Cepko, 2001). As the number of cells of each retinal cell types varies, different number of progenitor cells exit cell cycle to generate the appropriate numbers of cells of each type. The cells that exit cell cycle and become postmitotic leave the sub-ventricular zone and migrate to their appropriate retinal location. The RPCs receive cues from various cell intrinsic and extrinsic factors to proliferate and diversify into the various retinal cells (Cepko, 1993).

1.1.3 Regulation of retinal progenitor cell proliferation by glutamate

Extracellular and intracellular cues orchestrate cell cycle progression and the exit of RPCs. Many secreted factors positively control proliferation, which results in activation of cell cycle. These secreted factors usually maintain a concentration gradient in the retina. Hence, as RPCs undergo inter-kinetic movement during the cell cycle, they experience variable concentrations of these factors at different phases of the cell cycle (Baye and Link, 2008). Neurotransmitters, like glutamate, GABA and taurine are thought to regulate cell cycle (Martins and Pearson, 2008). However, the exact mechanisms of action for most of the neurotransmitters during development are not fully understood.

Specifically, glutamate provides an anti-proliferative signal for RPCs prior to neurogenesis and synapse formation. Pearson et al. (2002) demonstrated that although endogenous glutamate activated spontaneous Ca^{2+} transients in the ventricular zone (VZ) of developing chick retinas, it did not affect the time for RPCs to complete mitosis. Conversely, in embryonic murine retinal explants, glutamate reduced RPC proliferation by decreasing cyclin dependent kinase 2 (CDK2) activity (Martins et al., 2006). Figure 1.4 shows the potential mechanism for glutamate-induced cell cycle exit. Recent *in vitro* studies using explanted porcine retinas support findings that glutamate acts as an anti-proliferative signal and suggests that glutamate signaling during early development is important for regulation of rod photoreceptor differentiation and developmental apoptosis (Ghosh et al., 2012).

Figure 1.4. Glutamate signaling and the calcium cell cycle. Glutamatergic signaling activates the membrane-mediated influx of Ca2+ and inhibits G1-S progression of progenitor cells, and inhibits cell cycle entry. (Figure from Martins and Pearson, 2008).

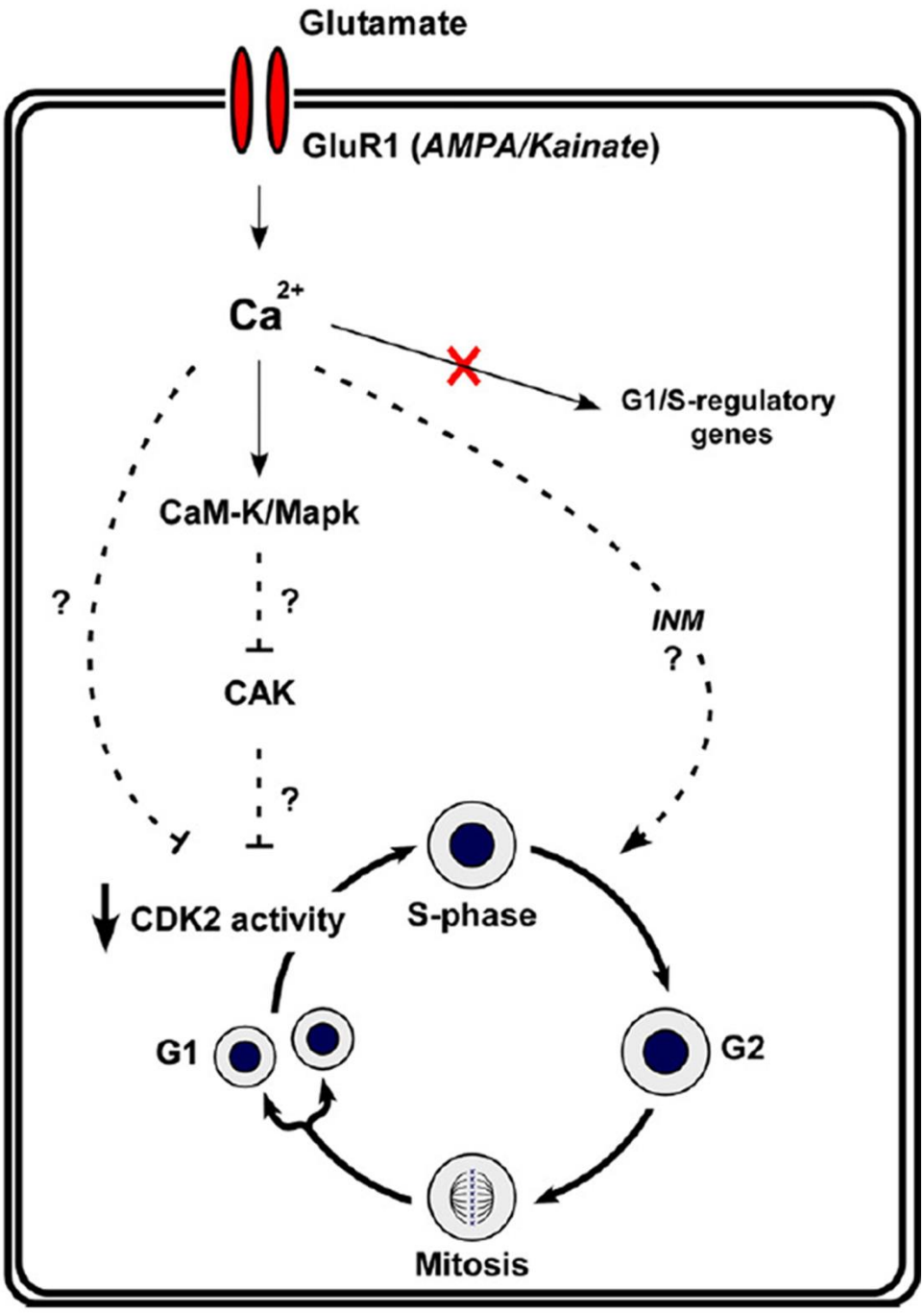

1.1.4 Glutamate receptor signaling

Glutamate is the main excitatory neurotransmitter of the adult retina and is present in high levels in embryonic and early postnatal retinas (Haberecht et al., 1996; Redburn et al., 1996). The membrane receptors that bind glutamate are broadly classified as ionotropic or metabotropic receptors (Brandstatter et al., 1998). Figure 1.5 gives a list of all the glutamate receptor subtypes and their permeability. Ionotropic glutamate receptors (iGluRs) function as gated ion channels while metabotropic receptors (mGluRs) couple with G-proteins and signal through second messengers (Yang, 2004). Further classification of iGluRs depends on their sensitivity to the agonists AMPA (alpha-amino-3-hydroxy-5-methyl-4-isoxazole-propionic acid), KA (kainate), or NMDA (N-methyl-D-aspartate) (Bleakman et al., 1998). The AMPA receptor family consists of four GLUR subtypes (GLUR1-4) while KA receptors consist on two subunit families, GLUR5-7 and KA1 and KA2 (Rosenmund et al., 1998; Kew et al,. 2005). NMDA receptors are classified into seven subunits: NR1, NR2A-D, NR3, and NR3B subunits. The ion permeability and functional traits of all iGluRs depend on their subunit composition (Bowie, 2012; Flores-Soto et al., 2012). The eight known mGluRs (mGluR1-8) in vertebrates are classified into three groups based on sequence homology, transduction mechanism, and agonist selectivity (Quraishi et al., 2007).

Figure 1.5. Glutamate receptor subtypes and their permeability. Glutamate receptors are classified as either ionotropic or metabotropic. Ionotropics receptors are further classified as either NMDA, AMPA, or KA. Metabotropic receptors are classified as either Group I, Group II, or Group III. The subunit composition helps to determine the ionotropic receptor permeability. (Figure from Kew and Kemp, 2005).

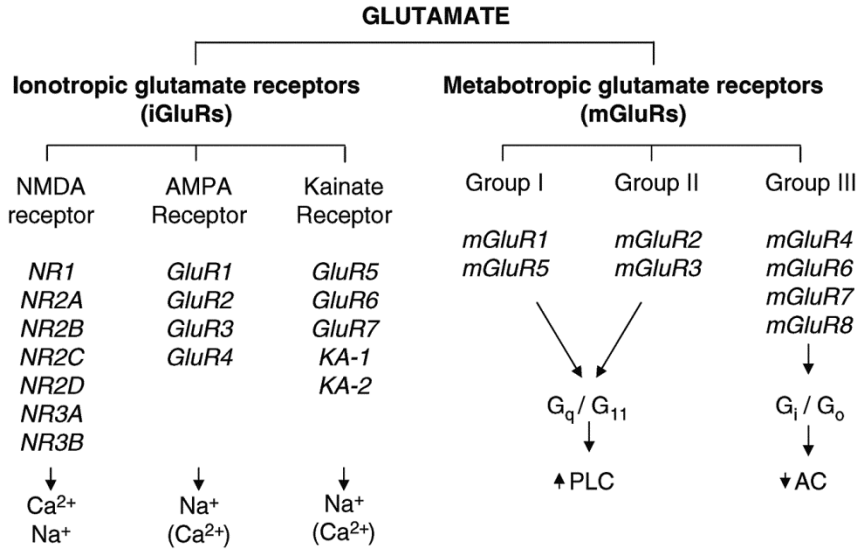

1.1.5 Glutamatergic synaptogenesis in the postnatal mouse retina

The development of ON and OFF pathways and the synaptic function of photoreceptors and bipolar cells is well characterized. Figure 1.6 presents a schematic representation of the major events of glutamatergic synaptogenesis in the developing mouse retina as characterized by vesicular glutamate transporter 1 (VGluT1) expression (Sherry et al., 2003). VGluT1, one of three VGLUT isoforms, is an 8-10 pass transmembrane protein located in synaptic vesicle membranes (Shigeri et al., 2004). VGluT1 uses a proton electrochemical gradient to load glutamate into vesicles for synaptic release and is the primary isoform associated with synaptic release in mouse and rat retina (Sherry et al., 2003; Shigeri et al., 2004; Stella et al., 2008). The first VGluT1 immunoreactive (IR) synapses develop in cone photoreceptors between postnatal day (PN) 4 and PN5. Rod photoreceptor terminals become VGluT1-IR around PN8. Bipolar cell dendrites make their first contact with cone pedicles at about PN8 and with rod spherules around PN10. In the IPL, the OFF sublamina IPLa becomes VGluT1-IR at PN8 before the ON sublamina IPLb at PN10.

1.1.6 Lead neurotoxicity

Lead (Pb^{2+}) is a potent and pervasive neurotoxicant that causes irreversible adverse effects on virtually every organ system in the body. Lead exists naturally in the environment, mainly in the inorganic form, and is commonly found in gasoline and paint (the US banned lead in gasoline and paint in 1977), as well as

Figure 1.6. Major events of glutamatergic synaptogenesis in the developing mouse retina as characterized by VGluT1. Schematic representation of the major events of glutamatergic synaptogenesis adapted from Sherry et al. (2003). The first vesicular glutamate transporter1-immunoreactive (VGluT1-IR) synapses are seen in cone photoreceptor synaptic terminals (pedicles) located in the outer plexiform layer (IPL) between postnatal day 4 (PN4) and PN5. Rod photoreceptor synaptic terminals (spherules) express VGluT1 around PN8. ON cone bipolar cell (BC) dendrites make their first (invaginating) synaptic contacts with pedicles about PN8-9. Rod BC dendrites make their first (invaginating) synaptic contacts with spherules about PN10-11. OFF cone BC axons make their initial synaptic contacts in the inner plexiform layer sublamina a (IPL-a) prior to the ON cone BC and rod BC axons make their initial synaptic contacts in the inner plexiform layer sublamina b (IPL-b).

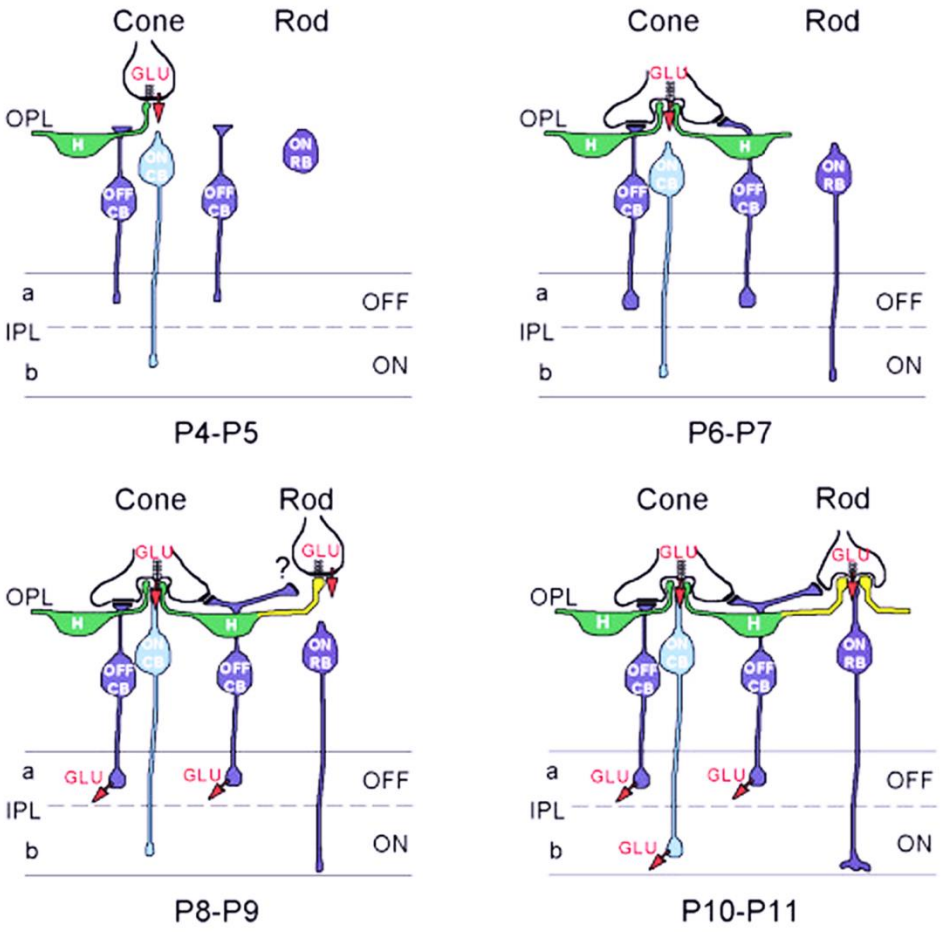

in consumer products such as computers, jewelry, toys and candy (Schwartz, 1994; ATSDR, 2007). Lead reaches soil and groundwater by leaching from abandoned industrial sites and pre-1978 homes, and thereby reaches food and water supplies (ATSDR, 2007). Blood-lead levels ([BPb]) are a reliable biomarker for determining recent exposure. While there is no threshold or safe level of [BPb] (ATSDR, 2007), the current level of concern is 5 µg/dL (CDC, 2013). Strong evidence shows a nonlinear dose-response effect of lead on children exposed during gestation, where low-level exposure ([BPb] <10 µg/dL) is more detrimental to measurements such as IQ than higher levels. Thus, no safe level of lead exists (Rothenberg et al., 2002; Canfield et al., 2003; Canfield et al., 2004; Ronchetti et al., 2006; Fox et al., 2008). The extent of lead toxicity depends on various factors such as age, duration, and level of exposure. In developing children, the central nervous system (CNS) is exceptionally susceptible to lead exposure because the blood-brain barrier is not fully developed and lead absorption is 5 to 10 times higher in children than in adults (Alexander, 1974; James et al., 1985; Nicholls and McLauchlan, 1990; Rice and Barone, 2000; ATSDR, 2007). Combined, these factors account for an incomplete blood-brain barrier can cause serious neurotoxicity in the developing nervous system that result from low [BPb] levels (Nicholls and McLachlan, 1991; ATSDR, 2007). In the womb, infants are exposed to lead through the mother's blood-placental barrier. Additionally, pregnant women release lead accumulated

in their bones, further exposing the infant to lead during pregnancy and lactation (Manton et al., 2003).

Lead exposure in children has severe effects on the developing CNS. Developmental lead exposure is linked with behavioral disorders such as attention deficit hyperactivity disorder, cognitive disorders including IQ deficits, and auditory and visual disorders (Needleman and Gatsonis, 1990; Otto and Fox, 1993; Schwartz, 1994; Rothenberg et al., 2002; Canfield et al., 2004; Toscano and Guilarte, 2005; ATSDR, 2007). Biological events including neurogenesis, proliferation, differentiation, synaptic organization and function, which occur early in development are not only crucial to proper adult function, but affect future development of the CNS. (Toscano and Guilarte, 2005). Developmental lead exposure also is linked to late-onset neurodegenerative disorders such as Alzheimer's and Parkinson's disease (Kuhn et al., 1998; Prince, 1998; Rice and Barone, 2000; Basha et al., 2005; Wu et al., 2008). Acute lead exposure can disrupt synaptic transmission and neurotransmitter release. Lead blocked evoked neurotransmitter release and enhanced spontaneous release at frog neuromuscular junction (Manalis et al., 1984). These effects occur at low lead concentrations, where the mechanism is competition between lead and calcium for changes in evoked release (Cooper and Manalis, 1983; Suszkiw, 2004).

The effect of lead exposure on glutamate receptors is an important area of neurotoxicology research. In rat hippocampal pyramidal neurons from cultured hippocampus, lead dose-dependently and selectively blocked synaptic NMDA

receptors at micomolar concentrations (Alkondon et al., 1990). Furthermore, exposure to lead during development, a time when NMDA receptors are more sensitive to lead, altered the subunit composition of NMDA receptors of hippocampal neuron synapses (Guilarte et al., 1992; Ujihara et al., 1992; Neal et al, 2011). Sui and Ruan (2000) found that in rat hippocampal slices in culture, lead exposure inhibited the cobalt uptake by both AMPA and KA receptors. Therefore, lead exposure can affect all of the iGluRs.

1.1.7 Gestational lead exposure (GLE) model in mouse and previous findings in this laboratory

Lead exposure produces markedly opposite effects on retinal structure and function that is dependent on the time-course of exposure. Moderate to high lead exposure during postnatal development or adulthood produced rod photoreceptor specific apoptosis and decreased rod-mediated (scotopic) retinal electroretinograms (ERGs) in humans, monkeys and rodents (Bushnell et al., 1977; Fox and Sillman, 1979; Otto and Fox, 1993; Fox and Chu, 1988; Fox et al., 1991; He et al., 2003). Conversely, children with low to moderate level GLE had supernormal scotopic a-wave and b-wave ERGs (Rothenberg et al., 2002; Fox et al., 2008; Nagpal and Brodie, 2009).

A GLE protocol, which simulated human retinal development, was developed for rodents in this laboratory (Fox et al., 2008; Leasure et al., 2008; Giddabasappa et al., 2011). Naïve rodent dams were exposed to one of three concentrations of lead-acetate, low (27 ppm), moderate (55 ppm) or high (109

ppm) for two weeks prior to and throughout mating and gestation until postnatal day 10 (PN10). Rodent brain and retinal development in this period is equivalent to human gestation (Raedler and Sievers 1975; Dobbing and Sands 1979; Rice and Barone 2000).

[BPb] for control and the three lead exposure groups were taken at E14, PN0, PN10, PN21, PN30, and PN60. GLE produced a dose-dependent increase in [BPb] resulting in a peak ≤0.7, 9, 23 and 42 µg/dL in control, low-, moderate- and high-exposure respectively, on PN0 and/or PN10 (Figures 1.7 and 1.8). By PN30 and at PN60, [BPb] of the GLE mice were not significantly different from control mice (Leasure et al., 2008; Giddabasappa et al., 2011). Body weights of GLE mice were not significantly different compared to controls at PN0, PN10, PN21, PN30, or PN60. There were no differences in fluid consumption of the dams between control and any GLE group during the exposure period.

Rats with low to moderate level GLE had supernormal scotopic a- and b-wave ERGs and increased b-wave sensitivity (Fox et al., 2008). In GLE rats, the scotopic supernormality was paralleled by a significant increase in the total number of rod photoreceptors and BCs (Fox et al., 2008). Recently, we utilized the same exposure protocol and characterized the GLE mouse retina similarly to rat retina (Giddabasappa et al., 2011). Retinal morphology of PN60 mice was characterized with cell-specific immunolabeling and nuclear staining on fixed-frozen vertical tissue sections. DAPI stained sections revealed that low-, moderate- and high GLE significantly increased ONL thickness by 18%, 25%,

and 8% respectively, INL thickness by 21%, 30%, and 18% respectively and total retina thickness by 26%, 30%, and 18% respectively (Figure 1.9). Quantitative morphometry showed a significant

Figure 1.7. Blood lead concentrations of GLE and control mice. Blood lead ([BPb]) at PN0, PN10 and PN21 significantly increased compared to controls. At PN30, [BPb] were equal to controls in all three treatment groups. *p<0.05, **p<0.01: compared to corresponding controls (Adapted from Leasure et al., 2008).

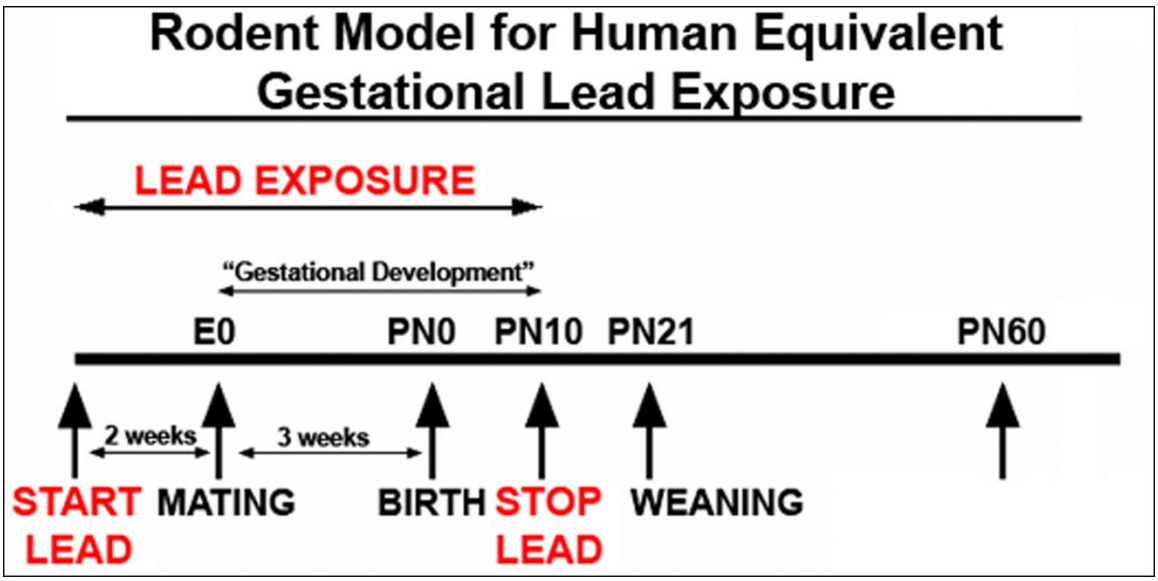

Figure 1.8. Mouse model for human-equivalent gestational lead exposure (GLE). Naïve females were continually exposed to either tap water one of three Pb2+-acetate solutions (low-27ppm, moderate-55ppm, high-109ppm) for two weeks prior to mating, through gestation, birth and until postnatal day 10 (PN10) when tap water was substituted. Water consumption for all four groups was monitored throughout this period. Mice not needed for developmental experiments (Chapter 4) were weaned and separated at PN21 and allowed to develop until PN60 (Adapted from Leasure et al., 2008).

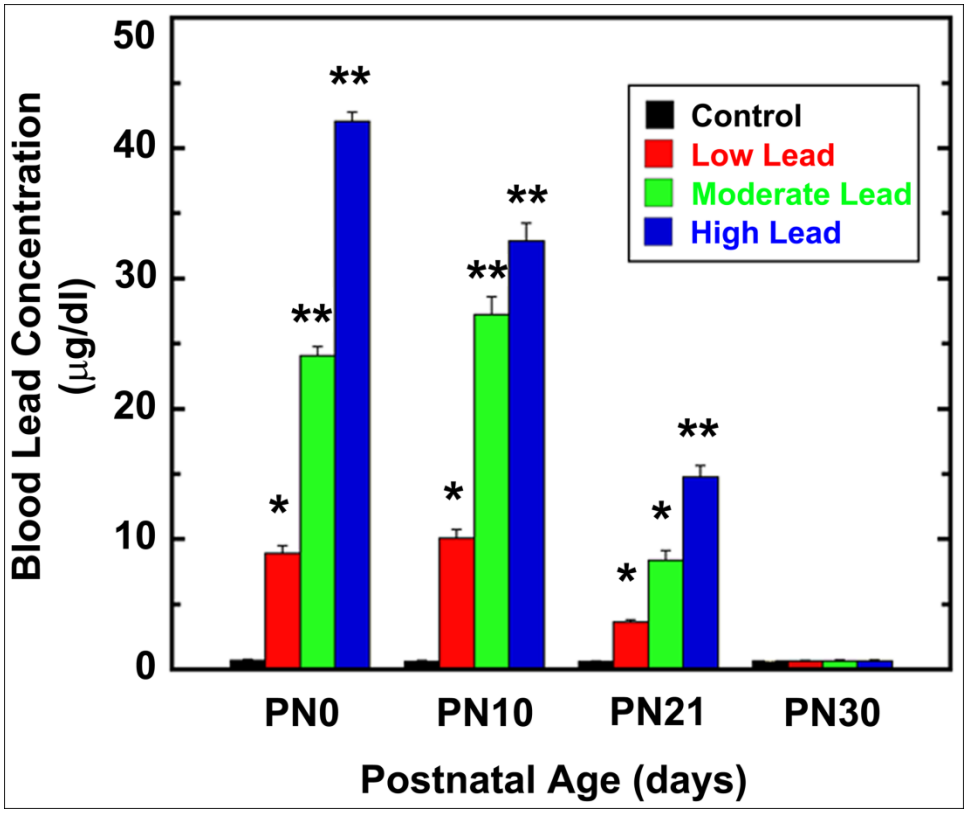

increase in the number of rod photoreceptors by 17%, 26%, and 9% in low-, moderate-, and high-GLE mice, respectively. There was no significant change in the number of cones between control and GLE mice (Figure 1.9) (Giddabasappa et al., 2011). These analyses demonstrated that the increase in ONL thickness was directly proportional to an increased number of rods. PKC-α (RBCs) and Chx10 (BCs) staining revealed a significant increase of 16-18%, 27,% and 20% in the number of BCs in the three GLE-treated retinas compared to control (Figure 1.9) (Giddabasappa et al., 2011). There was no change in the number of MGCs or HCs. Western blot data confirmed and extended all of these results. Moreover, there was no change in the number of apoptotic retinal cells between controls and GLE mice (Giddabasappa et al., 2011).

Figure 1.9. Central retina DAPI staining and morphometric and IHC cell counts in adult GLE retinas. (A) Nuclear staining revealed a significant dose-dependent increase in nuclear layers, ONL and INL as well as the synaptic layers, OPL and IPL of GLE retinas compared to control. The cell number in the GCL was unchanged in all GLE samples compared to controls. Scale bar = 20µm. (B) Morphometric and immunolabeled cell counts showed a significant increase in rods and bipolar cells. All counts are from central retina: ~250µm from the optic nerve head. Rods (DAPI) were significantly increased by 19%, 28% and 18% in low-, moderate- and high-level GLE, respectively, relative to control. In low-, moderate- and high-level GLE, compared to control, the Chx10-immunoreactive (IR) BCs were significantly increased by 16%, 27% and 25%, respectively, and the PKCα-IR rod BCs were significantly increased by 18%, 22% and 22%, respectively. There was no significant change in the number of any other cell type in the retina. *p<0.05: significantly different from corresponding controls. Results are from Giddabasappa et al., 2010.

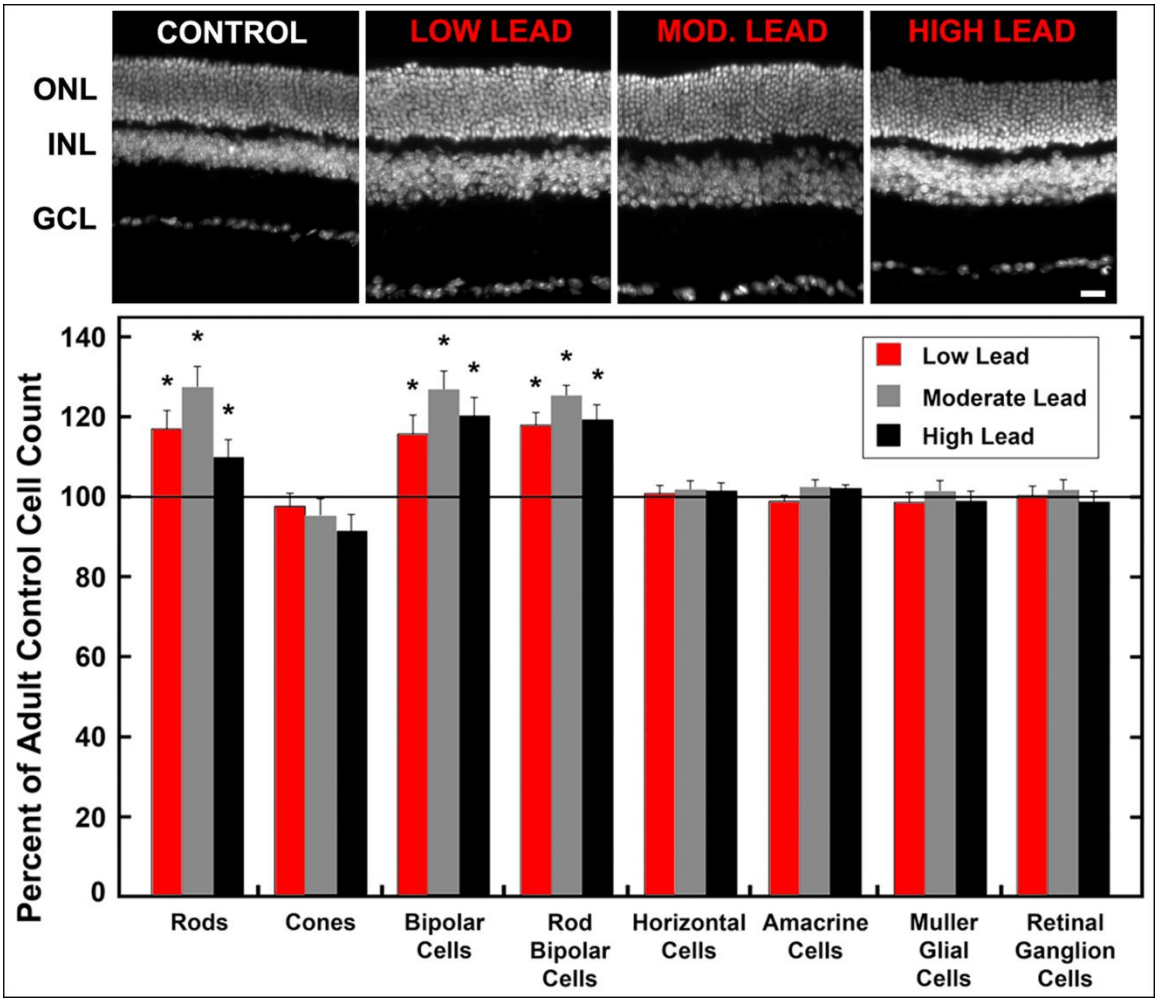

1.1.8 Hypothesis and overall goals

The present study examined the effects of GLE in developing, adult, and aging mouse retinas. The overall hypothesis was that GLE would adversely affect the spatiotemporal pattern and functional development of the glutamatergic system during early postnatal retinal development and that these effects would persist throughout the life of the animal. Therefore our goals were to examine: 1) the glutamatergic signaling profile prior to canonical synapse formation, 2) the development and temporal differentiation of two of the main glutamatergic neurons in the retina: rod photoreceptors and bipolar cells, and 3) functional synaptic development of rod photoreceptors and bipolar cells. In adult and aging control and GLE retinas, I examined the morphological and structural integrity of rod photoreceptors and bipolar cells and their synapses.

In summary, my findings in developing retina were that: 1) GLE increased and prolonged the response of the developing VZ to glutamate, 2) rod and bipolar cell precursors expressed functional glutamate receptors prior to their differentiation, 3) glutamate and nicotinic receptors influenced glutamate release and/or glutamate receptor activation prior to the development of typical glutamate synapses, 4) acute lead exposure altered glutamate signaling in the developing inner and outer retina, and 5) GLE delayed the differentiation and functional synaptic development of rod photoreceptors and bipolar cells. In aging retinas, I found that GLE accelerated and increased the age-related degeneration of rod photoreceptors and bipolar cells.

1.2 REFERENCES

Agency for Toxic Substances and Disease Registry (ATSDR). 2007. Toxicological profile for lead. Atlanta, GA: U.S. Department of Health and Human Services, Public Health Service.

Alkondon M, Costa CA, Radhakrishnan V, Aronstam RS, Albuquerque EX (1990) Selective blockade of NMDA activated channel currents may be implicated in learning deficits caused by lead. FEBS Lett 261:124-130.

Alexander FW (1974) The uptake of lead by children in differing environments. Environ Health Perspect 7:155-159.

Alexiades MR, Cepko C (1996) Quantitative analysis of proliferation and cell cycle length during development of the rat retina. Dev Dyn 205:293-307.

Basha MR, Murali M, Siddiqi HK, Ghosal K, Siddiqi OK, Lashuel HA, Ge YW, Lahiri DK, Zawia NH (2005) Lead (Pb) exposure and and its effect on APP proteolysis and Abeta aggregation. FASEB J 19:2083-2084.

Baylor DA (1987) Photoreceptor signals and vision. Proctor lecture. Invest Ophthalmol Vis Sci 28:34-49.

Baye LM, Link BA (2008) Nuclear migration during retinal development. Brain Res 1192:29-36.

Bleakman D, Lodge D (1998) Neuropharmacology of AMPA and kainate receptors. Neuropharmacology 37:1187-1204.

Bowie D (2012) Redefining the classification of AMPA selective ionotropic glutamate receptors. J Physiol 590:49-61.

Brandstatter JH, Koulen P, Wassle H (1998) Diversity of glutamate receptors in the mammalian retina. Vision Res 38:1385-1397.

Bushnell PJ, Bowman RE, Allen JR, Marlar RJ (1977) Scotopic vision deficits in young monkeys exposed to lead. Science 196:333-335.

Canfield RL, Gendle MH, Cory Slechta DA (2004) Impaired neuropsychological functioning in lead-exposed children. Dev Neuropsychol 26:513-540.

Canfield RL, Henderson CR, Cory-Slechta DA, Cox C, Jusko TA. Lanphear BP (2003) Intellectual impairment in children with blood lead concentrations below 10 microg per deciliter. N Engl J Med 348:1517-1526.

Carter-Dawson LD, LaVail MM (1979) Rods and cones in the mouse retina. I. Structural analysis using light and electron microscopy. J Comp Neuro 188:245-262.

Cepko CL (1993) Retinal cell fate determination. Prog Retin Eye Res 12:1-12.

Cooper GP, Manalis RS (1983) Influence of heavy metals on synaptic transmission: a review. Neurotoxicology 4:69-83.

Dyer MA, Cepko CL (2001) p27Kip1 and p57Kip2 regulate proliferation in distinct retinal progenitor cell populations. J Neurosci 21:4259-4271.

Flores-Soto ME, Chaparro-Huerta V, Escoto-Delgadillo M, Vazquez-Valls E, Gonzales-Castañeda RE, Beas-Zarate C (2012) Structure and function of NMDA-type glutamate receptor subunits. Neurologia 27:301-310.

Fox DA, Chu LW (1988) Rods are selectively altered by lead: II. Ultrastructure and quantitative histology. Exp Eye Res 46:613-625.

Fox DA, Kala SV, Hamilton WR, Johnson JE, O'Callaghan JP (2008) Low-level human equivalent gestational lead exposure produces supernormal scotopic electroretinograms, increased retinal neurogenesis, and decreased retinal dopamine utilization in rats. Environ Health Perspect 116:618-625.

Fox DA, Katz LM, Farber DB (1991) Low-level developmental lead exposure decreases the sensitivity, amplitude and temporal resolution of rods. Neurotoxicology 12:641-654.

Fox DA, Sillman AJ (1979) Heavy metals affect rod, but not cone, photoreceptors. Science 206:78-80.

Giddabasappa A, Hamilton WR, Chaney S, Xiao W, Johnson JE, Mukherjee S, Fox DA (2011) Low-level gestational lead exposure increases retinal progenitor cell proliferation and rod photoreceptor and bipolar cell neurogenesis in mice. Environ Health Perspect 119: 71-77.

Ghosh F, Taylor L, Arner K (2012) Exogenous glutamate modulates porcine retinal development in vitro. Dev Neurosci 34:428-439.

Guilarte TR, Miceli RC (1992) Age-dependent effects of lead on [3H]MK-801 binding to the NMDA receptor-gated ionophore: in vitro and in vivo studies. Neurosci Lett 148:27-30.

Güldenagel M, Söhl G, Plum A, Traub O, Teubner B, Weiler R, Willecke K (2000) Expression patterns of connexin genes in the mouse retina. J Comp Neurol 425:193-201.

Haberecht M, Redburn DA (1996) High levels of extracellular glutamate are present in retina during neonatal development. Neurochem Res 21:285-291.

Hack I, Peichl L, Brandstätter JH (1999) An alternative pathway for rod signals in the rodent retina: rod photoreceptors, cone bipolar cells, and the localization of glutamate receptors. Proc Natl Acad Sci USA 96:14130-14135.

He L, Perkins GA, Poblenz AT, Harris JB, Hung M, Ellisman MH, Fox DA (2003) Proc Natl Acad Sci USA 100:1022-1027.

James HM, Hilburn ME, Blair JA (1985) Effects of meals and meal times on uptake of lead from the gestational tract in humans. Human Toxicol 4:401-407.

Jeon CJ, Strettoi E, Masland RH (1998) The major cell populations of the mouse retina. J Neurosci 18:8936-8946.

Kew JN, Kemp JA (2005) Ionotropic and metabotropic glutamate receptor structure and pharmacology. Psychopharmacology 179: 4-29.

Kofuji P, Newmann EA (2004) Potassium buffering in the central nervous system. Neuroscience 129:1045-1056.

Kuhn W, Winkel R, Woitalla D, Meves S, Przuntek H, Müller T (1998) High prevalence of parkinsonism after occupational exposure to lead-sulfate batteries. Neurology 50:1885-1886.

Levine EM, Green ES (2004) Cell-intrinsic regulators of proliferation in vertebrate retinal progenitors. Semin Cell Dev Biol 15:63-74.

Marquardt T, Gruss P (2002) Generating neuronal diversity in the retina: one for nearly all. Trends Neurosci 25:32-38.

Martins RA, Linden R, Dyer MA (2006) Glutamate regulates retinal progenitors cells proliferation during development. Eur J Neurosci 24:969-980.

Martins RA, Pearson RA (2008) Control of cell proliferation by neurotransmitters in the developing vertebrate retina. Brain Res 1192:37-60.

Manton WI, Angle CR, Stanek KL, Kuntzelman D, Reese YR, Kuehnemann TJ (2003) Release of lead from bone in pregnancy and lactation. Environ Res 92:139-151.

Nagpal AG, Brodie SE (2009) Supranormal electroretinogram in a 10-year-old girl with lead toxicity. Doc Ophthalmol 118:163-166.

Neal AP, Worley PF, Guilarte TR (2011) Lead exposure during synaptogenesis alters NMDA receptors targeting via NMDA receptor inhibition. Neurotoxicology 32:281-289.

Needleman HL, Gatsonis CA (1990) Low-level lead exposure and the IQ of children. A meta-analysis of modern studies. JAMA 263:673-678.

Nelson R (1985) Spectral properties of cat horizontal cells. Neurosci Res Suppl 2:S167-183.

Nicholls DM, McLachlan DR (1990) Issues of lead toxicity. Basic Life Sci 55:237-246.

Otto DA, Fox DA (1993) Auditory and visual dysfunction following lead exposure. Neurotoxicology 14:191-207.

Pearson R, Catsicas M, Becker D, Mobbs P (2002) Purinergic and muscarinic modulation of the cell cycle and calcium signaling in the chick retinal ventricular zone. J Neurosci 22:7569-7579.

Prince M (1998) Is chronic low-level lead exposure in early life an etiologic factor in Alzheimer's disease? Epidemiology 9:618-621.

Quraishi SJ, Gayet J, Morgans CW, Duvoisin RM (2007) Distribution of group-III metabotropic glutamate receptors in the retina. J Comp Neurol 501:931-943.

Raedler A, Sievers J (1975) The development of the visual system of the albino rat. Adv Anat Embryol Cell Biol 50:3-88.

Rapaport DH, Wong LL, Wood ED, Yasumura D, LaVail MM (2004) Timing and topography of cell genesis in the rat retina. J Comp Neurol 474:304-324.

Raviola and Gilula (1975) Intramembrane organization of specialized contacts in the outer plexiform layer of the retina. A freeze fracture study in monkeys and rabbits. J Cell Biol 65:192-222.

Redburn DA Rowe-Rendleman C (1996) Developmental neurotransmitters signals for shaping neuronal circuitry. Invest Ophthalmol Vis Sci 37:1479-1482.

Rice D, Barone S (2000) Critical periods of vulnerability for the developing nervous system: evidence from humans and animal models. Environ Health Perspect 108 Suppl 3:511-533.

Ronchetti R, van de Hazel P, Schoeters G, Hanke W, Rennezova Z, Barreto M, Villa MP (2006) Lead neurotoxicity in children: is prenatal exposure more important than postnatal exposure? Acta Pediatr Suppl 95:45-49.

Rosenmund CY, Stern-Bach (1998) The tetrameric structure of a glutamate receptor channel. Science 280:1596-9.

Rothenberg SJ, Schnaas L, Salgado-Valladares M, Casanueva E, Geller AM, Hudnell HK, Fox DA (2002) Increased ERG a- and b-wave amplitudes in 7- to 10-year-old children resulting from prenatal lead exposure. Invest Ophthalmol Vis Sci 43-2036-2044.

Schwartz J (1994) Societal benefits of reducing lead exposure. Environ Res 66:105-124.

Sharpe LT, Stockman A (1999) Rod pathways: the importance of seeing nothing. Trend Neurosci 22:497-504.

Sherry DM, Wang MM, Bates J, Frishman LJ (2003) Expression of vesicular glutamate transporter 1 in mouse retina reveals temporal ordering in development of rod vs. cone and ON vs. OFF circuits. J Comp Neurol 465:480-498.

Shigeri Y, Seal RP, Shimamoto K (2004) Molecular pharmacology of glutamate transporters, EAATs and VGLUTs. Brain Res Rev 45:250-265.

Söhl G, Güldenagel M, Traub O, Willecke K (2000) Connexin expression in the retina. Brain Res Brain Res Rev 32:238-145.

Stella SL, Li S, Sabatini A, Vila A, Brecha N (2008) Comparison of the ontogeny of the vesicular glutamate transporter 3 (VGLUT3) with VGLUT1 and VGLUT2 in the rat retina. Brain Res 1215:20-29.

Sterling P, Freed MA, Smith RG (1988) Architecture of rod and cone circuits to the on-beta ganglion cell. J Neurosci 8:623-642.

Sui L, Ruan DY (2000) Impairment of the Ca2+-permeable AMPA/kainate receptors by lead exposure in organotypic rat hippocampal slice cultures. Pharmacol Toxicol 87:204-10.

Suszkiw, JB (2004) Presynaptic disruption of transmitter release by lead. Neurotoxicology 25:599-604.

Toscano CD, Guilarte TR (2005) Lead neurotoxicity: from exposure to molecular effects. Brain Res Brain Res Rev 49:529-554.

Turner DL, Cepko CL (1987) A common progenitor for neurons and glia persists in rat retina late in development. Nature 328:131-136.

Ujihara H, Albuquerque EX (1992) Developmental change of the inhibition by lead of NMDA-activated currents in cultured hippocampal neurons. J Pharmacol Exp Ther 263:868-75.

Yang XJ (2004) Roles of cell-extrinsic growth factors in vertebrate eye pattern formation and retinogenesis. Semin Cell Dev Biol 15:91–103.

Young RW (1985) Cell differentiation in the retina of the mouse. Anat Rec 212:199-205.

Young RW (1984) Cell death during differentiation of the retina in the mouse J Comp Neurol 229:362-373.

Wassle H (2004) Parallel processing in the mammalian retina. Nat Rev Neurosci 5:747-757.

Wu J, Basha MR, Zawia NH (2008) The environment, epigenetics and amyloidogenesis. J Mol Neurosci 34:1-7.

CHAPTER 2:

GESTATIONAL LEAD EXPOSURE DELAYS THE COMMITMENT AND FUNCTIONAL DEVELOPMENT OF ROD PHOTORECEPTORS AND BIPOLAR CELLS

2.1 Introduction

Developmental exposure to the environment neurotoxicant lead adversely affects the central nervous system (CNS) (Osman et al., 1999; Rothenberg et al., 2000; Wasserman et al., 2000; Canfield et al., 2003). The severity of these effects greatly depends on parameters such as the period of perinatal exposure, concentration and duration of exposure, and genetic susceptibility (Rice et al., 2000; Grandjean et al., 2006). Currently, at least 4 million households with children are exposed to lead and approximately half a million U.S. children between the ages of one to five have blood lead concentrations [BPb] >5 µg/dL – the CDC reference level for action. Blood lead concentrations are often highest in areas of low socioeconomic status (Gump et al., 2009).

The molecular mechanisms of the effects of lead in the CNS can be studied in detail by examining its effects on the retina: an easily accessible extension of the CNS. Postnatal lead exposure results in rod-selective apoptosis, persistent rod-mediated electroretinographic (ERG) subnormality, and scotopic behavioral deficits in humans, monkeys, and rodents (Fox et al., 1997; He et al., 2003; Fox and Boyes, 2013). In marked contrast, children, monkeys, and rats exposed to low- or moderate-dose lead during gestation exhibited ERG supermormality (Lilienthal et al., 1994; Rothenberg et al., 2002; Fox et al., 2008; Nagpal and Brodie, 2009). Our lab recently showed that low- and moderate-level gestational lead exposure (GLE) in mice and rats increased and prolonged retinal progenitor cell (RPC) proliferation and selectively increased the number of late

born neurons (rod photoreceptors and bipolar cells), but not late born Müller glial cells (Fox et al., 2008; Giddabasappa et al., 2011). Furthermore, GLE altered cell cycle dynamics by shortening the G1 phase of cell cycle, increasing the number of cells that re-entered cell cycle, and increasing the number of neural precursors that exited cell cycle throughout early postnatal development (Mukherjee, 2011). In the developing retina, tight regulation of cell cycle precedes the coordinated differentiation of the various cell types (Livesey and Cepko, 2001). Therefore, the goal of this study was to examine the spatiotemporal differentiation and functional development of late born neurons (rod photoreceptors and bipolar cells) in GLE retinas relative to age-matched controls.

The adult retina consists of six different types of neurons (rod and cone photoreceptors, horizontal, bipolar, amacrine, and ganglion cells) and one glial cell (Müller glia). These seven cell types develop in a specific histogenic order that is conserved across species (Young, 1985; Rapaport et al., 2004). In mice, early-born neurons (cone photoreceptors, horizontal, amacrine, and ganglion cells) exhibit peak neurogenesis prior to birth while late born neurons (rod photoreceptors and bipolar cells) and Müller glia peak after birth (Marquardt et al., 2002). Despite the significant time span in which retinal cells develops (E10.5 to PN14 in mouse), all of these cells originate from one common pool of multipotent RPCs (Turner and Cepko, 1987; 1990). To ensure production of the correct number of cell types, the developing retina must maintain constant regulation of proliferation, mitosis, and differentiation throughout development

(Dyer and Cepko, 2001). RPCs, like other neuronal progenitor cells, accomplish this by coordinating and managing the cumulative effects of intrinsic and extrinsic cues (Cepko, 1993; Edlund and Jessel, 1999; Dyer and Cepko, 2001). Intrinsic cues include the RPCs internal gene expression, competency, and predetermined differentiation clock (Agathocleous et al., 2009). Extrinsic cues include secreted growth factors, neurotransmitters, redox status, and surrounding cell communication (Martins and Pearson, 2008; Baye and Link, 2008; Kurihara et al., 2010).

One major goal of this study was to examine the functional development of rod photoreceptors and bipolar cells. In adult retinas, photoreceptors signal to bipolar cells via glutamatergic ribbon synapses in the retinal outer plexiform layer (OPL) (Rao-Mirotznik et al., 1995; Dieck and Brandstatter, 2006). Bipolar cells are classified as rod or cone bipolar cells based on whether rod or cone photoreceptors provide their presynaptic input in the OPL. While there is only one type of rod photoreceptor, there are nine different cone bipolar cell types in mammalian retina (Boycott and Wässle, 1991; Euler and Wässle, 1995; Ghosh et al., 2004). Bipolar cells are categorized as either ON or OFF bipolar cells, depending on whether they depolarize or hyperpolarize in the presence of light, respectively (Werblin and Dowling, 1969). Furthermore, rod bipolar cells are ON bipolar cells, whereas cone bipolar cells can be ON or OFF. All bipolar cells project their axons into different layers of the inner plexiform layer (IPL). Bipolar cells signal to amacrine and ganglion cells via a glutamatergic ribbon synapse.

OFF bipolar cells project axons into the distal 40% of the IPL (sublamina IPLa), whereas ON bipolar cells project axons into the proximal 60% of the IPL (sublamina IPLb) (Euler et al., 1996). ON and OFF cone bipolar cells directly communicate with ON and OFF retinal ganglion cells, respectively. Rod bipolar cells do not directly communicate to ON and OFF ganglion cells. Rather, they signal to glycinergic AII amacrine cells via conventional sign conserving glutamatergic synapses, which signal to OFF cone bipolar cells via sign inverting glycinergic synapses and connect to ON cone bipolar cells by electrical gap junctions (Shape and Stockman, 1999). Ganglion cells relay these signals to the vision centers of the brain.

Despite the complexity of circuitry in the retina, much progress has been made in characterizing the development of ON and OFF pathways and the synaptic function of photoreceptors and bipolar cells. Figure 1.6 (Chapter 1) presents schematic representation of the major events of glutamatergic synaptogenesis in the developing mouse retina as characterized by vesicular glutamate transporter 1 (VGluT1) expression (Sherry et al., 2003). VGluT1, one of three VGLUT isoforms, is an 8-10 pass transmembrane protein located in synaptic vesicle membranes (Shigeri et al., 2004). VGluT1 uses a proton electrochemical gradient to load glutamate into vesicles for synaptic release and is the primary isoform associated with synaptic release in mouse and rat retina (Sherry et al., 2003; Shigeri et al., 2004; Stella et al., 2008). Briefly, the first VGluT1 immunoreactive (IR) synapses develop in cone photoreceptors between

PN4 and PN5. Rod photoreceptor terminals become VGluT1-IR around PN8. Bipolar cell dendrites make their first contact with cone pedicles at about PN8 and with rod spherules around PN10. In the IPL, the OFF sublamina IPLa becomes VGluT1-IR at PN8 before the ON sublamina IPLb at PN10. I used this timeframe in control C57BL/6 mice as a basis to compare the development of VGLUT-IR OPL and IPL terminals in GLE retinas with that of control retinas.

GLE increased and prolonged RPC proliferation during early retinal development resulting in a dose-dependent increase in the number of rod photoreceptors and bipolar cells in adult GLE mice. Since photoreceptors and bipolar cells compose the primary components of the vertical glutamatergic signaling pathway in the retina, the overall goal of my research was examine alterations in this pathway at several critical time points during the rodent's lifespan. The specific goals of my PhD research were to: 1) characterize the spatiotemporal and functional synaptic development of rod photoreceptors and bipolar cells in developing GLE retinas, 2) examine the effect of GLE on proliferative glutamate signaling prior to conventional synapse formation, and 3) examine the integrity of GLE retinas, especially rod photoreceptors and bipolar cells, during normal aging. This chapter addresses the first of these three goals.

I hypothesized that GLE retinas would express higher onset levels of proteins associated with the commitment of rod photoreceptors and bipolar cells. This hypothesis was based on BrdU birthdating data that showed a significant increase in the number of postnatally born rod photoreceptors and bipolar cells in

GLE retinas (Giddabasappa et al., 2011). To test this hypothesis, I first analyzed the temporal expression of genes associated with rod photoreceptor and bipolar cell differentiation with real-time quantitative PCR (RT-qPCR) at early postnatal ages. These genes included, but were not limited to, rod-specific transcription factors *Nrl*, *Nr2e3*, and *Crx*, the rod-specific functional gene *Rho*, and the proliferative and/or postnatal bipolar-associated gene *Chx10.* Next, I examined the spatiotemporal expression of rod photoreceptor (rhodopsin) and bipolar cell (CHX10, PKCα, and SCGN) specific proteins by immunocytochemistry. Finally, I assessed the appearance of functional synapses in the outer and inner plexiform layers by immunohistochemically labeling for common synaptic proteins (VGluT1, PMCA, TRPM1, and SV2B) and examining the retinas with confocal microscopy.

In summary, I found a significant decrease in all the rod-specific genes tested at PN2 in GLE retinas. Furthermore, the spatiotemporal protein expression of rhodopsin and CHX10 revealed a 2-3 day delay in the commitment of rod photoreceptors and bipolar cells, respectively. These results are consistent with the retinal phenotype of the GLE mouse.

2.2 Materials and Methods

2.2.1 Mouse model of gestational lead exposure

All experimental and animal care procedures complied with the National Institutes of Health (NIH) Public Health Service Policy on Humane Care and Use of Laboratory Animals (NIH 2002) and were approved by the Institutional Animal Care and Use Committee of the University of Houston. All animals were treated humanely and with regard for alleviation of suffering. The protocol for housing, feeding, breeding, and lighting conditions were as previously described (Leasure et al., 2008; Giddabasappa et al., 2011). Briefly, naïve females were given either tap (control) or moderate-dose (55 ppm) lead acetate containing drinking water (GLE group) for two weeks before mating, during pregnancy, and until post-natal day 10, after which the lead was replaced with tap water. For embryonic-day 16.5 (E16.5) and E18.5 retinas, dams were mated overnight, checked for vaginal plugs in the morning and the pups were used for timed-pregnant experiments. Water, food, and weights were recorded throughout treatment. Mice were sacrificed by decapitation between 1000 and 1200 hours. Blood lead concentrations were measured as previously described for each pup to ensure relevant blood lead levels (Leasure et al., 2008). Pups in the control and GLE groups had peak blood lead concentration on PN0 and PN10 of 0.75 ± 0.06 and 22.11 ± 1.05 mg/dL, respectively. There were no statistical differences between control and GLE groups on any dam measure, litter measure, or body weight (Leasure et al., 2008).

2.2.2 RNA isolation

All supplies, equipment, surgical, and lab procedures were carried out under RNase-free conditions essentially as described (Fox et al., 2011). PBS was treated with DEPC. After decapitation, retinas were rapidly removed, placed into ice-cold PBS and cleaned. Neural retinas were transferred to an RNase-free tube and stored at -80°C until used. Four to five mice from different litters per treatment at the PN2, PN6, and PN10 were used. Briefly, RNA was isolated using the Trizol method (Chadderton et al., 1997). Retinas were suspended in 500 μl of Trizol, homogenized 20 times with a hand-held homogenizer, and incubated for 5 minutes at room tempperature. An equal volume of chloroform was added to each sample and incubated for 3 minutes at room temperature. The homogenate was centrifuged (12,000 rpm for 15 minutes at 4ºC) and the aqueous phase containing RNA was transferred into a new tube with an equal volume of 100% isopropyl alcohol added to precipitate the RNA. The solution was incubated for 10 minutes at room temperature and centrifuged (12,000 rpm for 30 minutes at 4ºC) to pellet the RNA. The pellet was washed with 100 μl of 75% ethanol, centrifuged (8,000 rpm for 5 minutes at 4°C), the supernatant was removed and the RNA pellet was dried and resuspended in 20 μL of RNase-free distilled water. To remove any DNA contamination, the sample was incubated with DNaseI for 30 minutes in a 37°C water bath and the suspension was centrifuged (10,000 x g for 1 minute). The RNA solution was transferred to a new tube and concentrated with 5 M ammonium acetate and 100% ethanol and the

mixture incubated at -80ºC for 30 minutes. The RNA was centrifuged (13,000 rpm for 30 minutes at 4ºC), the supernatant was discarded, and the RNA was resuspended in 10-20 µL of DEPC water and stored at -20ºC. RNA quantity and purity were measured with a Nanodrop spectrophotometer (ThermoFisher Scientific, Wilmington, DE).

2.2.3 Real-time-quantitative PCR (RT-qPCR)

Total RNA was synthesized into cDNA and performed as described (Graham et al., 2005). Briefly, 1 µg of total RNA was used for first-strand cDNA synthesis and added to oligo dT and random hexamer primers according to Bio-Rad specifications. All RT-qPCR experiments were run on the Bio-Rad iCylcer platform (Bio-Rad Laboratories, Hercules, CA). RT-qPCR primers were designed and validated within certain parameters: GC content 50-60%, melt temperature 55-65ºC, no secondary structures, no primer dimers or homodimers. Primer quality analysis was done using IDT DNA's Oligo Analyzer (http://www.idtdna.com/analyzer/Applications/OligoAnalyzer/). All primers designed were intron spanning. Primers were selected from the Roche Applied Science Universal Probe Library and Assay Design Center database. Primers were tested for alternative sites of homology with NCBI's BLAST (http://www.ncbi.nlm.nih.gov/BLAST) and the UCSC genome browser (http://genome.ucsc.edu/cgi-bin/hgGateway). Primer sequences are shown in

Table 2.1. Primers were validated by melt curve analysis for single peak of fluorescence.

All RT-qPCR experiments were performed in triplicate and using SYBR green. β-Actin was used as the internal control. The PCR mixture consisted of 12.7 µL of Bio-Rad supermix, 1 µL of cDNA template and 1.5 µL of gene specific forward and reverse primers all combined in a 0.5 mL PCR tube on a 96-well plate. A no template control, water control, and air [empty well] control were run for each plate. The PCR cycle conditions were: 95ºC for 3 minutes, followed by 40 cycles of 95ºC for 30 sec and 60ºC for 30 sec. A melt curve analysis was run at the end of each plate to ensure proper performance of primer pairs. This was performed starting at 60ºC and increasing the temp 0.5ºC per minute to 95ºC. Threshold for Ct values was manually adjusted for each plate to coincide with entrance into exponential growth phase of PCR. Ct values were then exported to Microsoft Excel for further analysis. The level of gene expression, relative to controls was determined using ΔΔCt (Yuan et al., 2008). ΔΔCt = ΔCt of gene of interest - ΔCt of β-actin. $2^{\Delta\Delta Ct}$ was used to compare the fold change in gene expression between GLE and control retinas.

Table 2.1
RT-qPCR Primer List

Gene Symbol	Accession Number	Forward Primer (5'–3')	Reverse Primer (5'–3')
Chx10	NM_007701	TGTTTCCTCCAGTGACCGAA	ACATCTGGGTAGTGGGCTTCAT
Crx	NM_007770	CACGTGAGGAGGTTGCTCTT	TCGCCCTACGATTCTTGAAC
Otx2	NM_144841	TTTGCGCCTCCAAACAACCT	ATGCAGCAAGTCCATACCCGAA
Nrl	NM_008736	TTCTGGTTCTGACAGTGACTACG	GGACTGAGCAGAGAGAGGTGTT
Nr2e3	NM_013708	GCTAAGCCAGCATAGCAAGG	GGAGCAATTTCCCAAACCTC
Rho	NM_145383	TGCAAGCCGATGAGCAACTT	AACGCCATGATCCAGGTGAA
Glul (Glutamine Synthetase)	NM_008131	AGGACTGCGCTGCAAGAC	CCATCAAAGTTCCACTCAGGT
Actb (Beta-actin)	NM_007393	AGAGAGGTATCCTGACCCTGAAGT	CACGCAGCTCATTGTAGAAGGTGT

2.2.4 Tissue processing and immunohistochemistry

All tissue processing and immunohistochemistry techniques were performed as described (Johnson et al., 2007; Fox et al., 2008; Giddabasappa et al., 2011). Briefly, adult or developing mice were decapitated and the eyes were quickly enucleated and placed in ice-cold PBS where the corneas were gently punctured at the limbus. The eyes were then immersion fixed in room temperature, buffered 4% paraformaldehyde (Ladd Research, Williston VT) for 30 minutes, washed in PBS three times for 10 minutes and cryoprotected in 30% w/v sucrose for 48 hours. Anterior segments were removed and the eyes were embedded in TissueTek OCT mounting medium (Electron Microscopy Services, Fort Washington, PA), flash frozen in liquid nitrogen and stored at -80°C. Three non-adjacent fixed-frozen transverse sections (10 µm) taken from the vertical meridian were mounted on Superfrost Plus glass slides (Thermo Fisher Scientific, Waltham, MA) and stored at -20°C.

All sections were taken from central retina: 200-400 µm from the optic nerve. The slides were thawed slowly, sections post-fixed with 4% paraformaldehyde, washed, and briefly immersed in a 1% sodium-borohydride (Sigma-Aldrich, St. Louis, MO) solution to reduce double bonds, allow proper epitope access for antibodies and decrease auto-fluorescence. Sections were washed with ddH_2O, then PBS and incubated for 2 hours with blocking buffer containing 10% normal goat serum (Jackson ImmunoResearch Labs Inc.) and 0.3% Triton-X100 in PBS. Primary antibodies were applied for 2 days at 4°C after

which slides were washed with PBS, blocked for 30 minutes, and secondary antibodies were applied. Table 2.2 lists the well-characterized and commercially available primary anitibodies that were used. For double-labeling experiments, primary antibodies from different host animals were applied simultaneously. Dilutions of Alexa 488, 555 and 647 (1:400) conjugated secondary antibodies were made in blocking buffer, applied to slides, and allowed to incubate in the dark at room temperature for one hour. Slides were washed with PBS, ddH_2O, dried, and mounted with Vectashield mounting medium (Vector Laboratories Inc. Burlinghame CA) and No.1 coverslip, and stored at 4°C. For experiments with DAPI labeling, sections were incubated with DAPI for one hour in the dark after secondary incubation. All antibodies were titrated through a broad range of working dilutions (3 orders of magnitude) to determine optimal working dilutions. Immunolabeling specificity was confirmed by processing retinal sections in the absence of primary antibody.

Table 2.2

Cell Specific Primary Antibodies Used for Immunohistochemistry (IHC)

Primary Antigen	Imunogen	Source	Catalog. No.	Target	Host	Dilution	IHC or WB
CHX10	Recombinant amino acids 1-131 N-terminal of human protein	Exalpha Biologicals	X1180P	RPCs in development Bipolar cells in adult	Sheep	1:200	IHC
PCNA	Purified PCNA	Chemicon	MA4076	Proliferative RPCs	Mouse	1:100	IHC
PKCa	Protein kinase C alpha	AbD Serotec	MCA1572	Rod bipolars	mouse	1:100	IHC
PMCA	Purified human erythrocyte ATPas	Affinity Bioreagents	MA3-914	OPL, IPL some amacrine and bipolar cells	Mouse	1:500	IHC
Secretagogin	Amino acids 186-276 C-Terminus of SCGN of human origin	Santa Cruz	SC-135395	Cone bipolars	Rabbit	1:1000	IHC
TRPM1-L	Synthetic peptide of transient potential cation, subfamily M, member 1 variant delta (long form)	Osenses	OST00037W	Dendrites of ON bipolar cells	Sheep	1:300	IHC
VGLUT1	Synthetic peptide from rat VGLUT1 protein	Chemicon	AB5905	Synaptic layers	Guinea Pig	1:1000	IHC

2.2.5 Statistical analyses

For all data, only one animal or one pooled group of animals from the same litter was used for each measure or sample. Data are presented as the mean ± SEM for four to nine animals per treatment group. Data were analyzed using an ANOVA followed by post-hoc analysis either with Fisher's Least Significance Difference Test or the Student's T-test when only two means were compared. In all figures, values with $p<0.05$ were considered significantly different from controls and were noted where appropriate by asterisks. In the text, values noted as significantly different from controls had $p<0.05$. IHC images were compiled and presented with Adobe Photoshop CS (Adobe Systems Inc., Mountain View CA). Quantitative cell counts were conducted from three non-adjacent retinal sections using unbiased stereological procedures (He et al., 2003; Giddabasappa et al., 2011). Values from each retina were averaged to obtain one representative value. Graphs were generated with KaleidaGraph (Synergy Software, Reading PA).

2.3 Results

2.3.1 GLE increased the developmental expression of proliferative and neurogenic genes while decreasing the expression of rod-specific gene expression.

Figure 2.1 shows the relative expression of the rod-specific transcription factors *Nrl* (A), *Nr2e3* (B), and *Crx* (C), and the rod-specific functional gene *Rho* (D). In both control and GLE retinas, the developmental gene expression pattern was similar for all four genes: a continuous increase from E18.5 to PN10. All four of the rod-associated genes tested were decreased significantly at PN2 in GLE retinas. Additionally, *Nrl* expression was decreased significantly at PN6. The RT-qPCR data are normalized with beta-actin so as not to reflect the increased number of cells. Therefore, these data suggests an overall decrease in rod-specific gene expression in GLE retinas at PN2. The gene expression profile for glutamine synthetase, which is predominately associated with Müller glia (Linser et al., 1984), showed no significant differences between control and GLE (data not shown).

Figure 2.2 shows the relative expression or the rod and bipolar proneural genes *Otx2* (A) and *Vsx2* (*Chx10*) (B) in developing retina. In control animals, *Otx2* expression continually increased from E18.5 to PN6 and peaked at PN6 when most late born retinal neurons have differentiated (Young 1985). This is consistent with *in situ* hybridization data for similar ages (Rath et al., 2007). The pattern of *Otx2* expression in GLE retinas followed that of control; however, gene

expression levels in GLE retinas were increased significantly at PN2 and PN6. In developing control retinas, *Chx10* expression declined from E16.5 to PN2 and increased from PN2 to PN10. This pattern of gene expression is consistent with the idea that CHX10 protein expression associates with all proliferative cells during the embryonic stages of retinal development, but becomes specific for bipolar cells as their numbers increase during postnatal ages (Levine and Green 2004; Hatekeyama and Kageyama, 2004) (Fig. 2.5B). By contrast, in GLE retinas, a decline in *Chx10* expression was never observed, rather the pattern of expression continually increased, with PN2 and PN6 expression levels significantly higher than that of controls. This difference correlates with increased differentiation of bipolar cells associated with the GLE phenotype (Giddabasappa et al., 2011).

Figure 2.1. Gestational lead exposure (GLE) decreased the relative gene expression of the rod-specific transcription factors *Nrl and* Nr2e3, the rod-cone transcription factor *Crx* and the rod functional marker rhodopsin (*Rho)* during retinal development. In both control and GLE retinas, the developmental pattern of **(A)** *Nrl*, **(B)** *Nr2e3*, **(C)** *Crx*, and **(D)** *Rho* gene expression were similar and their relative gene expression significantly increased from E16.5 to PN10. **(A)** In GLE retinas relative to age-matched controls, *Nrl* expression significantly decreased on PN2 and PN6. **(B-D)** In GLE retinas relative to age-matched controls, *Nr2e3*, *Crx* and *Rho* expression significantly decreased on PN2. Mean ± SEM values represent triplicate samples from four to five animals per treatment group per age. Values with an asterisk indicate $p<0.05$ compared to controls.

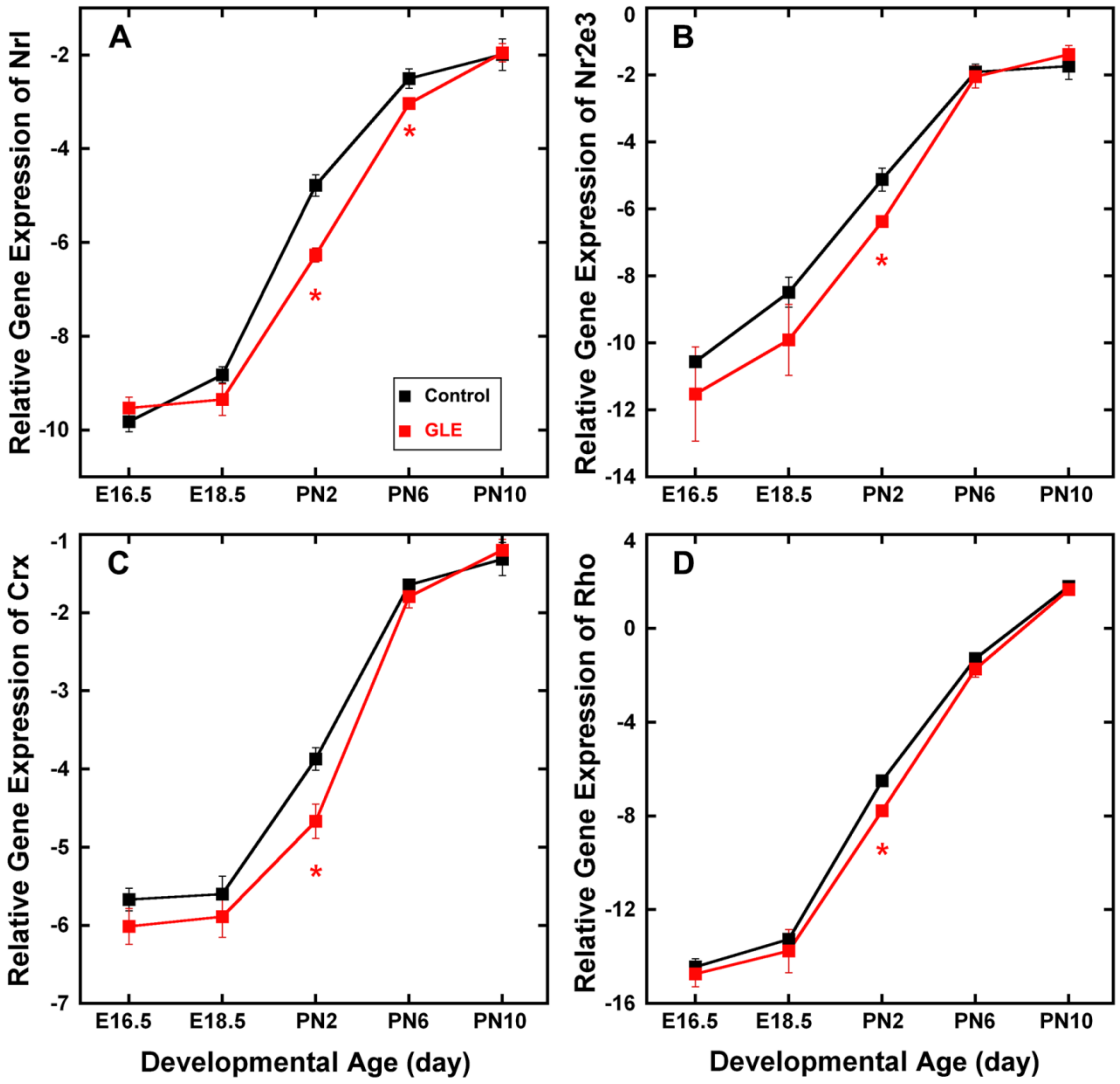
A
Relative Gene Expression of Nrl
-2
-4
-6
-8
-10
Control
GLE
*
*
E16.5
E18.5
PN2
PN6
PN10
B
Relative Gene Expression of Nr2e3
0
-2
-4
-6
-8
-10
-12
-14
*
C
Relative Gene Expression of Crx
-1
-2
-3
-4
-5
-6
-7
*
Developmental Age (day)
D
Relative Gene Expression of Rho
4
0
-4
-8
-12
-16
*
Developmental Age (day)

Figure 2.2. GLE increased the relative expression of the rod and bipolar cell proneural genes *Otx2 and Vsx2 (Chx10)* in developing retina. In control and GLE retinas, **(A)** *Otx2* and **(B)** *Chx10* gene expression significantly increased from embryonic day 16.5 (E16.5) to PN10. **(A)** For *Otx2*, the pattern of expression was similar in controls and GLE, peaking at PN6 when most late-born retinal neurons have differentiated (Young 1985). In GLE retinas relative to age-matched controls, *Otx2* expression significantly increased on PN2 and PN6. **(B)** For *Chx10*, the pattern of gene expression in controls and GLE retinas differed. In GLE retinas relative to age-matched controls, *Chx10* expression also significantly increased on PN2 and PN6. Mean ± SEM values represent triplicate samples from four to five animals per treatment group per age. Values with an asterisk indicate $p<0.05$ compared to controls.

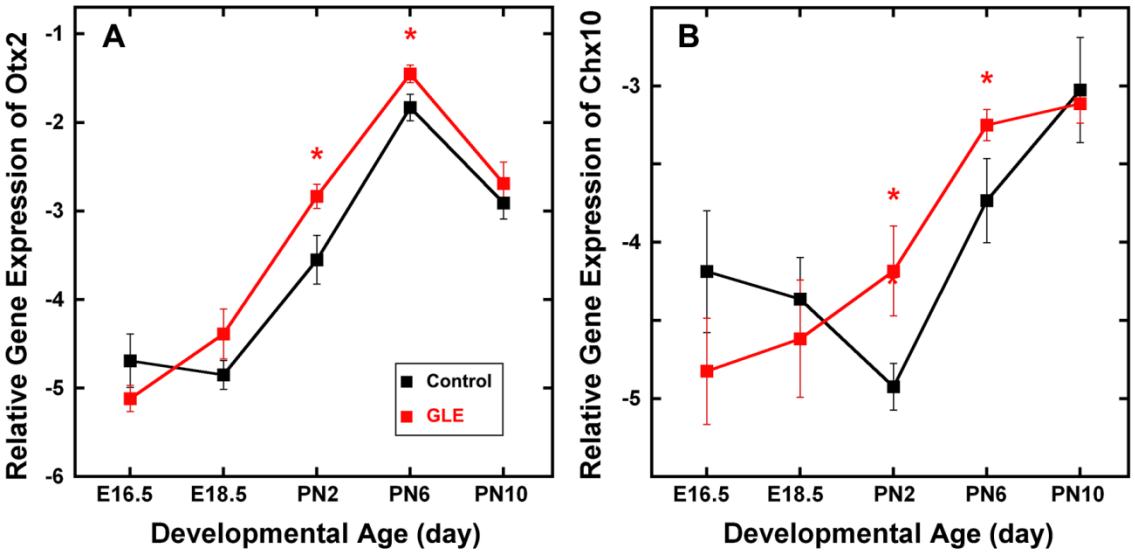

2.3.2 GLE delayed the differentiation of rod photoreceptors and bipolar cells

The RT-qPCR data revealed that GLE retinas had increased expression of proliferative genes throughout development, but decreased expression of rod-specific genes at PN2. Therefore, I examined the spatiotemporal localization of well-known photoreceptor specific proteins by immunohistochemistry. To determine the functional development of rod and cone photoreceptors, I analyzed the spatiotemporal appearance of the functional proteins Rhodopsin and Recoverin for ages E18.5, PN1, PN3, PN5, PN7 PN10, and PN60 in control and GLE retinas (Fig. 2.3). Rhodopsin is a rod-specific photopigment that initiates the phototransduction cascade in the presence of light (Hargrave and McDowell, 1992). Recoverin, a calcium-sensing protein present in all photoreceptors, regulates phototransduction by deactivating rhodopsin kinase (Baylor and Burns, 1998; Burgoyne and Weiss, 2001). Recoverin-immunoreactive (IR) only cells represent cone photoreceptors while rod photoreceptors double label with both recoverin and rhodopsin. In control retinas, rhodopsin-IR cell somas were first observed in the developing ONL at PN1 (Fig. 2.3B). This is consistent with published data in rat (Nir and Papermaster, 1984)**.** Rhodopsin expression increased throughout development, consistent with increased differentiation of RPCs into rod photoreceptors (Morrow and Cepko, 1998). By PN10 (Fig. 2.3F), rhodopsin-IR was seen in rod outer segments in control retinas. In GLE retinas.

Figure 2.3. GLE delayed the appearance of rod-specific rhodopsin immunoreactivity (IR), but not cone-rod recoverin-IR in developing retina. Developing retinas from **(A-U)** control and **(A'-U')** GLE mice were double-labeled with antibodies against rhodopsin (red: **A-G** and **A'-G'**) and recoverin (green: **H-N** and **H'-N'**), and co-labeling was examined in merged images (yellow: **O-U** and **O'-U'**). **(A, H,** and **O)**. In E18.5 control retinas, the inner segments (IS) were rhodopsin-IR and recoverin-IR, while only the somas of cones in the outer nuclear layer (ONL) were recoverin-IR bodies. There was no co-labeling. **(B-C, I-J,** and **P-Q)** In PN1 and PN3 control retinas, cells in the IS and ONL were rhodopsin-IR and recoverin-IR, although only a minimal amount of co-labeling occurred in the ISs. At PN3, a recoverin-IR outer plexiform layer (OPL) started to develop. **(D-E, K-L,** and **R-S)** In PN5 and PN7 control retinas, the ISs, ONL, and OPL were rhodopsin-IR and recoverin-IR, and an increased amount of co-labeling was seen in all layers. **(F, M,** and **T)** At PN10, outer segments (OS) were rhodopsin-IR and extensive co-labeling occurred in the ISs, ONL, and OPL. **(G, N,** and **U)** In the young adult retina at PN60, the OSs were intensely rhodopsin-IR and there was extensive in the ISs, ONL, and OPL. In the distal OPL, the smaller rod spherules were co-labeled, whereas the larger cone pedicles in the proximal OPL were only recoverin-IR. **(A'-B', H'-I',** and **O'-P')** In E18.5 and PN1 GLE retinas, there were almost no rhodopsin-IR ISs. In contrast, the ISs and ONL of cones were recoverin-IR. **(C', J',** and **Q')** In PN3 GLE retinas, cells in the IS and ONL were rhodopsin-IR and recoverin-IR, and many cells were co-labeled. At PN3, a recoverin-IR OPL started to develop. **(D'-E', K'-L',** and **R'-S')** In PN5 and PN7 GLE retinas, the ISs, ONL, and OPL were rhodopsin-IR and recoverin-IR, and an increased amount of co-labeling was seen in all layers. Relative to age-matched controls, the ONL thickness was increased. **(F', M',** and **T')** At PN10, OSs were rhodopsin-IR and extensive co-labeling occurred in the ISs, ONL, and OPL. Relative to age-matched controls, the ONL thickness was increased. **(G', N',** and **U')** In the young adult GLE retinas at PN60, the OSs, ONL and OPL were intensely rhodopsin-IR and almost completely co-labeled with recoverin. Relative to age-matched controls, the ONL and OPL thickness were increased, and the number of rod spherules increased. Scale bar = 40μm.

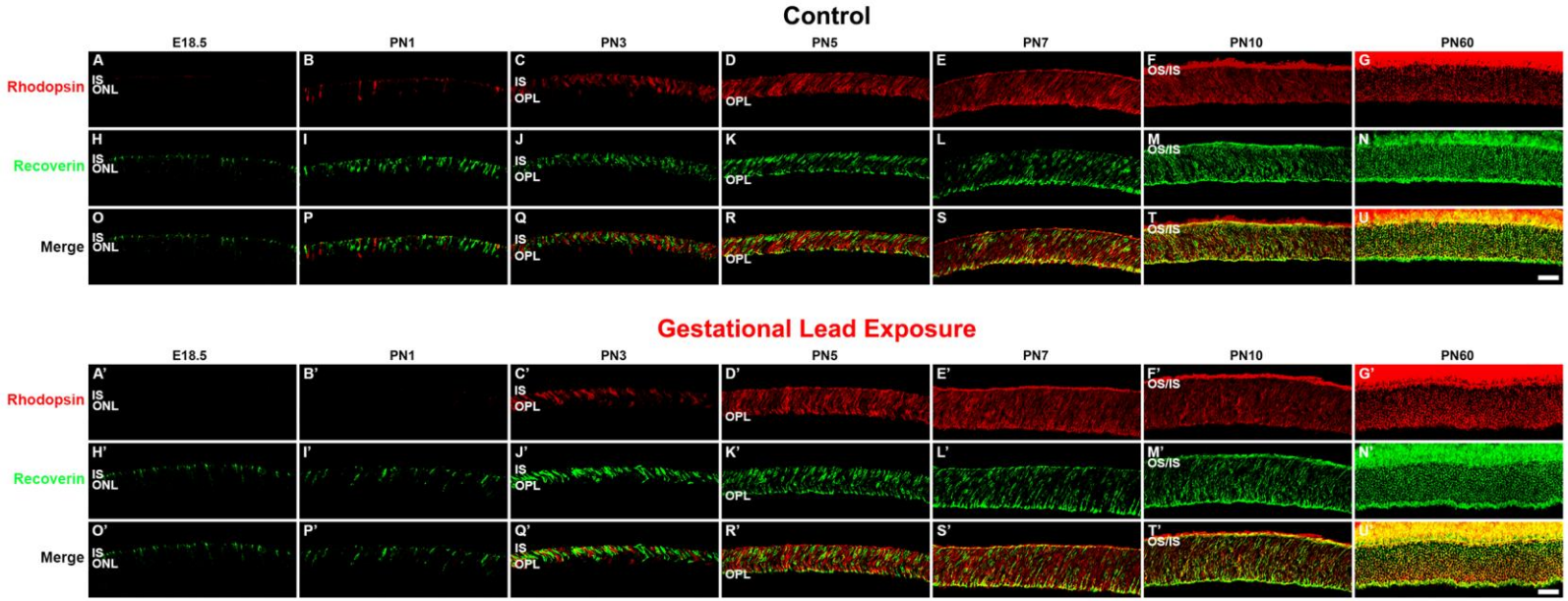
Control
E18.5
PN1
PN3
PN5
PN7
PN10
PN60
Rhodopsin
Recoverin
Merge
A
B
C
D
E
F
G
H
I
J
K
L
M
N
O
P
Q
R
S
T
U
IS
ONL
OPL
OS/IS
Gestational Lead Exposure
A'
B'
C'
D'
E'
F'
G'
H'
I'
J'
K'
L'
M'
N'
O'
P'
Q'
R'
S'
T'
U'

rhodopsin-IR cells were observed first in the ventricular zone at PN3: two days after controls (Fig. 2.3C'). Comparable to control retinas, rhodopsin expression in GLE retinas increased throughout development, however, the ONLs of GLE retinas were consistently thicker than age-matched controls beginning at PN5. Furthermore, rhodopsin-IR in the outer segments was not seen in age-matched PN10 GLE retinas (Fig. 2.3F'). In contrast, the onset of and developmental increase in recoverin-IR was similar in both control and GLE retinas. These data suggests that cones develop normally whereas rod photoreceptors are functionally delayed by approximately two days in GLE retinas.

To examine the differentiation of rod and cone bipolar cells, I analyzed the spatiotemporal protein expression of PKCα (Fig. 2.4), VSX2 (CHX10) (Fig. 2.4) and Secretagogin (SCGN) (Fig 2.6) in PN3, PN5, and PN7 control and GLE retinas. CHX10 is a homeobox domain transcription factor that is initially expressed in RPCs during the earliest stages of neuroretinal development (Liu et al., 1994). CHX10 expression persists in RPCs until the early postnatal ages, after which its expression permanently localizes to bipolar cells (Liu et al., 1994; Burmeister et al., 1996). In PN3 control retinas, I observed CHX10-IR in the ganglion cell layer (GCL), ventricular zone (VZ), and in two types of cells in the developing INL (Figure 2.4A). In the INL, cytoplasmic and nuclear labeling was seen in RPCs and immature bipolar cells, respectively.

Figure 2.4. GLE delayed the differentiation of VSX2 (CHX10)-IR rod and cone bipolar cells (BC) and protein kinase α (PKCα)-IR rod BCs. Developing retinas from **(A-F)** control and **(A'-F')** GLE mice were double-labeled with antibodies against CHX10 (green: **A-C** and **A'-C'**) and PKCα (red: **D-F** and **D'-F'**) **(A-C)** In PN3 control retinas, CHX10 labeled both proliferative and newly differentiated BCs in the inner nuclear layer (INL), as denoted by diffuse and intense labeling respectively, as well as cells in the ganglion cell layer (GCL). At PN5 and PN7, CHX10 labeled differentiated BCs in the inner nuclear layer (INL) as well as cells in the GCL. For confirmation, see Figure 2.6 for CHX10 and Cyclin D1 (CCND1), a cell cycle marker, labeling at PN1 and PN5. At PN7, a well-defined outer plexiform layer (OPL) was visible. **(A'-C')** In contrast, in PN3 GLE retinas, CHX10 labeled only proliferative cells and no differentiated CHX10-IR BCs were present. At PN5, CHX10-IR BCs were present, although they were spindle-shaped compared to the age-matched controls. **(D-F)** In PN3 control retinas, PKCα-IR was in inner segments (IS), minimally present in the INBL, and in the inner plexiform layer (IPL) and GCL. At PN5, PKCα-IR increased in the ISs, IPL and GCL and appeared in the OPL. At PN7, PKCα-IR was selectively and intensely expressed in rod BCs from their dendrites in the OPL and to their axon terminals in the most proximal INL. **(D'-F')** In PN3 GLE retinas, PKCα-IR was less intense and more diffuse than in age-matched controls. It was in ISs, diffusely spread throughout the INBL, and in the IPL and GCL. PN5 and PN7 GLE retinas were similar to controls, however, the OPL was less developed and fewer PKCα-IR rod BCs were present. VZ: ventricular zone. Scale bar = 40 μm.

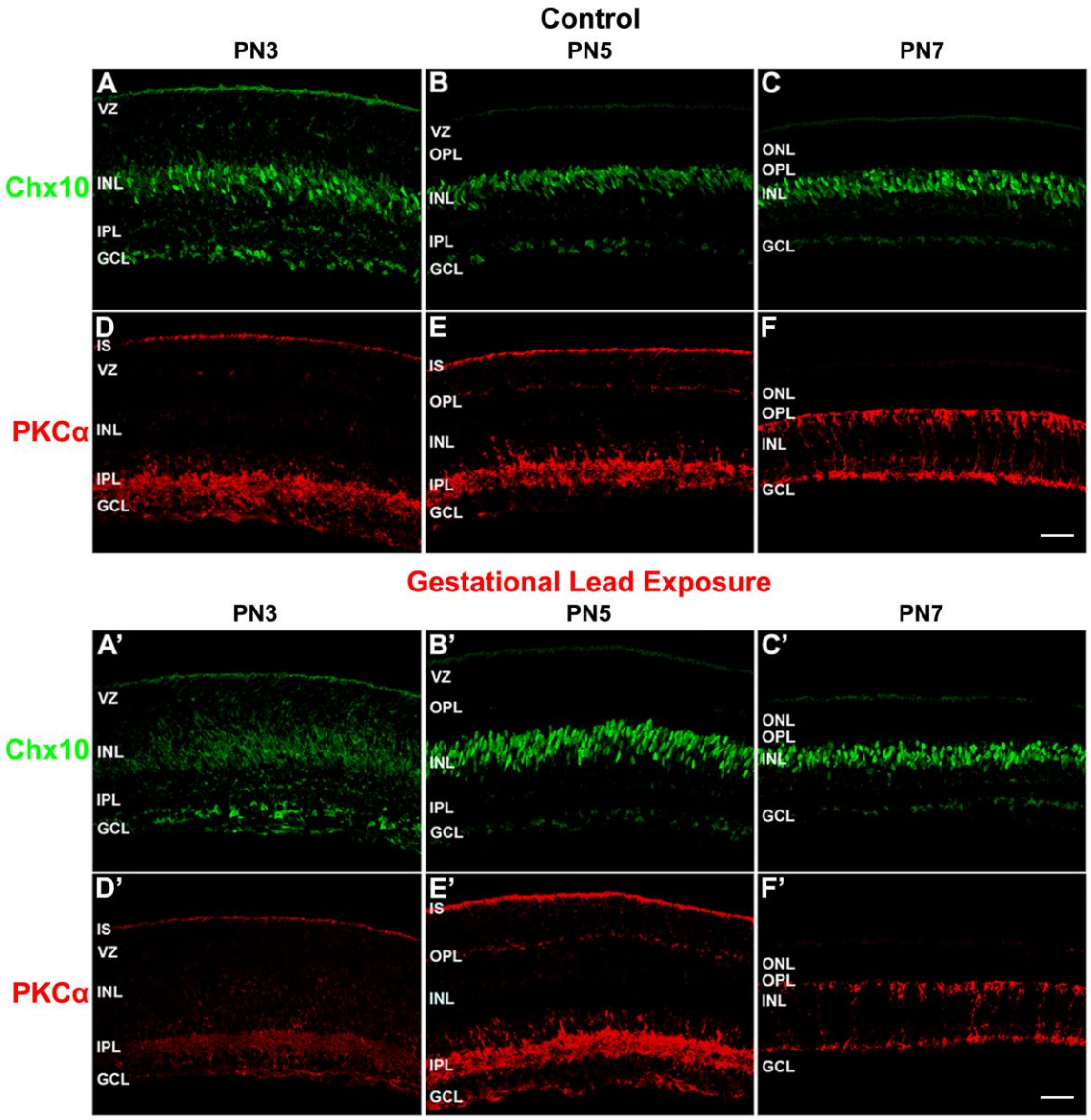
Control
PN3
PN5
PN7
A
VZ
INL
IPL
GCL
B
VZ
OPL
INL
IPL
GCL
C
ONL
OPL
INL
GCL
Chx10
D
IS
VZ
INL
IPL
GCL
E
IS
OPL
INL
IPL
GCL
F
ONL
OPL
INL
GCL
PKCα
Gestational Lead Exposure
PN3
PN5
PN7
A'
VZ
INL
IPL
GCL
B'
VZ
OPL
INL
IPL
GCL
C'
ONL
OPL
INL
GCL
Chx10
D'
IS
VZ
INL
IPL
GCL
E'
IS
OPL
INL
IPL
GCL
F'
ONL
OPL
INL
GCL
PKCα

Furthermore, the strongly labeled CHX-IR cells localized only to the center of the INL. Figure 2.5 demonstrates the difference between RPC-associated CHX10 and bipolar cell-associated CHX10. The appearance of CHX-IR bipolar cells at PN3 correlates with the peak of bipolar cell differentiation (Cepko, et al., 1996; Giddabasappa et al., 2011). By PN5 in control retinas, CHX10-IR was restricted to ganglion and bipolar cells and the diffuse label associated with RPCs was no longer present (Fig 2.4). In PN7 control retinas, the appearance of CHX10-IR bipolar cells was similar to that of the adult retina (PN60 data not shown). In PN3 GLE retinas, CHX10 labeled the VZ and cells in the INL and GCL. However, the strongly CHX10-IR bipolar cells observed in controls were not present in GLE retinas and CHX10-IR in the INL was restricted to proliferative cells. In PN5 GLE retinas, immature bipolar cells were strongly immunoreactive for CHX10 as in the age-matched control, however, the cells appeared as spindles and elongated in form. By PN7, the appearance of CHX10-IR bipolar cells in GLE retinas was similar to control. At PN10, I observed an increased number of CHX10-IR bipolar cells consistent with the GLE phenotype (data not shown; Giddabasappa et al., 2011).

Figure 2.5. CHX10 co-labels with cyclin D1 (CCND1) during early retinal development and subsequently specifies bipolar cell (BC) fate. Developing **(A-C)** PN1 and **(D-F)** PN3 control retinas double-labeled with antibodies against CHX10 (green: **A and D**) and CCND1 (red: **B and E**), and co-labeling was examined in merged images (yellow: **C and F**). **(A)** In PN1 controls retinas, CHX10-immunoreactivity (IR) was diffusely located throughout the retina in the cytosolic compartment. **(B)** CCND1, a cell cycle protein, was localized in the nucleus of proliferating cells in the ventricular zone (VZ). **(C)** CHX10-IR co-localized with CCND1-IR in the VZ. **(D)** In PN5 control retinas, CHX10-IR was localized in the nucleus of cells in the inner nuclear layer (INL) and cytosol of cells in the ganglion cell layer (GCL). The shape of the CHX10-IR in INL cells was changing from spindly to compact and round. **(E)** CCND1 localized to spindly proliferating cells in the INL. **(F)** CHX10 did not co-label with CCND1 in the INL. Scale bar = 40 μm.

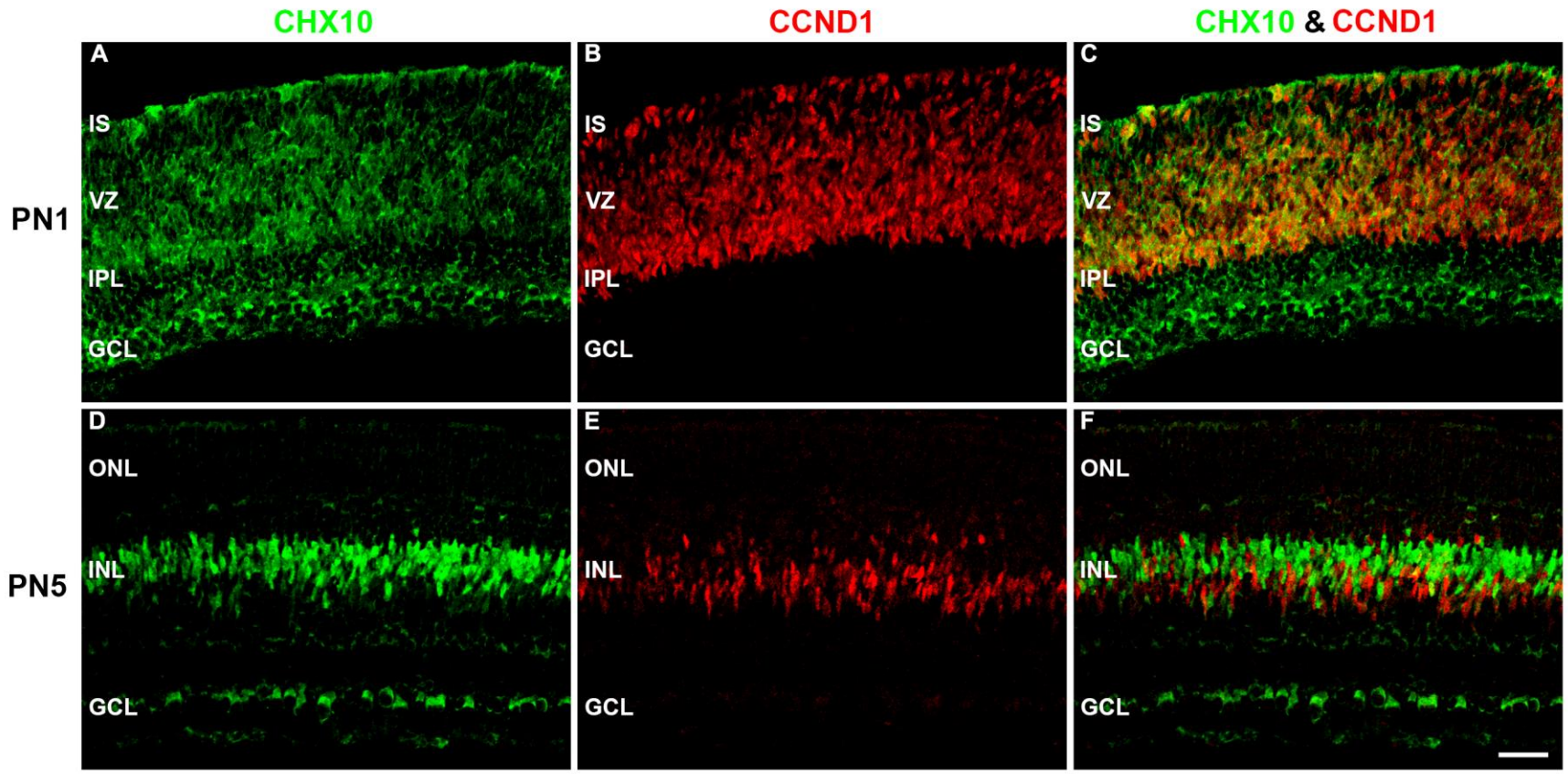
CHX10
CCND1
CHX10 & CCND1
A
B
C
IS
VZ
IPL
GCL
PN1
D
E
F
ONL
INL
GCL
PN5

Figure 2.4 also shows the spatiotemporal profile of PKCα in relation to CHX10-IR. PKCα, a calcium-activated serine/threonine protein kinase, labels the soma, dendrites, axon, and synaptic terminals of rod bipolar cells in adult mouse retina (Haverkamp and Wassle, 2000). In PN3 control retinas, PKCα minimally labeled the INL and strongly labeled the developing IS, IPL, and GCL. In PN5 control retinas, PKCα-IR increased in the ISs, IPL, and GCL and appeared in the OPL. By PN7, PKCα-IR was restricted to rod bipolar cell somas, axons, dendrites, and axon terminals. In PN3 GLE retinas, PKCα-IR was less intense and more diffuse than age-matched controls. GLE retinas were similar to controls at PN5 and PN7 although the OPL was less developed and fewer PKCα-IR rod BCs were present.

SCGN is an EF-hand (E-helix-loop-F-helix-hand) calcium-binding protein that localizes to subpopulations of ON and OFF cone bipolar cells, but not rod bipolar cells in the mammalian retina (Puthussery et al., 2010). Figure 2.6 shows the spatiotemporal immunoreactivity of SCGN in relation to PKCα for ages PN5, PN7, PN10 and PN60 in control (Fig 2.6A-L) and GLE (Figure 2.6M-X) retinas. In control retinas, SCGN-IR cone bipolar cells were first observed in the neuroblastic layer at PN5. These SCGN-IR cells appear elongated and some of their projections extended distally to the IS and proximally towards the GCL. By PN7, most of the SCGN-IR was restricted to somas of the INL, dendritic processes of the OPL, and axon terminals in sublamina a and b in developing IPL. SCGN labeled more intensely in IPL-a than IPL-b.

Figure 2.6. GLE delayed the differentiation of secretagogin (SCGN)-immunoreactive (IR) cone bipolar cells (BC). Developing retinas from **(A-L)** control and **(M-X)** GLE mice were double-labeled with antibodies against SCGN (red: **A-D** and **M-P**) and PKCα (green: **E-H** and **Q-T**), and co-labeling was examined in merged images (yellow: **I-L** and **U-X**). **(A-D)**. In PN5 control retinas, SCGN labeled cone somas in the inner nuclear layer (INL), their dendritic processes in the outer plexiform layer (OPL), and processes in the ganglion cell layer (GCL). At PN7, SCGN-IR increased and localized to immature cone somas in the INL, dendritic processes in the OPL, and axonal terminals in sublamina a (OFF layer) and sublamina b (ON layer) of the inner plexiform layer (IPL). SCGN-IR was more intense in IPL-a than IPL-b. At PN10, SCGN strongly labeled cone BC somas located throughout the INL, dendrites and axon terminals. By PN60, SCGN-IR cone somas were in the distal half of the INL, and the OPL and IPL reached their adult pattern and thickness. **(E-H)** The pattern of PKCα-IR in developing controls is similar to that shown in Figure 5. **(I-L)** Although SCGN and PKCα are in close approximation in the proximal IPL and especially the OPL, they do not co-label. **(M-P)** In PN5 GLE retinas, there were no SCGN-IR cells or processes. At PN7, SCGN-IR dramatically increased and was localized to immature cone somas in the INL, the OPL, and IPL-a and IPL-b: the former exhibiting more intense labeling. Relative to age-matched controls, the INL was thicker and the IPL was less organized. At PN10, SCGN moderately labeled cone BC somas located throughout the INL, dendrites and axon terminals. Relative to age-matched controls, the INL and IPL were less developed and organized. By PN60, SCGN-IR cone somas were in the distal half of the INL, and the OPL and IPL reached their adult pattern and thickness. Relative to age-matched controls, the OPL, INL and IPL were significantly thicker. **(Q-R)** The pattern of PKCα-IR in developing GLE retinas is similar to that shown in Figure 5. **(U-X)** Although SCGN and PKCα are in close approximation in the proximal IPL and especially the OPL, they do not co-label. Scale bar = 40 μm.

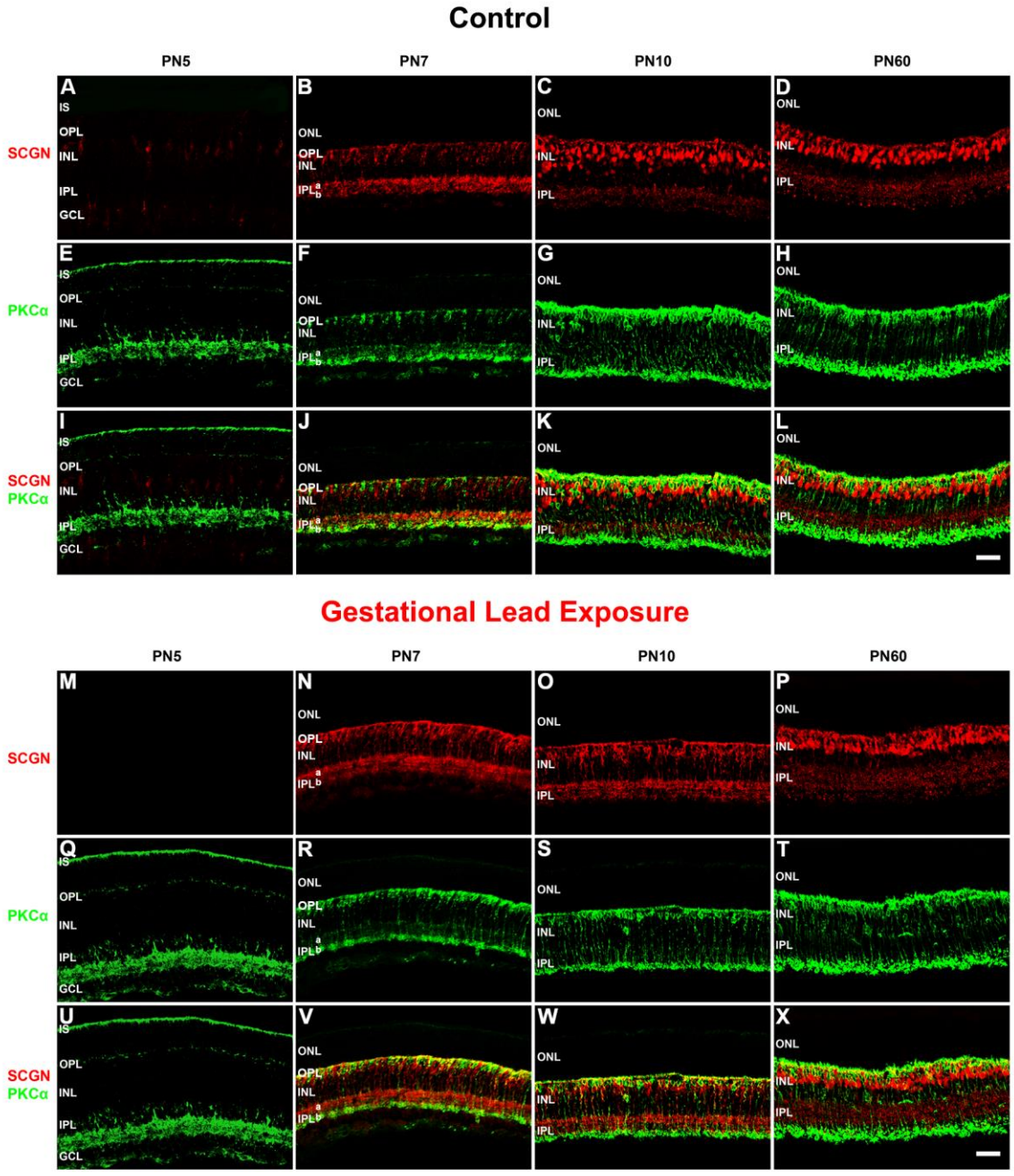
Control
PN5
PN7
PN10
PN60
SCGN
PKCα
SCGN
PKCα
A
B
C
D
E
F
G
H
I
J
K
L
IS
OPL
INL
IPL
GCL
ONL
Gestational Lead Exposure
PN5
PN7
PN10
PN60
SCGN
PKCα
SCGN
PKCα
M
N
O
P
Q
R
S
T
U
V
W
X

By PN10 in control retinas, the pattern of SCGN-IR in the INL changed from moderately labeled linear projections to intensely labeled soma. Furthermore, the dendrites and axon terminals of these SCGN-IR cone bipolar cells exhibited punctate and well-defined labeling in the OPL and IPL, respectively. PKCα and SCGN double labeled control retinas showed no co-localization. The appearance of SCGN-IR somas, dendrites and axon terminals observed in PN10 control retinas closely resembled the appearance of the label in the PN60 adult. These results correlate with similar data in mouse (Puthussery et al., 2010). In GLE retinas, SCGN expression was delayed at PN5. By PN7, however, there was an increase in the number of SCGN-IR cone bipolar cells when compared to age-matched controls. Interestingly, the SCGN immunolabel revealed that, unlike PN10 control retinas, PN10 GLE retinas appeared similar to PN7 retinas rather than PN60 retinas. The punctate dendritic and axon terminals observed in PN10 control retinas were not present in age-matched GLE retinas. Together, these data indicate that bipolar cell differentiation and synaptic development is delayed in GLE retinas.

2.3.3 GLE altered the synaptic development of the outer and inner plexiform layers.

GLE delayed the expression of functional and differentiation proteins in rod photoreceptors and bipolar cells, respectively. Since these neurons directly communicate with each other in the vertical glutamatergic signaling pathway of the retina (Sharpe and Stockman, 1999), I determined whether the spatiotemporal appearance of proteins associated with synaptic function and glutamate release were altered in these neurons. Figure 2.7 shows the spatiotemporal expression of one of these functional synaptic proteins: VGluT1. In control retinas, I first observed sporadic VGluT1-IR puncta below the VZ at PN3 (Figure 2.7). At PN5, VGluT1 labeling in control retinas localized to the developing OPL. In controls, OPL associated VGluT1-IR increased at both PN7 and PN10 as the OPL matured. VGluT1 first localized in IPL-a of control retinas at PN5 and then IPL-b at PN10. These data correlate with VGluT1 data in mouse retina, demonstrating the appearance of VGluT1 in: 1) cone terminals at PN2, 2) rod terminals at PN8, 3) OFF cone bipolar cell terminals at PN6 and PN8, and 4) ON cone and rod bipolar cell terminals at PN10 (Sherry et al., 2003). In GLE retinas, VGLUT-IR puncta were first observed at PN3, similar to controls, however, VGluT1-IR in PN5 and PN7 GLE retinas revealed a delay in OPL and IPL-a maturation. Furthermore, in PN10 GLE retinas, VGluT1 did not strongly label the IPL-b sublamina as in age-matched control retinas. At PN60, VGluT1-IR

revealed the increased thicknesses of the OPL and IPL associated with the adult GLE phenotype (Giddabasappa et al., 2011).

Next, I examined the spatiotemporal expression of the plasma membrane calcium ATPases (PMCAs) throughout development (Figure 2.8). The PMCA family consists of four high-affinity isoforms that extrude cytosolic calcium upon hydrolysis of ATP (Garcia et al., 1999). Neurons use PMCA to return to or maintain basal levels of intracellular calcium after the stimulation of voltage operated calcium channel and subsequent neurotransmitter release (Garcia et al., 1999). In the adult mammalian retina, all four PMCA isoforms are expressed and strongly label the plexiform layers (Krizaj et al., 2002). I used the commercial pan-PMCA antibody that recognizes all four isoforms and intensely labels rod spherules and the apical portion of cone pedicles (Johnson et al., 2007). PMCA-IR was observed in control retinas as early as PN3 where diffusely labeled cells in the neuroblastic layer, GCL, and the developing IPL. In PN5 control retinas, PMCA-IR increased so that PMCA labeled strongly in the OPL and IPL, and weakly in the VZ, INL and GCL. In PN7 and PN10 control retinas, PMCA showed greater localization to the outer and inner plexiform layers and some cells in the INL. At PN60 PMCA-IR laminated in the OPL such that the distal layer (rod spherules) was labeled intensely, whereas the proximal OPL (cone pedicles) was only lightly labeled. Furthermore, IPL-a and IPL-b were distinguishable in PN60 controls. In GLE retinas, PMCA–IR was similar to control at most ages except for PN5 where development of the OPL appeared severely delayed. At PN60, the

pattern of PMCA-IR was similar in control and GLE except that the distal OPL and entire IPL were thicker and had more intense PMCA-IR in GLE.

To further examine the development of the presynaptic and postsynaptic components associated with glutamate synaptic transmission, I analyzed the spatiotemporal profile of synaptic vesicle protein 2B (SV2B) and the transient receptor potential melastatin 1-long isoform (TRPM1-L) protein during development (Fig 2.9). SV2B is one of three SV2 isoforms (SV2A, SV2B, and SV2C) of a protein present on presynaptic vesicles that regulates excitatory calcium-dependent vesicle release (Wan et al., 2010). In mouse retina, SV2B is the expressed in the OPL and IPL (Kriegstein and Schmitz, 2003; Wang et al., 2003) and is the major SV2 isoform that regulates rod photoreceptor neurotransmitter release (Morgans et al., 2009). TRPM1 is member of the group 1 transient receptor potential (TRP) nonselective cation channels (Venkatachalam and Montell, 2007). In the retina, TRPM1 is required for the light response of ON bipolar cells and characteristically labels ON bipolar cell dendrites, soma, and IPL (Morgans et al., 2009; 2010; Krizaj et al., 2010). Therefore, in the developing OPL, SV2B denotes presynaptic maturation whereas TRPM1-L-IR denotes postsynaptic maturation. I used the long isoform of TRPM1 as characterized by Koike et al (2010).

Figure 2.7. GLE delayed the synaptic expression of the vesicular glutamate transporter1 (VGluT1) in the developing outer (OPL) and inner plexiform layers (IPL). Developing retinas from **(A-E)** control and **(F-J)** GLE mice were labeled with an antibody against VGluT1. **(A)** In control PN3 retinas, sporadic VGluT1-immunoreactivity (IR) was in the OPL. **(B-C)** In PN5 and PN7 retinas, the VGluT1-IR amount and intensity increased in the OPL and was seen in IPL sublamina a (OFF layer: IPL-a). **(D)** At PN10, VGluT1-IR in the OPL laminated into discrete puncta in the distal (rod spherules) and clumps in the proximal (cone pedicles) layers as well as into IPL-a and IPL-b (ON layer). **(E)** By PN60, the adult pattern of VGluT1 occurred in the OPL and IPL. **(F-G)** In control PN3 and PN5 retinas, sporadic VGluT1-IR was in the OPL. In contrast to controls, the IPL-a was not VGluT1-IR at PN5. **(H)** In PN7 retinas, a minimal amount of VGluT1-IR was seen in the OPL and IPL-a. **(I)** At PN10, VGluT1-IR in the OPL increased in GLE retinas and was similar to controls. Although VGluT1-IR was present in IPL-a, only a minimal amount occurred in IPL-b. **(J)** At PN60, the amount and intensity of VGluT1 in the OPL and IPL of GLE retina, relative to age-matched controls, was increased such that these layers were thicker. Scale bar = 40 μm.

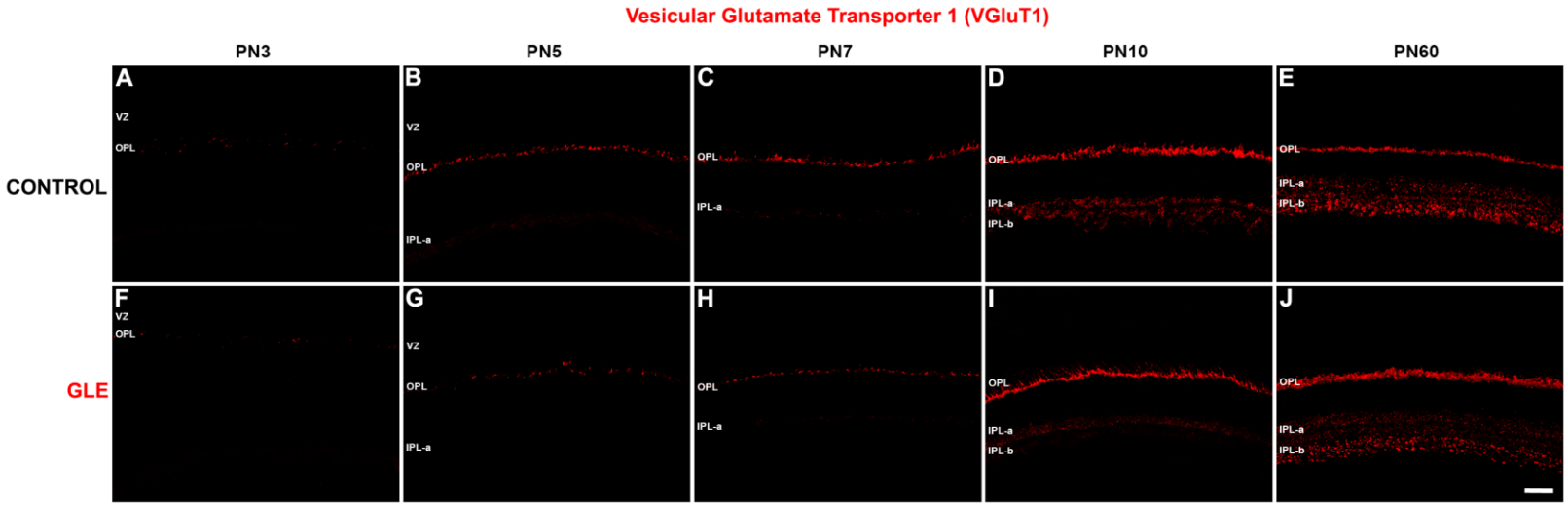
Vesicular Glutamate Transporter 1 (VGluT1)
PN3
PN5
PN7
PN10
PN60
CONTROL
GLE
A
B
C
D
E
F
G
H
I
J
VZ
OPL
IPL-a
IPL-b

Figure 2.8. GLE delayed the synaptic expression of plasma membrane calcium ATPase (PMCA) in the developing outer plexiform layer (OPL). Developing retinas from **(A-E)** control and **(F-J)** GLE mice were labeled with an antibody against pan-PMCA. **(A)** In control PN3 retinas, PMCA-IR was seen in inner segments (IS), and throughout the inner plexiform layer (IPL) and ganglion cell layer (GCL). **(B-C)** In PN5 and PN7 retinas, PMCA-IR was visible in the ISs and intensely labeled the OPL, IPL, and GCL. **(D)** At PN10, PMCA-IR was more localized. Intensely PMCA-IR occurred in the OPL and IPL, and labeling was visible in the distal and proximal inner nuclear layer (INL). **(E)** At PN60, PMCA-IR laminated in the OPL such that the distal layer (rod spherules) was intensely labeled, whereas the proximal OPL (cone pedicles) was only lightly labeled. Somas throughout the INL were PMCA-IR. Both sublamina a and b of the IPL (IPL-a and IPL-b) were intensely PMCA-IR. **(F)** In PN3 GLE retinas, PMCA-IR occurred in the IPL and GCL, but not in ISs. **(G)** In PN5 GLE retinas, PMCA-IR was in the ISs, but was less intense in the OPL, IPL, and GCL compared to age-matched controls. **(H-I)** At PN7 and PN10, the pattern of PMCA-IR was similar in control and GLE. **(J)** At PN60, the pattern of PMCA-IR was similar in control and GLE except that the distal OPL and entire IPL were thicker and had more intense PMCA-IR in GLE. Scale bar = 40 μm.

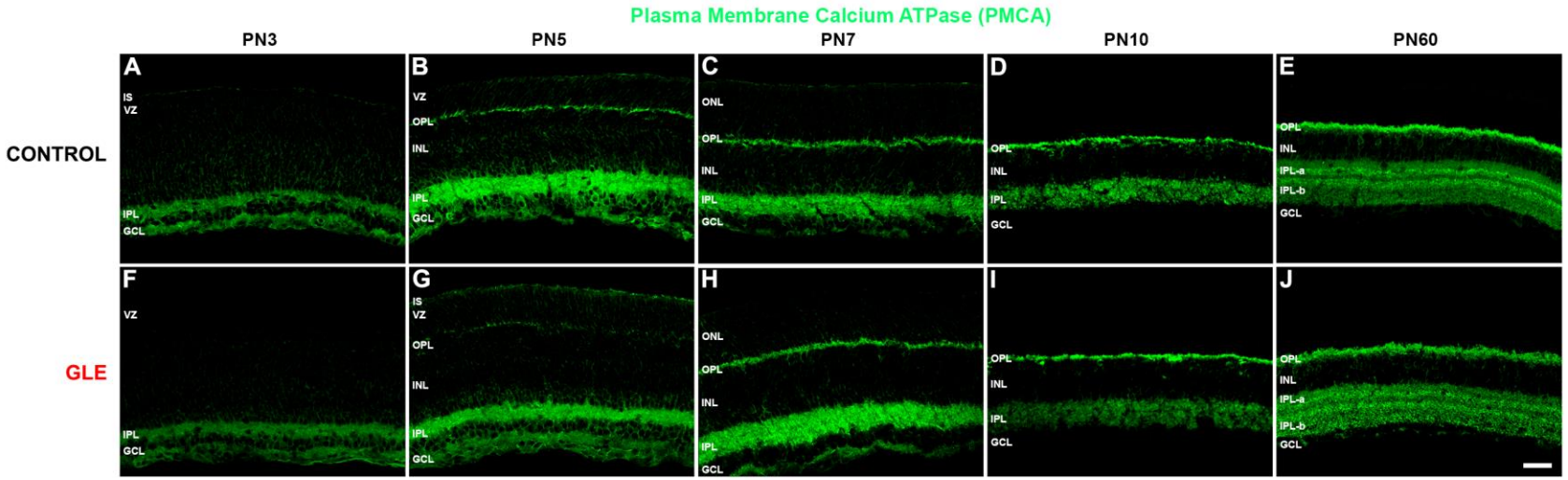
Plasma Membrane Calcium ATPase (PMCA)
PN3
PN5
PN7
PN10
PN60
CONTROL
GLE
A
B
C
D
E
F
G
H
I
J
IS
VZ
OPL
INL
IPL
GCL
ONL
IPL-a
IPL-b

In control retinas, SV2B was visible in the OPL at PN3 and PN5. SV2B dimly labeled the IPL of control retinas at PN5. At PN7, SV2B labeled the OPL and both sublamina – a and – b in the IPL. By PN10, SV2B-IR in the IPL was such that IPL-a and IPL-b sublamina and rod bipolar cell terminals in IPL-b were clearly distinguishable. These results correlate with published data on SV2B-IR in mouse (Wang et al., 2003). SV2B labeling in GLE retinas differed at: 1) PN3 where the SV2-IR puncta were not uniformly localized to the developing OPL, 2) PN5 and PN7 where the OPLs were sparse and less intense when compared to age-matched controls, 3) PN5 where SV2B-IR in the IPL was less than that of age-matched controls, and 4) PN10 where rod bipolar terminals were not clearly defined in IPL-b.

TRPM1-L diffusely labeled the inner segments (IS), IPL, and ganglion cell layer of PN3 control retinas. At PN5, TRPM1-L intensely labeled the IS and weakly labeled the developing OPL. TRPM1-L-IR intensified in the IS, OPL, and IPL of PN7 and PN10 control retinas and the somas of bipolar cells just proximal to the OPL were visible. IN GLE retinas, TRPM1-L-IR was similar to that of control retinas except at PN7 where the OPL was not brightly labeled. SV2B and TRPM1-L did not co-localize at PN3 and PN5 in control or GLE retinas. In the OPLs of PN7 control retinas, SV2B labeled photoreceptor terminals directly above TRPM1-L-IR bipolar cell dendrites. In the OPLs of age-matched GLE retinas, SV2B-IR photoreceptor terminals were in the same plane as TRPM1-IR bipolar cell dendrites. Furthermore, there was very little overlap in the two

proteins in PN10 control retinas. GLE retinas, however, showed significantly more overlap of OPL associated SV2B and TRPM1-L proteins.

Table 2.3 presents a summary of the aforementioned immunohistochemical results. Taken together this data suggest a delay in the functional development of rod photoreceptors and bipolar cells in the OPL, and bipolar cells in the IPL of GLE retinas.

Figure 2.9. GLE delayed the appearance of presynaptic synaptic vesicle protein 2B (SV2B) and postsynaptic ON bipolar cell (BC) protein transient receptor potential M1-long (TRPM1-L) in the developing outer (OPL) and inner plexiform layers (IPL). Developing retinas from **(A-L)** control and **(M-X)** GLE mice were double-labeled with antibodies against SV2B (red: **A-D** and **M-P**) and TRPM1-L (green: **E-H** and **Q-T**), and co-labeling was examined in merged images (yellow: **I-L** and **U-X**). **(A-B)** In PN3 and PN5 control retinas, SV2B was visible in the outer plexiform layer (OPL). In PN5 retinas, punctate SV2B-IR was just visible in the inner plexiform layer (IPL). **(C)** At PN7, SV2B-IR occurred more intensely in the OPL, and both sublamina a and sublamina b of the IPL: with higher intensity in IPL-a than IPL-b. **(D)** By PN10, SV2B-IR laminated in the OPL such that there were discrete puncta in the distal (rod spherules) and clumps in the proximal (cone pedicles) layer. The IPL laminated into IPL-a and -b separated by a layer that was not labeled. **(E)** In PN3 control retinas, TRPM1-L diffusely labeled the inner segments (IS), IPL, and ganglion cell layer (GCL). **(F)** By PN5 TRPM1-L intensely labeled the IS and weakly labeled the developing OPL. **(G)** At PN7, the intensity or TRPM1-L-IR intensified in the ISs, OPL, and IPL. Furthermore, the TRPM1-L labeled the distal somas of bipolar cells right below the OPL. **(H)** This pattern of TRPM1-L-IR persisted at PN10. **(I-J)** No colabel was observed at PN3 and PN5. **(K-L)** In the OPLs of PN7 and PN10 control retinas, SV2B labeled just above TRPM1-L-IR with little to no overlap. No colabel was observed in the IPL. **(M)** In PN3 GLE retinas, SV2B-IR puncta in the developing OPL was not uniformly localized as in the age-matched control. **(N-O)** The OPLs of PN5 and PN7 GLE retinas were less mature than age-matched controls. Very little SV2B was observed in the IPL of PN5 GLE retinas, however, by PN7 SV2B labeled both IPL-a and –b with IPL-a labeling more strongly. **(P)** In PN10 GLE retinas, SV2B-IR in the OPL and IPL increased, however, IPL-a and IPL-b did not show differential labeling as in the control. **(Q-T)** TRPM1-L-IR in GLE retinas were similar to controls except at PN7 where the OPL was not labeled as brightly. **(U-V)** SV2B and TRPM1-L did not colocalize at PN3 and PN5 in GLE retinas as in controls. **(W-X)** PN7 and PN10 GLE retinas differed from control such that at PN7 SV2B labeled in the same plane as, rather than above, TRPM1-L and at PN10 SV2B co-localized with TRPM1-L more than in controls. Scale bar = 40 µm.

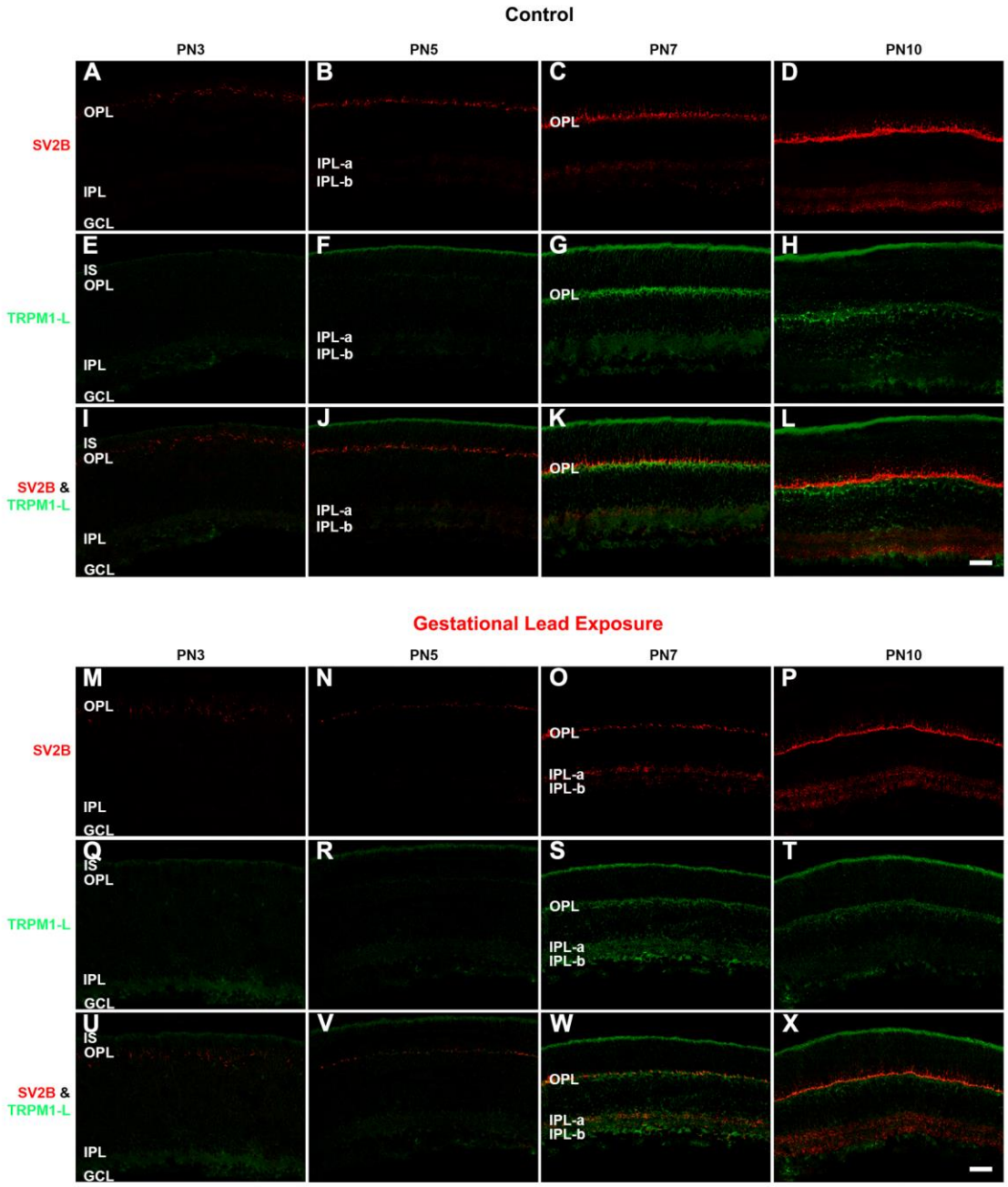
Control
PN3
PN5
PN7
PN10
SV2B
TRPM1-L
SV2B & TRPM1-L
A
B
C
D
E
F
G
H
I
J
K
L
M
N
O
P
Q
R
S
T
U
V
W
X
OPL
IS
IPL
GCL
IPL-a
IPL-b
Gestational Lead Exposure

Table 2.3

Summary of Developmental Appearance of Cellular and Synaptic Proteins in Control and GLE Retinas

	Developmental Age (day)					
Retinal Layer	E18.5	PN1	PN3	PN5	PN7	PN10
CONTROL						
OS						RHO
IS	RECVRN	RHO	PRKCA, PMCA	TRPM1-L		
ONL	RECVRN	RHO				
OPL			RECVRN, VGluT1 SV2B, TRPM1-L (low)	RHO, PRKCA, VGluT1, SCGN, PMCA, TRPM1-L (high)		
INL			CHX10 (RPCs & BCs), PRKCA	CHX10 (BCs), SCGN	CHX10	
IPL			PRKCA, PMCA, TRPM1-L (low)	VGluT1 (IPL-a), PMCA (high) SV2B (low)	SCGN	VGluT1 (IPL-b: high), SCGN (punctate) SV2B (IPL-a: low)
GCL			CHX10, PRKCA, PMCA	SCGN		
GESTATIONAL LEAD EXPOSURE						
OS						RHO (low)
IS	RECVRN		RHO, PRKCA	PMCA TRPM1-L (low)		
ONL	RECVRN		RHO			
OPL			RECVRN, VGluT1, TRPM1-L (low)	RHO, PRKCA, PMCA (low), VGluT1, TRPM1-L (low)	SCGN, TRPM1-L (low)	
INL			CHX10 (RPCs), PRKCA	CHX10 (RPCs & BCs)	CHX10 (BCs), SCGN	
IPL			PRKCA, PMCA	VGluT1 (IPL-a), PMCA (low)	SCGN SV2B	VGluT1 (IPL-b: low), SGCN (not punctate), SV2B (IPL-a: high)
GCL			CHX10, PRKCA, PMCA	PMCA (low)		

Proteins highlighted in red were delayed in appearance the GLE retinas.

2.4 Discussion

The overall goal of this study was to examine the functional development of the two late-born neural populations altered in the adult mouse retina after GLE: rod photoreceptors and bipolar cells (Giddabasappa et al., 2011). There were three main interrelated findings. First, RT-qPCR showed that the expression of genes associated with neurogenic cell cycle exit (*Otx2* and *Chx10* postnantally) were increased, whereas the expression of four rod specific transcription factors (*Nrl, Nr2e3, Crx,* and *Rho*) were decreased in PN2 GLE retinas. Second, immunohistochemical and confocal imaging studies revealed a two- to three-day delay in proteins associated with the differentiation and maturation of rod photoreceptors and bipolar cells. Third, immunohistochemical and confocal imaging studies also showed decreased expression of several essential proteins associated with synaptic function in both the OPL and IPL. Together, these data support the overall conclusion that the functional development of rod photoreceptors and bipolar cells was delayed in GLE retinas by two to three days.

A delay in the expression of rod and bipolar cell functional markers was an unexpected finding since birth-dating experiments revealed an increase in the number of these cells that underwent terminal mitosis during postnatal development without a phase shift in the timing (Giddabasappa et al., 2011). This, in combination with the data presented here, supports the idea that RPC terminal mitosis and neuronal differentiation are two separate events and that the

former does not always immediately follow the latter. *In vitro* and *in vivo* studies demonstrate that the early-born rod photoreceptors possess an intrinsically determined ability to postpone rhodopsin expression after terminal mitosis (Wantanbe et al., 1990; Morrow et al 1998). Morrow et al. (1998) demonstrated that in developing rat retina *in vitro* there were two phases of rod differentiation: 1) an early phase born prior to E19 in which terminal mitosis did not correlate with initial rhodopsin expression (average of 8.5- to 12.5- day difference between terminal mitosis and differentiation) and 2) a late phase born after E19 in which initial rhodopsin expression correlated with terminal mitosis (average difference of 5.5 – 6.5 days between terminal mitosis and differentiation). Although the postnatal microenvironment cannot prematurely induce early-born rods to express rhodopsin (Wanatanbe et al., 1990; Morrow et al., 1998), it is unknown whether early-born rods can further delay their expression of rhodopsin. Since the initial delay in rhodopsin expression occurs at PN2 in GLE retinas, it is likely that GLE affected the early cohort of rod photoreceptors.

There are only a few examples in the literature that cite a delayed commitment or maturation of differentiated late-born neurons during retinal development. Ciliary neurotrophic factor (CNTF) delayed rhodopsin expression and thereby negatively regulated rod differentiation (Kirsch et al., 1998; Schulz-Key et al., 2002). Neophytou et al (1997), using an *in vitro* preparation, showed that Müller glia derived leukemia-induced factor (LIF) also inhibited rod development. Although Affymetrix data from our lab does not suggest changes in

the genes associated with CNTF or its receptors during retinal development (data not shown), these data represent whole retinal expression. Therefore, I cannot rule out the possibility that CNTF or other cytokine receptors are differentially expressed on individual postmitotic RPCs in GLE retinas. One report notes a delay in bipolar cell development. Wu and Chiao (2007) demonstrated that dark-rearing rabbits delayed the morphological maturation of bipolar cells by two to three days as characterized by histology and confocal microscopy.

One possible explanation for the delay in rod photoreceptor differentiation in GLE retinas can be understood by examining the interactions of genes presented in our data. Here I show that increases in the gene expression of *Otx2* and *Chx10* overlap with the decreased expression of *Nrl, Nr2e3, Crx,* and *Rho*. The *Otx2* gene is a master regulator in rod photoreceptor cell fate determination and although the homogenous knockout is lethal, the conditional knockout of *Otx2* causes postmitotic rod precursors to switch cell fate and become amacrine-like cells (Acampora et al., 1995; Nishida et al., 2003). Furthermore, *Otx2* is an upstream promoter of *Crx* transcription and maintenance of rod photoreceptors and bipolar cells requires the expression of these two genes in concert (Nishida et al., 2003; Koike et al., 2007). Once Otx2 initiates Crx, Crx then initiates other genes in the rod differentiation pathway (Chen et al., 1997; Henning et al., 2008; Bibb et al., 2011). The ablation of *Otx2* in the conditional knockout strongly down-regulated many of the genes associated with photoreceptor differentiation, transcription, and phototransduction including *Crx*, *Nrl*, *Nr2e3*, and *Rho* (Koike at

al., 2007). On the protein level, however, Mukherjee (2011) demonstrated that GLE mice expressed more OTX2-IR rod and bipolar cell precursors in early postnatal development. These protein data correlate with an increase in PN2 *Otx2* gene expression, but since genes associated with rod photoreceptor differentiation are down-regulated in the PN2 GLE animals, this does not correlate with the aforementioned data, demonstrating the ability of Otx2 to promote rod specific genes. Therefore, it is likely that the down-regulation of rod-specific genes in GLE retinas is a consequence of factors not mediated by the *Otx2* gene.

RT-qPCR demonstrated that *Chx10* expression was decreased significantly in PN2 control retinas, possibly signifying the switch from RPC associated *Chx10* to bipolar cell associated *Chx10*. In GLE retinas, this decrease in expression was not observed since GLE retinas consistently maintained higher numbers of proliferative cells prior to their differentiation. This small, but significant, decrease in *Chx10* expression observed in PN2 control retinas may signify a critical time point in normal retinal development at which the developing retina switches from a proliferative state to a maturational state. Interestingly, Giddabasappa and Fox using Affymetrix analysis (unpublished data), identified five gene expression clusters: four of which indicated PN2 as a critical time point in normal retinal development. Two of the clusters, termed Clusters 4 and 5, demonstrated a marked decrease and increase in gene expression after PN2, respectively. Furthermore, Cluster 4 (i.e., decreased gene expression post PN2)

had the highest number of genes associated with cell proliferation, cell cycle and differentiation, while Cluster 5 (i.e., increased gene expression post PN2) had the highest number of genes associated with visual perception and receptor activity. In GLE retinas, many proliferative genes associated with Cluster 4 were up-regulated at or after PN2, while many functional Cluster 5 genes were down-regulated at PN2 (Giddabasappa and Fox, unpublished data; Mukherjee, 2011). If PN2 is a critical switch point between the expression of proliferative and differentiating genes, then the global overexpression of such proliferative genes may be sufficient to delay the subsequent expression of many neuronal differentiation markers. Consequently, no single gene or protein would be responsible for the delay and this would explain why both rod photoreceptors and bipolar cells are affected.

Finally, I showed that GLE decreased the expression of several functional proteins associated with synaptic function in both the OPL and IPL. The photoreceptor ribbon synapse is a complex structure that is specialized for fast, sustained neurotransmitter release (Heidelberger et al., 2005). Critical proteins associated with proper photoreceptor synaptic function include calcium channels, ion pumps, cytoskeletal scaffolds, presynaptic endocytotic and exocytotic proteins, and postsynaptic receptors (Mercer et al., 2011). Specifically, I assessed proteins involved in presynaptic calcium extrusion (PMCA), neurotransmitter uptake into synaptic vesicles (VGluT1), synaptic vesicle release (SV2B), and postsynaptic glutamate signaling (TRPM1) rather than scaffolding

proteins structurally associated with the synaptic ribbon (Morgans et al., 1998). I showed that although both GLE and control animals initially express VGluT1 at PN3, GLE animals exhibited decreased of VGluT1 in the developing OPL at PN7. Furthermore, I showed that PMCA-IR is decreased in GLE retinas at PN5. At PN3, VGluT1-IR in the OPL is indicative of cone synapses forming their first glutamatergic connections with horizontal cells, while rod photoreceptors first form connections around PN8 in mouse (Figure 2.2) (Sherry et al., 2003). Therefore, the pattern of VGluT1 label in the OPL of developing GLE retinas indicates that cone photoreceptor terminals develop normally, whereas rod terminals were delayed in their ability to package glutamate into vesicles. This was confirmed by the decrease in PMCA labeling observed in the OPL at PN5. PMCA localizes to photoreceptor terminals during the first postnatal week the rat (Rentaria et al., 2005). In adult mouse retinas, most PMCA is associated with rod spherules rather than cone pedicles (Krizaj et al., 2002; Johnson et al., 2007). Therefore, limited PMCA-IR in the OPL of PN5 GLE retinas may be a consequence of immature rod synapses. Interestingly, this delay is not seen at PN7 as with VGluT1 labeling. The fact that the delay in PMCA label is two days before the major delay in OPL VGluT1 label suggests that in normal maturation of the rod synapse, the mechanisms for calcium extrusion develop before that of glutamate packaging. Therefore, the photoreceptor terminal primarily establishes a means for maintaining calcium homeostasis before glutamate release is possible.

In addition to the delay of rod terminal development in the OPLs of GLE retinas, I observed a delay in IPL maturation at PN10. There are two possible explanations for this phenomenon: 1) the delayed commitment of bipolar cells, as observed by CHX10-IR in PN3 GLE retinas, resulted in an overall delay in the synaptic development of these cells, or 2) since GLE retinas exhibit an increase in the number of all bipolar cell types without changing their postsynaptic partners (retinal ganglion cells for cone bipolars and AII amacrine cells for rod bipolars), more time may be required for these cells to form proper connections and therefore appear mature. Both of these possibilities may be true since: 1) SCGN-IR at PN10 in GLE retinas demonstrated that cell bodies of cone bipolar cells appeared immature, 2) VGluT1-IR showed differences in the development of IPL-b in GLE retinas, and 3) the IPL-b contains over half of all the synaptic connections made by bipolar cells (Gosh and Wässle, 2004). It is unknown whether GLE mice express ectopic or uncharacteristic synaptic connections in their IPLs; however, it is likely that the ganglion cells increase their number of dendrites to accommodate the increased number of cone bipolar cells. The area where the GLE phenotype of increased bipolar cells may mostly affect the types of synaptic connections, however, is in the OPL. Normally, each rod photoreceptor communicates with only one rod bipolar cell. However, one rod bipolar cell combines the signals of many rod photoreceptors. Conversely, one cone communicates with many ON- and OFF-cone bipolar cells. Although the increase in rod photoreceptors is sufficient to accommodate the concurrent

increase in rod bipolar cells in GLE retinas, there is no change in the number of cone photoreceptors. Therefore, it is unknown if the increase in cone bipolar cells results in more synaptic ribbons in the available cones or if the cone bipolar cells make unusual contacts with the available rod photoreceptors. Although rare, some OFF-cone bipolar cells do make direct non-invaginating contacts with rod spherules (Soucy et al., 1998; Hack et al., 1999). Claes et al. (2004) demonstrated that in extreme cases (i.e., retinal degeneration) the plasticity of rod photoreceptors allows them to express multiple non-characteristic pre-synaptic ribbons. Furthermore, Hamilton (2011) showed that in GLE retinas, horizontal cells increased their dendritic sprouting: indicative of an overall increase in invaginating ON-bipolar cell contacts with either rod or cone photoreceptors. More work is required, however, to characterize and quantify the types of synaptic connections made in the OPLs of GLE retina.

In conclusion, I demonstrated that postponed differentiation and functional development of rods and bipolar cells accompanies the increased and prolonged proliferation observed in GLE retinas. I showed that GLE retinas expressed increased levels of genes associated with proliferation; however, the initial expression of genes associated with differentiation and synaptic function was delayed. Since the retina is a model system for the CNS, the delayed level of synaptic maturation I observed in retinas of GLE mice likely represents what occurs in the brain. Specifically, these data mark the time of neuronal differentiation and synaptogenesis as a vulnerable period for lead exposure in

mice and may correlate to similar vulnerabilities in humans (Rodier, 1994; 1995). Overall, this study shows that the timing of normal retinal morphological and cellular development is delayed following low-level GLE. The functional and behavioral consequences of delayed synaptic development are evident in neurological and psychiatric disorders such as autism, schizophrenia, and intellectual disability (Melom and Littleton, 2011). The links between developmental lead exposure and many of these disorders are well characterized (Cory-Slechta, 1995; Opler et al., 2008; Baranowska-Bosiacka et al., 2012) although the cellular and molecular mechanisms remain unknown.

2.5 REFERENCES

Acampora D, Mazan S, Lallemand Y, Avantaggiato V, Maury M, Simeone A, Brûlet (1995) Forebrain and midbrain regions are deleted in *Otx2-/-* mutants due to a defective anterior neuroectoderm specification during gastrulation. Development 121:3279-3290.

Agathocleous M, Harris W (2009) Differentiated cells in the vertebrate retina. Annu Rev Cell Dev Biol 25:45-69.

Baranowska-Bosiacka I, Gutowska I, Rybicka M, Nowacki P, Chlubek D (2012) Neurotoxicity of lead. Hypothetical molecular mechanisms of synaptic function disorders. Neurol Neurochir Pol 46:569-578.

Baye LM, Link BA (2008) Nuclear migration during retinal development. Brain Res 1192:29-36.

Baylor DA, Burns ME (1998) Control of rhodopsin activity in vision. Eye 12:521-525.

Bibb LC, Holt J, Tarttelin EE, Hodges M, Gregory-Evans K, Rutherford A, Lucas RJ, Sowden JC, Gregory-Evans CY (2001) Temporal and spatial expression patterns of the *Crx* transcription factor and its downstream targets. Critical differences during human and mouse eye development. Hum Mol Genet 10:1571-1579.

Boycott BB, Wässle H (1991) Morphological classification of bipolar cells of the primate retina. Eur J Neurosci 3:1069-1088.

Burgoyne RD, Weiss JL (2001) The neuronal calcium sensor family of Ca^{2+}-binding proteins. Biochem J 353:1-12.

Burmeister M, Novak J, Liang M, Basu S, Ploder L, Hawes NL, Vidgen D, Hoover F, Goldman D, Kalnins VI, Roderick TH, Taylor BA, Hankin MH, cInnes RR (1996) Ocular retardation mouse caused by *chx10* homeobox null allele: impaired retinal progenitor proliferation and bipolar cell differentiation. Nat Genet 12:376-384.

Canfield RL, Henderson CR, Jr., Cory-Slechta DA, Cox C, Jusko TA, Lanphear BP (2003) Intellectual impairment in children with blood lead concentrations below 10 microg per deciliter. N Engl J Med 348:1517-1526.

Chadderton T, Wilson C, Bewick M, Glück S (1997) Evaluation of three rapid RNA extraction reagents: relevance for use in RT-PCR's and measurement of low level gene expression in clinical samples. Cell Mol Biol 43:1227-1234.

Chen S, Wang Q, Nie Z, Sun H, Lannon G, Copeland NG, Gilbert DJ, Jenkins NA, Zack DJ (1997) Crx, a novel otx-like paired-homeodomain protein, binds to and transactivates photoreceptor cell-specific genes. Neuron 19:1017-1030.

Cepko CL, Austin CP, Yang X, Alexiades M, Ezzeddine D (1996) Cell fate determination in the vertebrate retina. Proc Natl Acad Sci 93:589-595.

Claes E, Seeliger M, Michalakis, Biel, Humphries, Haverkamp S (2004) Morphological characterization of the retina of CGNA -/-Rho-/- mutant mouse lacking functional cones and rods. Invest Ophthalmol Vis Sci 45:2039-2048.

Cory-Slechta DA (1995) Relationships between lead-induced learning impairments and changes in dopaminergic, cholinergic, and glutamatergic neurotransmitter system functions. Annu Rev Pharmacol Toxicol 35:391-415.

Dieck S, Brandstätter JH (2006) Ribbon synapses of the retina. Cell Tissue Res 326:339-346.

Dyer MA, Cepko CL (2001) Regulating proliferation during retinal development. Nat Rev Neurosci 2:333-342.

Edlund T and Jessell TM (1999) Progression from extrinsic to intrinsic signaling in cell fate specification: a view from the nervous system. Cell 96:211-224.

Euler T, Schneider H, Wässle H (1996) Glutamate responses of bipolar cells in a slice preparation of the rat retina. J Neurosci 16:2934-2944.

Euler I, Wässle H (1995) Immunocytochemical identification of cone bipolar cells in the rat retina. J Comp Neurol 361:461-478.

Fox DA, Campbell ML, Blocker YS (1997) Functional alterations and apoptotic cell death in the retina following developmental or adult lead exposure. Neurotoxicology 18:645-664.

Fox DA, Boyes WK. 2013. Toxic responses of the ocular and visual system. In: Casarett & Doull's Toxicology: The Science of Poisons (Klaassen CD, ed). 8th ed. New York: McGraw-Hill, Chapter 17, in press.

Fox DA, Kala SV, Hamilton WR, Johnson JE, O'Callaghan JP (2008) Low-level human equivalent gestational lead exposure produces supernormal scotopic

electroretinograms, increased retinal neurogenesis, and decreased retinal dopamine utilization in rats. Environ Health Perspect 116:618-625.

Fox DA, Hamilton WR, Johnson JE, Xiao W, Chaney S, Mukherjee S, Miller DB, O'Callaghan JP (2011) Gestational lead exposure selectively decreases retinal dopamine amacrine cells and dopamine content in adult mice. Toxicol Appl Pharmacol 256:258-267.

Garcia M, Strehler E (1999) Plasma membrane calcium ATPases as critical regulators o calcium homeostasis during neuronal cell function. Front Biosci 4:d869-882.

Giddabasappa A, Hamilton WR, Chaney S, Xiao W, Johnson JE, Mukherjee S, Fox DA (2011) Low-level gestational lead exposure increases retinal progenitor cell proliferation and rod photoreceptor and bipolar cell neurogenesis in mice. Environ Health Perspect 119:71-79.

Gosh KK, Bujan S, Haverkamp S, Feigenspan A, Wässle H (2004) Types of bipolar cells in the mouse retina. J Comp Neurol 469:70-82.

Graham DR, Overbeek PA, Ash JD (2005) Leukemia inhibitory factor blocks expression of Crx and Nrl transcription factors to inhibit photoreceptor differentiation. Invest Ophthalmol Vis Sci 46:2601-2610.

Grandjean P, Landrigan PJ (2006) Developmental neurotoxicity of industrial chemicals. Lancet 368:2167-2178.

Gump BB, Reihman J, Stewart P, Lonky E, Granger DA, Matthews KA (2009) Blood lead (Pb) levels: further evidence for an environmental mechanism

explaining the association betwenn socioeconomic status and psychophysiological dysregulation in children. Health Psychol 28:614-620.

Hack I, Peichl L, Brandstätter H (1999) An alternative pathway for rod signals in the rodent retina: rod photoreceptors, cone bipolar cells, and the localization of glutamate receptors. Proc Natl Acad Sci USA 96:14130-14135.

Hamilton WR (2011) Gestational lead exposure alters GABAergic and dopaminergic systems in the mouse retina. PhD Dissertation The University of Houston.

Hargrave PA, McDowell JH (1992) Rhodopsin and phototransduction: a model system for G protein-linked receptors. FASEB J 6:2323-2331.

Hatakeyama J and Kageyama R (2004) Retinal cell fate determination and bHLH factors. Semin Cell Dev Biol 15:83-89.

Haverkamp S, Wassle H (2000) Immunocytochemical analysis of the mouse retina. J Comp Neurol 424:1-23.

He L, Perkins GA, Poblenz AT, Harris JB, Hung M, Ellisman MH, Fox DA (2003) Bcl-xL overexpression blocks bax-mediated mitochondrial contact site formation and apoptosis in rod photoreceptors of lead-exposed mice. Proc Natl Acad Sci USA 100:1022-1027.

Heidelberger R, Thoreson WB, Witkovsky P (2005) Synaptic transmission at retinal ribbon synapses. Prog Retinal Eye Res 24:682-720.

Henning AK, Peng G, Chen S (2008) Regulation of photoreceptor gene expression be crx-associated transcription factor network. Brain Res 1192:114-133.

Johnson JE, Jr., Perkins GA, Giddabasappa A, Chaney S, Xiao W, White AD, Brown JM, Waggoner J, Ellisman MH, Fox DA (2007) Spatiotemporal regulation of ATP and Ca^{2+} dynamics in vertebrate rod and cone ribbon synapses. Mol Vis 13:887-919.

Kihara AH, Santos TO, Osuna-Melo EJ, Paschon V, Vidal K, Akamine PS, Castro TO, Resende RR, Hamassaki DE, Britto L (2010) Connexin-mediated communication controls cell proliferation and is essential in retinal histogenesis. Int J Devl Neuroscience 28:39-52.

Kirsch M, Schulz-Key S, Wiese A, Fuhrmann S, Hofmann H (1998) Ciliary neurotrophic factor blocks rod photoreceptor differentiation from postmitotic precursor cells in vitro. Cell Tissue Res 291:207-216.

Koike C, Nishida A, Ueno S, Saito H, Sanuki R, Sato S, Furukawa A, Aizawa S, Matsuo I, Suzuki N, Kondo M, Furukawa T (2007) Functional roles of Otx2 transcription factor in postnatal mouse retinal development. Mol Cell Biol 27:8318-8329.

Krizaj D, Demarco S, Johnson J, Strehler E, Copenhagen DR (2002) Cell-specific expression of plasma membrane calcium ATPase isoforms in retinal neurons. J Comp Neurol 451:1-21.

Kurihara T, Kubota Y, Ozawa Y,Takubo K, Noda K, Simon MC, Johnson RS, Suematsu, Tsubota K, Ishida S, Goda N, Suda T, Okano H (2010) von Hippel-Lindau protein regulates transition from fetal to adult circulatory system in retina. Development 137:1563-1571.

Leasure JL, Giddabasappa A, Chaney S, Johnson JE Jr, Pothakos K, Lau YS, Fox DA (2008) Low-level human equivalent gestational lead exposure produces sex-specific motor and coordination abnormalities and late-onset obesity in year-old mice. Environ Health Perspect 115:355-361.

Levine EM, Green ES (2004) Cell-intrinsic regulators of proliferation in vertebrate retinal progenitors. Semin Cell Dev Biol 15:63-74.

Lilienthal H, Kohler K, Turfeld M, Winneke G (1994) Persistent increases in scotopic B-wave amplitudes after lead exposure in monkeys. Exp Eye Res 59:203-209.

Linser PJ, Sorrentino M, Moscona AA (1984) Cellular compartmentalization on carbonic anhydrase-C and glutamine synthetase in the developing and mature mouse neural retina. Brain Res 315:65-71.

Liu I, Chen J, Ploder L, Vidgen D, Kooy D, Kalnins VI, McInnes RR (1994) Developmental expression of a novel murine homeobox gene (chx10): evidence for roles in determination of the neuroretina and inner nuclear layer. Neuron 13:377-393.

Livesey FJ and Cepko CO (2001) Vertebrate neural cell-fate determination: lessons from the retina. Nat Rev 2:109-118.

Marquardt T and Gruss P (2002) Generating neuronal diversity in the retina: one for nearly all. Trends Neurosci 25:32-38.

Martins RA, Pearson RA (2008) Control of cell proliferation by neurotransmitters in the developing vertebrate retina. Brain Res 1192:37-60.

Melom JE , Littleton JT (2011) Synapse development in health and disease. Current Opinion in Genetics and Development 21:256-261.

Mercer AJ, Thoreson WB (2011) The dynamic architecture of photoreceptor ribbon synapses: cytoskeletal, extracellular matrix, and intramembrane proteins. Vis Neurosci 28:453-471.

Morgan J, Wong R (2005) Developmental of cell types and synaptic connections in the retina. Webvision: The Organization of the Retina and Visual System. http://www.ncbi.nlm.nih.gov/books/NBK11558/

Morgans CW, Far OE, Berntson A, Wässle H, Taylor WR (1998) Calcium extrusion from mammalian photoreceptor terminals. J Neurosci 18:2467-2474.

Morrow EM, Belliveau MJ, Cepko CL (1998) Two phases of rod photoreceptor differentiation during rat retinal development. J Neurosci 18:3738-3748.

Mukherjee S (2011) Mechanisms of retinal progenitor cell proliferation and neuronal-glial cell fate choice in a gestational lead exposure model. Ph.D. Dissertation. The University of Houston.

Negpal AG, Brodie SE (2009) Supranormal electroretinogram in a 10-year-old girl with lead toxicity. Doc Ophthalmol 118:163-166.

Neophytou C, Vernallis AB, Smith A, Raff MC (1997) Müller-cell-derived leukaemia inhibitory factor arrests rod photoreceptor differentiation at a postmitotic pre-rod stage of development. Development 124:2345-2354.

Nir I, Cohen D, Papermaster DS (1984) Immunocytochemical localization of opsin in the cell membrane of developing rat retinal photoreceptors. J Cell Biol 98:1788-1795.

Nishida A, Furukawa A, Kioke C, Tano Y, Aizawa S, Matsuo I, Furukawa T (2003) *Otx2* homeobox gene controls retinal photoreceptor cell fate and pineal gland development. Nat Neurosci 6:1255-1263.

Opler MG, Buka SL, Groeger J, McKeague I, Wei C, Factor-Litvak P, Bresnahan M, Graziano J, Goldstein JM, Seidman LJ, Brown AS, Susser ES (2008) Prenatal exposure to lead, delta-aminolevulinic acid, and schizophrenia: further evidence. Environ Health Perspect 116:1586-1590.

Osman K, Pawlas K, Schutz A, Gazdzik M, Sokal JA, Vahter M (1999) Lead exposure and hearing effects in children in Katowice, Poland. Environ Res 80:1-8.

Puthussery T, Gayet-Primo J, Taylor WR (2010) Localization of the calcium-binding protein secretagogin in cone bipolar cells of the mammalian retina. J Comp Neurol 518:513-525.

Rapaport DH, Wong LL, Wood ED, Yasumura D, LaVail MM (2004) Timing and topography of cell genesis in the rat retina. J Comp Neurol 474:304-324.

Rao-Mirotznik, Harkins AB, Buchsbaum G, and Sterling P (1995) Mammalian rod terminal: architecture of a binary synapse. Neuron 14:561-569.

Rath MF, Morin F, Shi Q, Klein DC, Møller M (2007) Ontogenetic expression of the *Otx2* and *Crx* homeobox genes in the retina of the rat. Exp Eye Res 85:65-73.

Rentería RC, Strehler EE, Copenhagen DR, Krizaj D (2005) Ontogeny of plasma membrane Ca^{2+} ATPase isoforms in the neural retina of the postnatal rat. Vis Neurosci 22:263-274.

Rice D, Barone S Jr (2000) Critical periods of vulnerability for the developing nervous system: evidence from humans and animal models. Environ Health Perspect 108:511-533.

Rothenberg SJ, Poblano A, Schnaas L (2000) Brainstem auditory evoked response at five years and prenatal and postnatal blood lead. Neurotoxixol Teratol 22:503-510.

Rothenberg SJ, Schnaas L, Salgado-Valladares M, Casanueva E, Geller AM, Hudnell HK, Fox DA (2002) Increased ERG a- and b-wave amplitudes in 7- to 10-year-old children resulting from prenatal lead exposure. Invest Ophthalmol Vis Sci 43-2036-2044.

Schulz-Key S, Hofmann H, Beisenherz-Huss C, Barbisch C, Kirsch M (2002) Ciliary neurotrophic factor as a transient regulator of rod development in rat retina. Invest Ophthalmol Vis Sci 43:3099-3108.

Sherry DM, Wang MM, Bates J, Frishman LJ (2003) Expression of vesicular glutamate transporter 1 in mouse retina reveals temporal ordering in development of rod vs. cone and ON vs. OFF circuits. J Comp Neurol 465:480-498.

Shigeri Y, Seal RP, Shimamoto K (2004) Molecular pharmacology of glutamate transporters, EAATs and VGLUTs. Brain Res Rev 45:250-265.

Soucy E, Wang Y, Nirenberg S, Nathans J, Meister M (1998) A novel signaling pathway from rod photoreceptors to ganglion cells in mammalian retina. Neuron 21:481-493.

Stella SL, Li S, Sabatini A, Vila A, Brecha N (2008) Comparison of the ontogeny of the vesicular glutamate transporter 3 (VGLUT3) with VGLUT1 and VGLUT2 in the rat retina. Brain Res 1215:20-29.

Turner DL, Cepko CL (1987) A common progenitor for neurons and glia persists in rat retina late in development. Nature 328:131-136.

Turner DL, Snyder EY, Cepko CL (1990) Lineage-independent determination of cell type in the embryonic mouse retina. Neuron 4:833-845.

Wasserman GA, Musabegovic A, Liu X, Kline J, Factor-Litvak P, Graziano JH (2000) Lead exposure and motor functioning in 4(1/2)-year-old children: the Yugoslavia prospective study. J Pediatr 137:555-561.

Watanabe T, Raff MC (1990) Rod photoreceptor development in vitro: intrinsic properties of proliferating neuroepithelial cells change as development proceeds in the rat retina. Neuron 2:461-467.

Werblin F, Dowling JE (1969) Organization of the retina of the mudpuppy, Nectrurus maculosus, II. Intracellular recording. J Neurophysiol 32:339-355.

Wu M, Chiao C (2007) Light deprivation delays morphological differentiation of bipolar cells in the rabbit retina. Brain Res 1170:13-19.

Young RW (1985) Cell differentiation in the retina of the mouse. Anat Rec 212:199-205.

Yuan JS, Wang D, Stewart CN (2008) Statistical methods for efficiency adjusted real-time PCR quantification. Biotechnol J 3:112-123.

CHAPTER 3:

GESTATIONAL LEAD EXPOSURE ALTERED THE GLUTAMATERGIC RESPONSE PROFILE OF DEVELOPING RETINA

3.1 Introduction

The seven cell types in the adult murine retina arise from a common pool of mulitpotent progenitor cells from embryonic day 11.5 (E11.5) to postnatal day 10 (PN10) (Turner and Cepko, 1987; 1990). Tight regulation of retinal progenitor cell (RPC) proliferation and cell cycle exit is therefore required to ensure proper proportions of all the adult cell types (Dyer and Cepko, 2001). This regulation occurs through the concerted actions of both extrinsic and intrinsic cues (Cepko, 1993; Dyer and Cepko, 2001). Current data suggests a competence model in which a RPC's competence state is intrinsically defined, and positively or negatively regulated by both intrinsic and extrinsic cues (Livesey and Cepko, 2001). Intrinsic cues include gene and protein expression internally regulated by the RPC. For example, transcription factors and membrane receptors, and a predetermined 'differentiation clock' (Agathocleous et al., 2009). Extrinsic cues include secreted molecules such as neurotrophic/growth factors, neurotransmitters, and even the surrounding redox state of the tissue (Martins and Pearson, 2008; Baye and Link, 2008; Kurihara et al., 2010).

Neurotransmitters promote or inhibit the proliferation of RPCs when they act as extrinsic cues (Martins and Pearson, 2008). Specifically, glutamate provides an anti-proliferative signal for RPCs prior to neurogenesis and synapse formation. Pearson et al. (2002) demonstrated that although endogenous glutamate activated spontaneous Ca^{2+} transients in the ventricular zone (VZ) of developing chick retinas, it did not affect the time for RPCs to complete mitosis.

Conversely, in embryonic murine retinal explants, glutamate reduced RPC proliferation by decreasing cyclin dependent kinase 2 (CDK2) activity (Martins et al., 2006). Recent *in vitro* studies, using explanted porcine retinas, support findings that glutamate acts as an anti-proliferative signal and suggest that glutamate signaling during early development is important for regulation of rod photoreceptor differentiation and developmental apoptosis (Ghosh et al., 2012).

Glutamate is the main excitatory neurotransmitter in the adult retina and its extracellular levels are maintained at low levels to prevent neurotoxicity. However, in developing neonatal rabbit retina, extracellular glutamate levels can reach levels that are toxic in the adult (>70 μM) (Haberecht et al., 1996; Redburn et al., 1996). High levels of extracellular glutamate occur in the early neonatal retina because Müller glia cells, the cells responsible for glutamate uptake in the adult retina, are the last retinal cells to completely develop (Young, 1985; Marquardt and Gruss, 2002). The exact mechanism of glutamate release for embryonic and early postnatal retina is unknown, but may involve a non-canonical release mechanism as is observed in the hippocampus (Demarque et al., 2002). This is feasible since most cells in the developing retina are immunoreactive for glutamate (Fletcher et al., 1997).

Despite the uncertainty on how glutamate release occurs, the mechanism for glutamate signaling at the receptor level is fairly constant. The membrane receptors that bind glutamate are broadly classified as ionotropic or metabotropic receptors (Brandstatter et al., 1998) Ionotropic glutamate receptors (iGluRs)

function as gated ion channels while metabotropic receptors (mGluRs) couple with G-proteins and signal through second messengers (Yang, 2004). Further classification of iGluRs depends on their sensitivity to the agonists AMPA (alpha-amino-3-hydroxy-5-methyl-4-isoxazole-propionic acid), KA (kainate), or NMDA (N-methyl-D-aspartate) (Bleakman et al., 1998). The AMPA receptor family consists of four GLUR subtypes (GLUR1-4) while KA receptors consist on two subunit families, GLUR5-7 and KA1 and KA2 (Rosenmund et al., 1998; Kew et al,. 2005). NMDA receptors are classified into seven subclasses: NR1, NR2A-D, NR3, and NR3B subunits. The ion permeability and functional traits of all iGluRs depend on their subunit composition (Bowie, 2012; Flores-Soto et al., 2012). The eight known mGluRs (mGluR1-8) in vertebrates are classified into three groups based on sequence homology, transduction mechanism, and agonist selectivity (Quraishi et al., 2007). This study primarily focuses on the effects of gestational lead exposure (GLE) on iGluRs during retinal development.

The genes for AMPA (Zhang et al., 1996) and NMDA (Wantanabe et al., 1994) glutamate receptors are expressed in the embryonic rodent VZ as characterized by *in situ hybridization*. Interestingly, most AMPA genes are expressed at higher levels during development than in the adult (Zhang et al., 1996). The localization and timing of iGluR gene expression suggests their role in processes other than canonical synaptic transmission. Similarly, NMDA and non-NMDA glutamate receptor proteins are expressed embryonically and/or during early postnatal stages in chick, rabbit, and rodent retina (chick: Silveira dos

Santos and Hamassaki-Britto, 2001; rabbit: Wong, 1995; rodent: Wanatanabe et al., 1994; Grunder et al., 2000; 2000b; Sucher et al., 2003). However, many of the protein studies on glutamate receptor expression during early postnatal ages focused on the developing inner plexiform layer (IPL) and ganglion cell layer (GCL). Functional data, as characterized by calcium signaling, confirms the conclusions reached from gene expression data and show that some cells located in the VZ respond to different glutamate agonists in rabbit retina (Wong, 1995). Furthermore, cells in the VZ preferentially respond to non-NMDA glutamate agonist, whereas, differentiating ganglion and amacrine cells respond to both NMDA and non-NMDA glutamate agonist (Wong, 1995).

The effect of lead exposure on glutamate receptors is an important area of neurotoxicology research. In rat hippocampal pyramidal neurons from cultured hippocampus, lead dose-dependently and selectively blocked synaptic NMDA receptors at micomolar concentrations (Alkondon et al., 1990). Furthermore, exposure to lead during development, a time when NMDA receptors are more sensitive to lead, altered the subunit composition of NMDA receptors of hippocampal neuron synapses (Guilarte et al., 1992; Ujihara et al., 1992; Neal et al, 2011). Sui and Ruan (2000) found that in rat hippocampal slices in culture, lead exposure impaired both AMPA and KA receptors. Therefore, lead exposure can affect all of the iGluRs.

Goals of the present study on retinal glutamatergic signaling and lead neurotoxicity

GLE increased and prolonged RPC proliferation during early retinal development resulting in a dose-dependent increase in the number of rod photoreceptors and bipolar cells in adult GLE mice (Giddabasappa et al., 2011). Since photoreceptors and bipolar cells compose the primary components of the vertical glutamatergic signaling pathway in the retina, my research examined alterations in this pathway at several critical time points during the rodent lifespan. The goals of my PhD research were to: 1) characterize the spatiotemporal and functional synaptic development of rod photoreceptors and bipolar cells in developing GLE retinas, 2) examine effect of GLE on proliferative glutamate signaling prior to conventional synapse formation, and 3) examine the integrity of GLE retinas, especially rod photoreceptors and bipolar cells, during normal aging.This chapter addresses the second of these goals.

Glutamate functions as an extrinsic anti-proliferative signal for RPCs in the early stages of retinal development. Lead can inhibit the activity of all iGluR types. Therefore, I hypothesized that lead inhibited activation of glutamate receptors on RPCs in GLE retinas and delayed cell cycle exit in these cells. To test this hypothesis, I first analyzed the spatiotemporal localization of cells responsive to different iGluR agonists (glutamate, AMPA, KA, and NMDA) in developing control and GLE mouse retinas. I used the well characterized and commercially available probe agmatine (AGB), which is a small divalent cation

that selectively enters activated iGluRs and thereby maps the excitation history of a cell that expresses functional glutamate receptors (Marc et al., 2005). Once AGB enters a cell, it can be visualized by standard immunohistochemical techniques (Marc et al., 2005; Sun et al., 2006). Next, I used commercially available antibodies to immunohistochemically identify the glutamate responsive cells present in early postnatal retinas. Since nicotinic activation of developing inner retina influences the profile of calcium waves in the developing outer retina (Syed et al., 2004), I determined whether a similar phenomenon occurs with developmental glutamate signaling. I performed acute pharmacological experiments in which I activated the developing inner retina with a nicotinic agonist and characterized the entry of AGB in the outer retina. Additional pharmacological experiments with ATP and KCl were performed. Furthermore, to test whether lead directly inhibited the activation of iGluRs in developing retinas, I incubated control retinas in the presence of low micromolar concentrations of lead and exogenous glutamate agonists and examined the entry of AGB. Finally, I used quantitative RT-qPCR to determine whether there were any changes in the gene expression of iGluR subunits in GLE retinas, compared to age-matched controls, throughout development when compared to age-matched controls.

Briefly, my results reveal the presence of glutamate responsive cells located in the VZ and developing inner retina (IPL and GCL) of early postnatal control retinas. Glutamate responsive cells located in the inner retina are composed of differentiated amacrine and ganglion cells, whereas all of the cells

observed in the VZ were postmitotic. GLE increased the peak number of these postmitotic glutamate responsive cells and extended the timeframe in which these cells responded to glutamate in the developing outer retina. Immunohistochemical experiments revealed that many of the postmitotic glutamate responsive cells were rod and bipolar cell precursors. Pharmacological experiments showed that the outer and inner retina could be directly or indirectly stimulated by different ligand-gated ion channels to increase AGB permeation. Finally, acute *in vitro* lead exposure decreased AGB entry into the outer and inner retina of following AMPA or KA stimulation: an effect opposite to that seen with GLE retinas. Together, my results will provide future insight into how iGluRs and other ligand-activated ion channels in developing outer and inner retina contribute to RPC proliferation and neuronal differentiation.

3.2 Material and Methods

3.2.1 Mouse model of gestational lead exposure

All experimental and animal care procedures complied with the National Institutes of Health (NIH) Public Health Service Policy on Humane Care and Use of Laboratory Animals (NIH 2002) and were approved by the Institutional Animals Care and Use Committee of the University of Houston. All animals were treated humanely and with regard for alleviation of suffering. The protocol for housing, feeding, breeding, and lighting conditions were as previously described (Leasure et al., 2008; Giddabasappa et al., 2011). Briefly, naïve female were given either tap (control) or moderate-dose (55 ppm) lead acetate drinking water (GLE group) for two weeks before mating, during pregnancy, and until PN10, after which the lead was replaced with tap water. For E18.5 retinas, dams were mated overnight and checked for vaginal plugs in the morning. Water, food, and weights were recorded throughout treatment. Mice were sacrificed by decapitation between 1000 and 1200 hours. Blood lead concentrations were measured as previously described for each pup to ensure relevant blood lead levels (Leasure et al., 2008). Pups in the control and GLE groups had peak blood lead concentration on PN0 and/or PN10 of 0.75 ± 0.06 and 22.11 ± 1.05 mg/dL, respectively. There were no statistical differences between control and GLE groups on any dam measure, litter measure, or body weight (Leasure et al., 2008).

3.2.2 Agmatine (AGB) labeling

After decapitation, mouse eyes were enucleated and immediately placed in cold HEPES buffer (125 mM NaCl, 5 mM KCl, 2 mM $MgCl_2$, 1.5 mM $CaCl_2$, 30 mM HEPES, and 10 mM glucose, 305 ± 5 mOsm, pH 7.4). The optic nerve was cut at the globe and the opening was used to gently separate the retinal pigment epithelium (RPE) from the retina under a dissecting microscope. The RPE was peeled back, cornea was removed, and the retina with the attached lens remained. The lens served as a reference point when sectioning the tissue. To avoid mechanical or stress-induced entry of AGB, the retinas were not touched with forceps, cut, or exposed to bright room light once they were isolated. The retina and attached lens were moved with a plastic transfer pipette to fresh, warm (37°) HEPES for 5 minutes in a slow shaking water bath to equilibrate. The HEPES was removed gently by suction and fresh HEPES that contained AGB plus the desired agonist and/or antagonist for 5 minutes, as described in the Results. For inhibitory experiments, the antagonist was added during the first 5 minutes of equilibration. After 5 minutes of the HEPES-AGB buffer, the reaction was stopped by directly adding buffered paraformaldehyde and glutaraldehye fixative (4% paraformaldehyde, 0.01% glutaraldehyde, 0.03% w/v sucrose, 0.01% v/v $MgSO_4$) for 30 minutes. The retinas were washed in PBS, cryoprotected in 30% sucrose overnight, frozen in OCT and stored in a -80°C freezer until processed.

3.2.3 Tissue processing and immunohistochemistry

All tissue processing and immunohistochemistry techniques were performed as described (Johnson et al., 2007; Fox et al., 2008; Giddabasappa et al., 2011). Three non-adjacent fixed-frozen transverse sections (10 µm) taken from the vertical meridian were mounted on Superfrost Plus glass slides (Thermo Fisher Scientific, Waltham, MA) and stored at -20°C. The slides were thawed slowly, sections post-fixed with 4% paraformaldehyde, washed, and briefly immersed in a 1% sodium borohydride (Sigma-Aldrich, St. Louis, MO) solution to reduce double bonds, allow proper epitope access for antibodies and decrease auto-fluorescence. Sections were washed with ddH_2O, then PBS and incubated for 2 hours with blocking buffer containing10% normal goat serum (Jackson ImmunoResearch Labs Inc.) and 0.3% triton in PBS. Primary antibodies were applied for 2 days at 4°C after which slides were washed with PBS, blocked for 30 minutes, and secondary applied. For double-labeling experiments, primary antibodies from different host animals were applied simultaneously. Table 3.1 lists all antibodies used, their source, and their dilutions. Dilutions of Alexa 488, 555 and 647 (1:400) conjugated secondary antibodies were made in blocking buffer, applied to slides, and allowed to incubate in the dark at room temperature for one hour. Slides were washed with PBS, ddH_2O, dried, and mounted with Vectashield mounting medium (Vector Laboratories Inc. Burlinghame CA) and No.1 coverslip, and stored at 4°C. For experiments with DAPI labeling, sections were incubated with DAPI for one hour in the dark after secondary incubation. All

antibodies were titrated through a broad range of working dilutions (3 orders of magnitude) to determine optimal working dilutions. Immunolabeling specificity was confirmed by processing retinal sections in the absence of primary anitibody.

Table 3.1
Cell Specific Primary Antibodies Used for Immunohistochemistry (IHC)

Primary Antigen	Imunogen	Source	Catalog. No.	Target	Host	Dilution	IHC or WB
Agmatine (AGB)	Agmatine conjugated BSA	Millipore	AB1568-2000T	AGB permeated cells	rabbit	1:1000	IHC
Agmatine (AGB)	Agmatine conjugated BSA	Abcam	AB62667	AGB permeated cells	chicken	1:100	IHC
OTX2	Full length recombinant human OTX2	Chemicon	AB9566	Rod and bipolar cell precursors	rabbit	1:100	IHC
PCNA	Purified PCNA	Chemicon	MA4076	Proliferative RPCs	Mouse	1:100	IHC
MCM6	C-Terminal of MCM6 of human origin	Santa Cruz	SC-9843	RPCs	Goat	1:100	IHC

3.2.4 Real-time quantitative PCR (RT-qPCR)

Total RNA was synthesized into cDNA as described (Graham et al., 2005). Briefly, 1 µg of total RNA was used for first-strand cDNA synthesis and added to oligo dT and random hexamer primers according to Bio-Rad specifications. All RT-qPCR experiments were run on the Bio-Rad iCycler platform (Bio-Rad Laboratories, Hercules, CA). RT-qPCR primers were designed and validated within certain parameters: GC content 50-60%, melt temperature 55-65ºC, no secondary structures, and no primer dimers or homodimers. Primer quality analysis used IDT DNA's Oligo Analyzer (http://www.idtdna.com/analyzer/Applications/OligoAnalyzer/). All primers designed were intron spanning. Primers were selected from the Roche Applied Science Universal Probe Library and Assay Design Center database. Primers were tested for alternative sites of homology with NCBI's BLAST (http://www.ncbi.nlm.nih.gov/BLAST) and the UCSC genome browser (http://genome.ucsc.edu/cgi-bin/hgGateway). Primer sequences are shown in Table 3.2. Primers were validated by melt curve analysis for single peak of fluorescence.

Table 3.2
RT-qPCR primer list

Gene	Accession Number	Forward Primer (5'-3')	Reverse Primer (3'-5')	Product Size (bp)
Actb	NM_007393	AGAGAGGTATCCTGACCCTGAAGT	CACGCAGCTCATTGTAGAAGGTGT	105
Gria1 (AMPA1)	NM_008165.4	AGGGATCGACATCCAGAGAG	TGCACATTTCCTGTCAAACC	63
Gria2 (AMPA2)	NM_001083806.1	CCAATGGGATAAGTTCGCATA	GCACAGCTTGCAGTGTTGA	65
Gria3 (AMPA3)	NM_016886.3	AGCCGTGTGATACGATGAAA	GCAAGGTTTACAGGCGTTCT	100
Gria4 (AMPA4)	NM_001113181.1	CTGCCAACAGTTTTGCTGTG	AAATGGCAAACACCCCTCTA	66
Grik1 (GluR5)	NM_010348.3	AGCTCTCATGCAGCAAGGAT	TCCTCCAACTATTCTGGTCGAT	64
Grik2 (GluR6)	NM_001111268.1	AAAAACGCTCAATTGGAAAAGA	GACGCTGGCACTTCAGAG	79
Grik3 (GluR7)	NM_001081097.2	AGGTCACTCATCGTCACCACT	ATCAGACTTGCGGAACATGA	60
Grik4 (KA1)	NM_175481.5	GAGCTGATCGCTCGGAAA	TCTCACGTTCCGCTGTGA	64
Grik5 (KA2)	NM_008168.2	CCCCTCAGCTAGCCTCATCT	GCCTCGCACCAGTTCTTCTA	67
Grin1 (NMDA1)	NM_001177657.1	GCTGGAGGAGCGTGAGTC	AGCAGAGCCGTCACATTCTT	138
Grin2a (NMDA2a)	NM_008170.2	ATTCAACCAGAGGGGCGTA	TTCAAGACAGCTGCGTCATAG	87
Grin2b (NMDA2b)	NM_008171.3	GGGTTACAACCGGTGCCTA	CTTTGCCGATGGTGAAAGAT	65

All RT-qPCR experiments were performed in triplicate and using SYBR green. β-Actin was used as the internal control. The PCR mixture consisted of 12.7 µL of Bio-Rad supermix, 1 µL of cDNA template and 1.5 µL of gene specific forward and reverse primers all combined in a 0.5 mL PCR tube on a 96-well plate. A no template control, water control and air [empty well] control were run for each plate. The PCR cycle conditions were: 95ºC for 3 minutes, followed by 40 cycles of 95ºC for 30 sec and 60ºC for 30 sec. A melt curve analysis was run at the end of each plate to ensure proper performance of primer pairs. This was performed starting at 60ºC and increasing the temp 0.5ºC per minute to 95ºC. Threshold for Ct values was manually adjusted for each plate to coincide with entrance into exponential growth phase of PCR. Ct values were then exported to Microsoft Excel for further analysis. The level of gene expression, relative to controls was determined using ΔΔCt (Yuan et al., 2008). ΔΔCt = ΔCt of gene of interest - ΔCt of β-actin. To compare GLE versus control, $2^{\Delta\Delta Ct}$ to obtain the fold change of gene expression was used.

3.2.5 Statistical analyses

For all data, only one animal or one pooled group of animals from the same litter was used for each measure or sample. Data are presented as the mean ± SEM for four to nine animals per treatment group. Data were analyzed using an

ANOVA followed by post-hoc analysis with Fisher's Least Significance Difference Test or the Student's T-test when only two means were compared. In all figures, values with $p<0.05$ were considered significantly different from controls and were noted where appropriate by asterisks. In the text, values noted as significantly different from controls had $p<0.05$.

3.3 Results

3.3.1 AGB standardization

To validate our AGB technique, I incubated adult (PN60) control retinas in the presence of AGB and either glutamate, KA, or NMDA. To examine the sensitivity the AGB activation technique in GLE retinas to determine if it reproduced our previously published morphologic data on the GLE model (Giddabasappa et al., 2011), I incubated PN60 adult GLE retinas with AGB and glutamate. Figure 3.1 shows the immunohistochemical images from these experiments. Figure 3.1A shows that without added agonist, there is very little basal uptake of AGB in adult control retinas. One goal in the development of our free-float technique was to reduce the possibility of mechanical damage to the retina. Figure 3.1B demonstrates that physical damage or trauma to the retina during the removal or incubation process produces a significant increase in AGB uptake and thus alters the results and their interpretation. Figures 3.1C and 3.1D show the AGB responses after the addition of either KA or NMDA to the incubation buffer. KA markedly increases AGB-immunoreactivity (IR) in the outer and inner segments (OS and IS, respectively), outer and inner plexiform layers (OPL and IPL, respectively), and cells in both the inner nuclear and ganglion cell layers (INL and GCL, respectively). NMDA, however, elicited a more cellular pattern of labeling in the INL and GCL in addition to labeling the OS, IS, OPL, and IPL. This demonstrates that different agonists elicit different responses, as described (Marc, 2005; Sun and Kalloniatis, 2006). Figures 3.1E and 3.1F show

AGB entry in response to glutamate in PN60 control and GLE retinas. In control retinas that were stimulated by glutamate, AGB lightly labeled the OS, IS, and bipolar cells in the INL while strongly labeling the OPL, IPL, and amacrine and ganglion cells. There were several differences noted in glutamate-stimulated GLE retinas compared to age-matched controls. First, the overall retinal thickness of GLE retinas was increased, consistent with our previously published data (Giddabasappa et al., 2011). Second, bipolar cells in the INL were increased in number also consistent with our previously published data on the GLE model (Giddabasappa et at., 2011). Third, the OS, IS, and bipolar cells in GLE retinas labeled more intensely for AGB. Fourth, and interestingly, the IPL labeled less intensely with AGB in GLE retinas. Overall, these results describe the effect that dissection and incubation techniques have on the results and confirm the sensitivity of the AGB technique in adult control and GLE retinas.

Since our main goal was to examine glutamate signaling during early postnatal development in control and GLE retinas, we standardized our techniques and the glutamate agonist-dependent AGB responses in PN2 control retinas. In control retinas, the peak of both rod photoreceptor and bipolar cell neurogenesis (the two neurons affected in the GLE model) occurs around PN2 (Giddabasappa et al., 2011). Furthermore, in the GLE model, PN2 is a peak time when the phenotypic increase in retinal progenitor cell proliferation in the GLE retinas is most notable. Figure 3.2 shows AGB uptake in PN2 control retinas in response to varying the AGB concentrations (Figures 3.2A and 3.2B), and

Figure 3.1. The ionotropic glutamate receptor agonists kainate (KA), N-methyl-D-aspartate (NMDA) and glutamate (Glu) as well as forceps-induced injury activate agmatine (AGB) permeation in retinas of adult control and gestational lead exposure (GLE) mice. Adult (postnatal day 60: PN60) control **(A-E)** and GLE **(F)** retinas. Retinas were isolated and incubated in 25 mM AGB only **(A, B)**, 25 mM AGB and 60 µM KA **(C)**, 25 mM AGB and 1 mM NMDA **(D)** or 25 mM AGB and 1 mM Glu **(E, F)**. **(A)** Basal permeation of AGB without any agonist was minimal. It weakly and variably labeled cone photoreceptor inner segments (ISs: arrows), horizontal cells (HCs) in the distal inner nuclear layer (INL: arrowheads) and some cells in the ganglion cell layer (GCL). **(B)** Intentional injury produced by penetrating the distal retina (photoreceptor layer) with the tip of a #5 Dumont forceps (white V) activated AGB permeation into rod and cone photoreceptor ISs and somas in the outer nuclear layer (ONL) as well as HCs. Moreover, the injury slightly increased the basal or background AGB-immunoreactivity (IR) throughout the retina. **(C)** KA stimulation increased AGB permeation into photoreceptor outer segments (OSs), ISs, and their synaptic terminal in the outer plexiform layer (OPL), the external limiting membrane (elm), HCs (large arrowheads), bipolar cells (BCs) in the distal inner nuclear layer (arrows: INL), amacrine cells (ACs) in the proximal INL (small arrowheads), the inner plexiform layer (IPL), and GCL. **(D)** Activation of NMDA receptors markedly increased AGB permeation into OSs and ISs, and the GCL as well as increased labeling throughout the distal and proximal INL. No AGB-IR was seen in Müller glial cells (arrows). (**E**) Glutamate stimulation markedly increased AGB permeation into the OPL, distal INL and GCL and increased permeation in the OS, IS and elm. **(F)** Adult retinas from GLE mice have a 25-30% selective increase in the number of rod photoreceptors and bipolar cells as well as an increased retinal thickness, as reported (Giddabasappa et al. 2011). Glutamate markedly increased AGB permeation into the OS, IS, elm, ONL, OPL, distal and proximal INL, and the GCL. Compared to control retinas with 1 mM glutamate shown in E, the GLE retinas stimulated with glutamate had increased AGB permeation. Similar abbreviations are used in all subsequent figures. Scale bar = 40 µm.

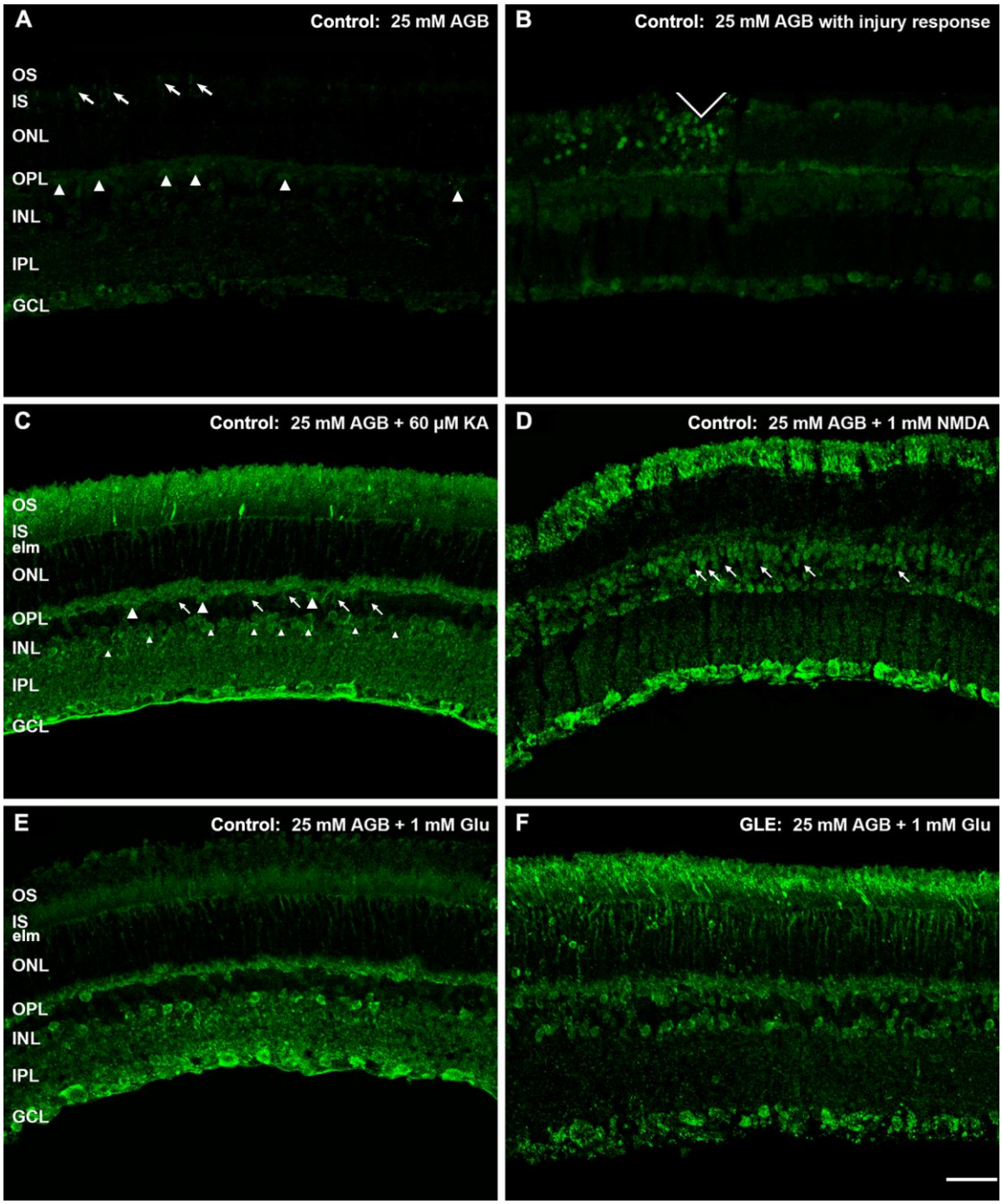
A
Control: 25 mM AGB
OS
IS
ONL
OPL
INL
IPL
GCL
B
Control: 25 mM AGB with injury response
C
Control: 25 mM AGB + 60 µM KA
OS
IS
elm
ONL
OPL
INL
IPL
GCL
D
Control: 25 mM AGB + 1 mM NMDA
E
Control: 25 mM AGB + 1 mM Glu
OS
IS
elm
ONL
OPL
INL
IPL
GCL
F
GLE: 25 mM AGB + 1 mM Glu

Figure 3.2. In PN2 control retinas, AGB permeation increased with increasing concentrations of AGB and ionotropic agonists. Retinas were isolated and incubated in AGB **(A, B)**, AGB and glutamate (Glu) **(C, D)**, AGB and AMPA **(E, F)** or AGB and kainate (KA) **(G, H)**. **(A)** Basal permeation of AGB with 25 mM AGB was minimal. Only a few cells in the most distal retina above the ventricular zone (VZ), which are photoreceptor ISs as shown in Figure 2.3, exhibited AGB-IR. **(B)** With 50 mM AGB, the basal permeation of AGB increased in cone ISs and the VZ. In the VZ, isolated clusters of AGB-IR cells became visible that were not seen with 25 mM AGB. Incubating retinas with AGB plus Glu **(C, D)**, AMPA **(E, F)** or KA **(G, H)** differentially increased AGB permeation in ISs, clusters of cells in the distal VZ, amacrine cells in the proximal IPL and cells in the GCL. Retinas incubated in 50 mM AGB plus double the concentration of agonist **(D, F and H)** markedly increased the amount and intensity of AGB-IR cells in the VZ. To minimize basal AGB permeation and increase the detection of agonist-mediated effect, 25 mM AGB was used in all subsequent experiments. Scale bar = 40 µm.

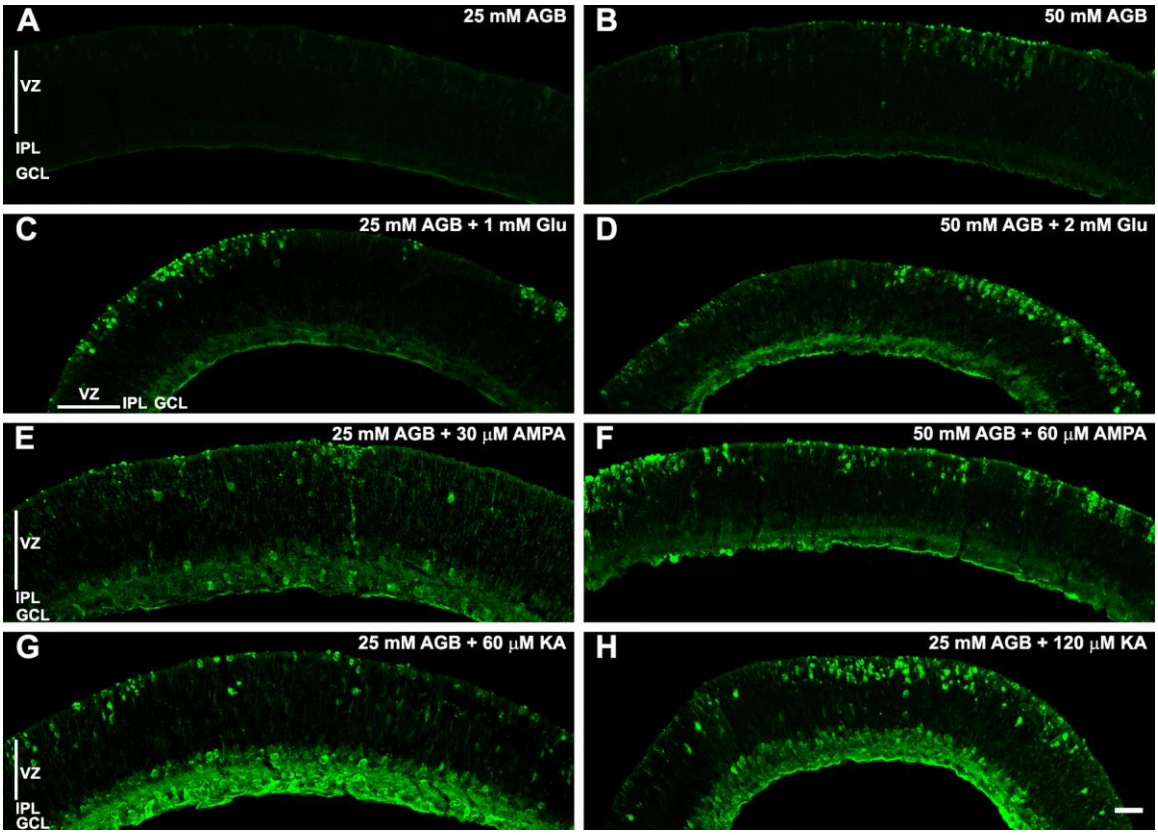

different final concentrations of glutamate (Figures 3.2B and 3.2C), AMPA (Figures 3.2D and 3.2E), and KA (Figures 3.2F and 3.2G). When control PN2 retinas were incubated in 25 mM AGB without agonist, very little AGB entry occurred. Since these tissues were washed in equilibration buffer prior to the incubation with AGB (see METHODS), this is indicative of minimal basal levels of non-specific glutamate release and/or signaling at this age. Incubation of PN2 control retinas with glutamate or its analogs AMPA and KA resulted in detectable entry of AGB into previously unidentified cells in the distal ventricular zone (VZ), the developing IPL, and amacrine and ganglion cells. Figure 3.3 shows that in PN2 control retinas, AGB-IR cells in the distal VZ often appeared as clone like clusters and AGB-IR cells throughout the retina were either brightly or dimly labeled. Increasing the concentration of AGB and glutamate agonist in the incubation buffer increased the intensity and number of AGB-IR cells in the VZs of PN2 control retinas. Increasing the concentration of AGB from 25 to 50 mM increased the basal level of AGB entry (Figure 3.2B). Therefore, 25 mM AGB was used as the standard for all experiments. Subsequent figures will present the spatiotemporal labeling pattern of AGB entry into developing postnatal control and GLE retinas following stimulation with either glutamate, AMPA, KA, or NMDA.

Figure 3.3. AMPA and KA incubation revealed brightly and dimly labeled AGB-IR cells in the VZs and IPLs of PN2 control retinas. High magnification images of AMPA **(A)** and KA **(B)** induced AGB permeation in PN2 control retinas. Incubation with both agonist resulted in dim (arrows) and bight (arrowheads) AGB-IR cells in the VZ and near the developing IPL. Furthermore, both agonists induced AGB permeation in clusters of cells in the distal VZ (ovals). Scale bar = 40 μm.

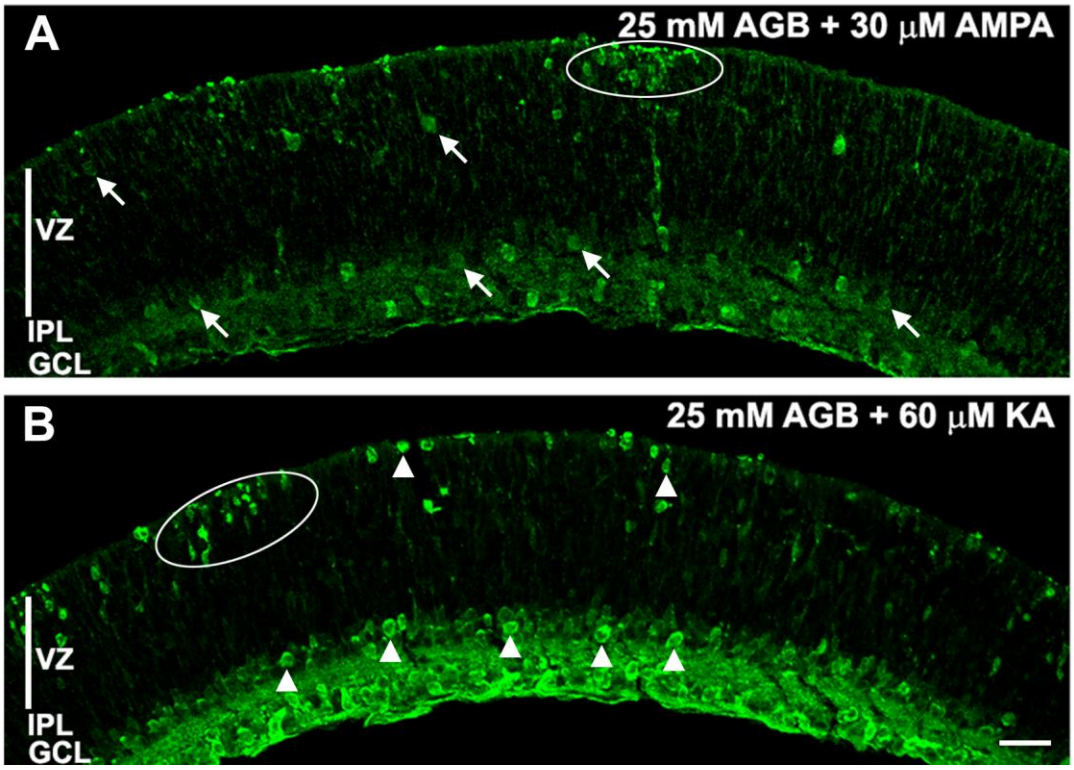

Figure 3.4. Basal permeation of AGB in the absence of exogenous glutamate receptor agonists in developing control and GLE retinas. Control **(A-C; G-I)** and GLE **(D-F; J-L)** retinas from PN0, PN2, PN4, PN6, PN8 and PN10 mice were incubated in buffer containing 25 mM AGB in the absence of exogenous glutamate agonists and processed as described in the Methods. **(A-C)** In control PN0, PN2 and PN6 retinas, minimal and diffuse basal AGB-IR was observed in the distal VZ, IPL and GCL. **(D-F)** PN0 GLE retinas were relatively similar to PN0 controls. However, in PN2 GLE retinas, the amount and intensity of AGB-IR markedly increased in the ISs, clusters of cells in the distal VZ, and cells in the distal IPL and GCL. In PN4 GLE retinas, AGB-IR decreased in the ISs and slightly increased in cells in the distal IPL and GCL. **(G-I)** In PN6 controls, AGB-IR localized to ISs, clusters of cells in the ONL, HCs in the distal INL, and cells in the IPL and GCL. In PN8 controls, AGB-IR localized to ISs, HCs, the entire IPL and GCL. In PN10 retinas, AGB-IR was minimal and localized to ISs, OPL and GCL. **(J-L)** PN6 GLE retinas were relatively similar to PN6 controls. In PN8 GLE retinas, the amount and intensity of AGB-IR increased in the ISs and ONL, although it was relatively similar to PN8 controls in the remainder of the retina. In PN10 GLE retinas, cellular AGB-IR was observed in the ISs, OPL, INL, IPL and GCL. Scale bar = 40 µm.

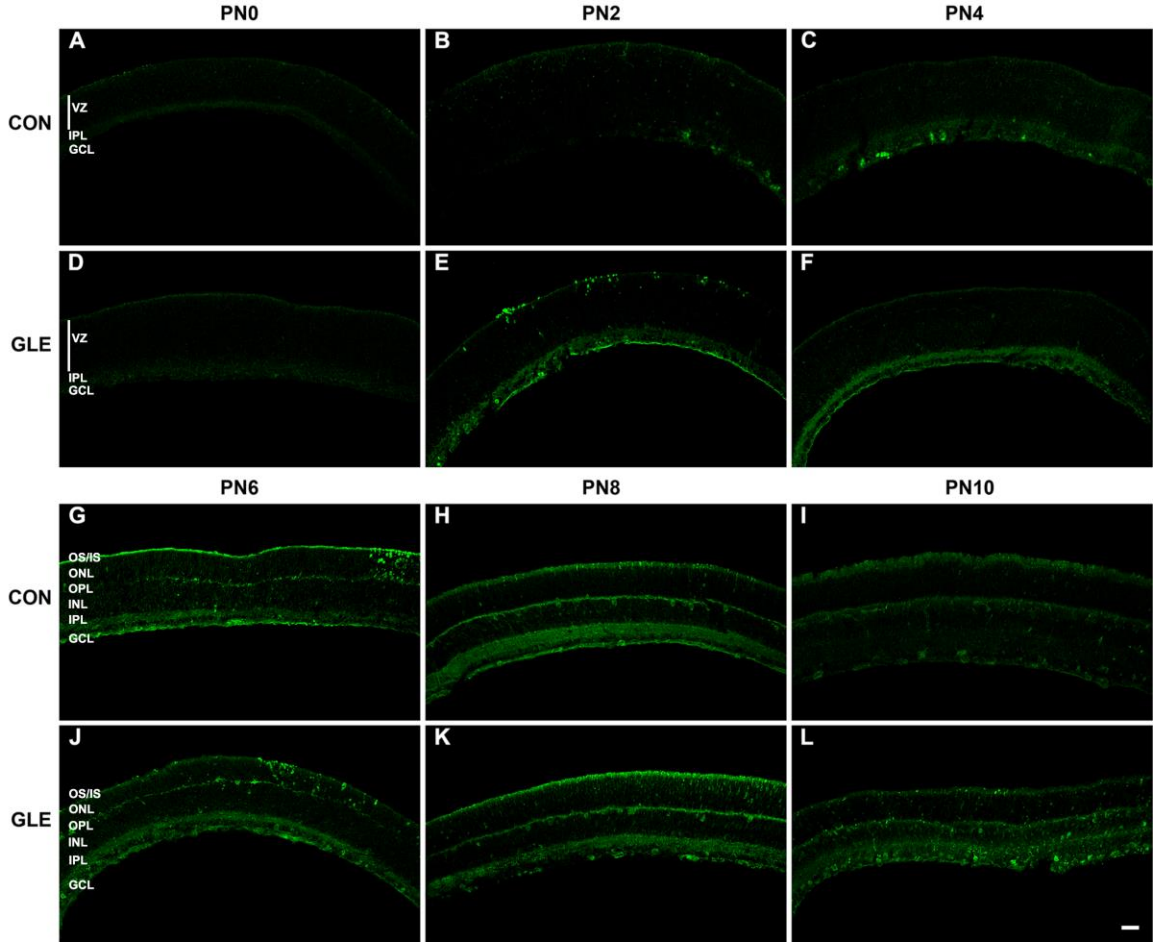
PN0
PN2
PN4
A
B
C
CON
VZ
IPL
GCL
D
E
F
GLE
VZ
IPL
GCL
PN6
PN8
PN10
G
H
I
CON
OS/IS
ONL
OPL
INL
IPL
GCL
J
K
L
GLE
OS/IS
ONL
OPL
INL
IPL
GCL

3.3.2 Spatiotemporal pattern of agonist-induced AGB activation in control and GLE retinas

To characterize the spatiotemporal pattern of glutamate receptor driven entry of AGB into cells of the developing retina, we incubated control and GLE retinas at PN0, PN2, PN4, PN6, PN8, and PN10 with AGB only (Figure 3.4), glutamate (Figure 3.5), AMPA (Figure 3.6), KA (Figure 3.7), or NMDA (Figure 3.8). In control retinas, very little basal AGB entry was detected at ages PN0, PN2, and PN4 (Figure 3.4A-C). At PN6, PN8 and PN10 the basal activity in control retinas slightly increased and revealed the structural organization of the retina (Figure 3.4G-I). The basal activity of AGB entry in GLE retina (Figures 3.4D-F and J-L) was similar to control retinas except at ages PN2 (Figure 3.4E) and PN10 (Figure 3.4L) when the basal levels were slightly higher in GLE retinas.

The spatiotemporal pattern of glutamate-induced AGB entry revealed strongly labeled AGB-IR throughout development in control (Figures 3.5A-C and G-I) and GLE retinas (Figures 3.5D-F and J-L). In control PN0 retinas, we observed AGB-IR cells in the distal VZ and near the IPL, which also labeled with AGB. In control PN2 retinas, the number of the AGB-IR cells in the distal VZ and near the developing IPL increased. By PN4, the intensity and number of the AGB-IR cells in the distal VZ decreased while the intensity of AGB-IR in the developing IPL increased. At PN6 in control retinas, the appearance of the AGB-IR cells in the developing ONL appeared as clusters of brightly labeled cells. In

Figure 3.5. Permeation of AGB after activation with 1 mM Glu in developing control and GLE retinas. Control **(A-C; G-I)** and GLE **(D-F; J-L)** retinas from PN0, PN2, PN4, PN6, PN8 and PN10 mice were incubated in buffer containing 25 mM AGB plus 1 mM Glu and processed as described in the Methods. AGB-IR cells in this and all subsequent figures were classified as low, moderate or high intensity. **(A-C)** In control PN0, PN2 and PN4 retinas, a moderate intensity of AGB-IR was consistently observed in ISs and moderate-to-high intensity AGB-IR clusters of cells in the distal VZ. The peak number and intensity of AGB-IR cells in the VZ occurred on PN2. Cells in the IPL and GCL exhibited a low-to-moderate intensity of AGB-IR on PN0 and PN2, which increased to a high intensity on PN4. **(D-F)** PN0 GLE retinas were relatively similar to PN0 controls. However, in PN2 and PN4 GLE retinas, the amount and intensity of AGB-IR markedly increased in the ISs and in clusters of cells in the distal VZ. The peak number and intensity of AGB-IR cells in the VZ was similar on PN2 and PN4. Cells in the distal IPL and GCL exhibited a moderate-to-high AGB-IR at PN0, PN2 and PN4. **(G-I)** In PN6 controls, moderate-to-high intense AGB-IR localized to ISs and clusters of cells in the ONL. Low intensity AGB-IR was seen in HCs in the distal INL, and cells in the IPL and GCL. In PN8 and PN10 controls, moderate-to-high intense AGB-IR localized to ISs, HCs, BCs and ACs in the INL, IPL and GCL. In PN8 and PN10 retinas, no AGB-IR was seen in the ONL. **(J-L)** In PN6 and PN8 GLE retinas, high intensity AGB-IR localized to ISs, large clusters of cells in the ONL, OPL, INL, IPL and GCL. In PN10 GLE retinas, moderate intensity AGB-IR was seen in the ISs, OPL, distal and proximal INL, whereas high intensity AGB-IR occurred in the GCL. Overall, GLE retinas exhibited an increased number of intensely labeled AGB-IR cells in the distal VZ and/or ONL at PN2, PN4, PN6, and PN8. Scale bar = 40 µm.

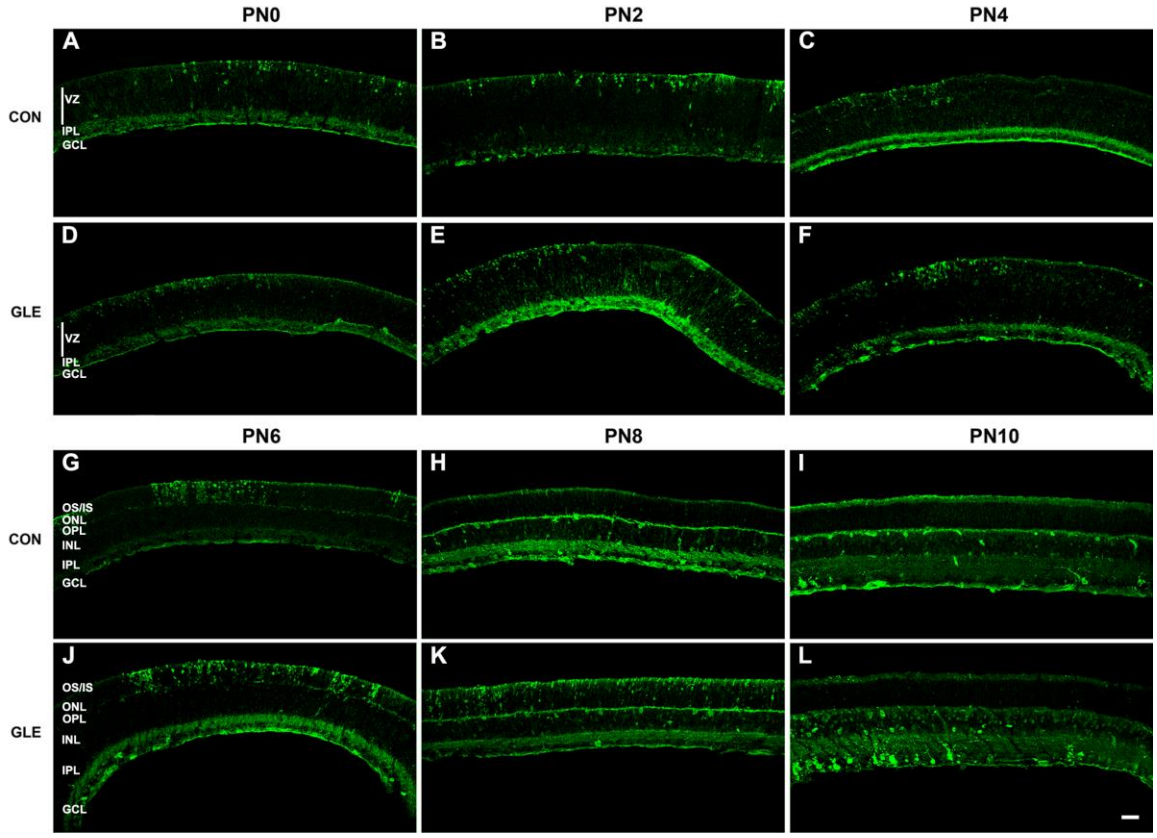
PN0
PN2
PN4
A
B
C
CON
VZ
IPL
GCL
D
E
F
GLE
VZ
IPL
GCL
PN6
PN8
PN10
G
H
I
CON
OS/IS
ONL
OPL
INL
IPL
GCL
J
K
L
GLE
OS/IS
ONL
OPL
INL
IPL
GCL

control PN8 and PN10 retinas, these clusters were no longer present and AGB strongly labeled the developing IS, both plexiform layers, and amacrine and ganglion cells. Some bipolar cells were also labeled.

In GLE retinas, the developmental pattern of glutamate-induced AGB-IR was different from controls at every age At PN0, the AGB-IR cells in the VZ of GLE retinas were lighter in intensity than age-matched controls. In GLE PN2 retinas, AGB-IR cells in the distal VZ were fewer in number, but brighter in intensity when compared to age-matched controls. At PN4, GLE retinas exhibited an increase in the number and intensity of AGB-IR cells in the VZ. By PN6 when the ONL was identifiable, GLE retinas had more cluster-like cells in this layer compared to controls. It is also interesting to note that while these cells were no longer present in the ONLs of control retinas, they were still present in GLE retinas. At PN10, most of the ganglion, amacrine and bipolar cells that labeled with AGB in GLE retinas were more intensely labeled compared to the age-matched controls. In summary, GLE retinas exhibited an increase in the number and/or intensity of AGB-IR cells throughout development following glutamate stimulation.

Figure 3.6 shows the spatiotemporal pattern of AGB-IR in developing control (Figures 3.6A-C and G-I) and GLE (Figures 3.6D-F and J-L) retinas following activation with AMPA. As with glutamate, stimulation of the developing retina with AMPA increased AGB-IR at every age. However, the overall AMPA-induced AGB response was greater than that of glutamate. In control PN0

retinas, AGB brightly labeled a few clusters of cells in the distal VZ, horizontal cells, amacrine cells, ganglion cells, and the developing IPL. This pattern persisted in PN2 control retinas and additionally, the APMA-induced AGB-IR in the distal VZ was lighter and more diffuse rather than bright and somal. At PN4, AGB-IR in the VZ was mostly limited to horizontal cells and the developing OPL. At PN6, AGB labeled a few cell clusters in the ONL, both plexiform layers, and amacrine and ganglion cells. Bipolar cells were first seen spanning the INL at this age. As the control retina matured, this overall pattern of AGB-IR was maintained. At PN10, AGB intensely labeled the IS, OPL, IPL, horizontal, bipolar, amacrine, and ganglion cells.

In comparison to age-matched controls, the response to AMPA was different in GLE retinas. At PN0 and PN2 there were more clusters of AGB-IR cells in the distal VZ and the IPL labeled less intensely At PN4, AGB labeled many more clusters of distal VZ cells and the OPL was less developed. At PN6, more ONL cells labeled with AGB, but there was no appearance of developing bipolar cells. At PN10, all AGB-IR cells labeled more intensely than in controls although the IS was not as developed. As with glutamate induced AGB-IR, AMPA induced AGB-IR revealed an increase in the intensity and/or number of AGB-IR cells in the VZ and ONL throughout development. In summary, these results reveal a delay in the functional development of the AMPA specific glutamatergic system in GLE retinas.

Figure 3.6. Permeation of AGB after activation with 30 µM AMPA in developing control and GLE retinas. Control **(A-C; G-I)** and GLE **(D-F; J-L)** retinas from PN0, PN2, PN4, PN6, PN8 and PN10 mice were incubated in buffer containing 25 mM AGB plus 30 µM AMPA and processed as described in the Methods. **(A-C)** In control PN0, PN2 and PN4 retinas, a low intensity of AGB-IR was consistently observed in ISs and small clusters of moderate-to-high intensity AGB-IR cells were scattered in the distal VZ. The peak number and intensity of AGB-IR cells in the VZ was similar on PN0 and PN2. Cells in the IPL and GCL exhibited a moderate intensity of AGB-IR on PN0 and PN2, which increased to a high intensity on PN4. **(D-F)** In PN0, PN2 and PN4 GLE retinas, the amount and intensity of AGB-IR steadily increased in the ISs. Similarly, the number of moderate-to-high intensity clusters of AGB-IR cells in the distal VZ increased. The peak number and intensity of AGB-IR cells in the VZ was similar on PN4. Cells in the distal IPL and GCL exhibited a moderate-to-high AGB-IR at PN0, PN2 and PN4. **(G-I)** In PN6 and PN8 controls, there were intense small clusters of AGB-IR cells in the ONL, but none at PN10. In PN6, PN8 and PN10 controls, moderate-to-high intensity AGB-IR localized to ISs, apparent photoreceptor processes in the ONL, the OPL, INL, IPL and GCL. Intense AGB-IR HCs were present at all ages and by PN10 there were distinct intense AGB-IR OSs, BCs and ACs. **(J-L)** In PN6 GLE retinas, there were large clusters of intense AGB-IR cells in the ONL. In PN8 retinas, there were dispersed intense AGB-IR cells in the ONL and by PN10 there were none. Similar to controls, in PN6, PN8 and PN10 GLE retinas there were moderate-to-high intensity AGB-IR localized to ISs, apparent photoreceptor processes in the ONL, the OPL, INL, IPL and GCL. Intense AGB-IR HCs were present at all ages and by PN10 there were distinct intense AGB-IR BCs and ACs although the OSs were not yet AGB-IR. Scale bar = 40 µm.

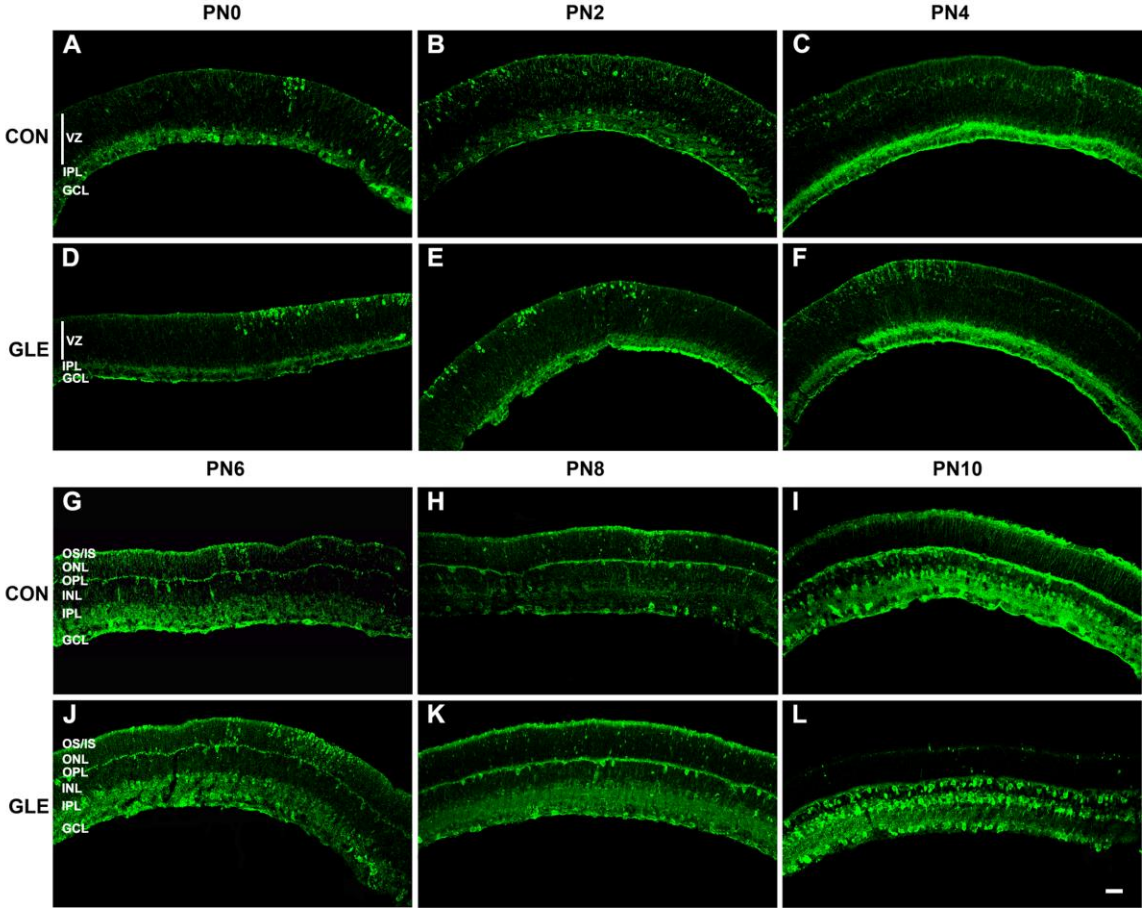
PN0
PN2
PN4
A
B
C
CON
VZ
IPL
GCL
D
E
F
GLE
VZ
IPL
GCL
PN6
PN8
PN10
G
H
I
CON
OS/IS
ONL
OPL
INL
IPL
GCL
J
K
L
GLE
OS/IS
ONL
OPL
INL
IPL
GCL

Figure 3.7. Permeation of AGB after activation with 60 µM KA in developing control and GLE retinas. Control **(A-C; G-I)** and GLE **(D-F; J-L)** retinas from PN0, PN2, PN4, PN6, PN8 and PN10 mice were incubated in buffer containing 25 mM AGB plus 60 µM KA and processed as described in the Methods. **(A-C)** In control PN0 retinas, a cluster and scattered individual moderate-to-high intensity AGB-IR cells were located in the distal VZ. At PN2, a cluster and a few AGB-IR cells were present in the VZ and none at PN4. In control PN2 and PN4 retinas, a low intensity of AGB-IR was consistently observed in ISs. The peak number and intensity of AGB-IR cells in the VZ was similar on PN0. Cells in the IPL and GCL exhibited a moderate intensity of AGB-IR on PN0, PN2 and PN4. **(D-F)** In PN0 and PN2 GLE retinas, the number of moderate-to-high intensity clusters of AGB-IR cells in the distal VZ increased. The peak number and intensity of AGB-IR cells in the VZ was on PN2 and there were none on PN4. PN0, PN2 and PN4 controls expressed similar amounts and moderate-intensity AGB-IR ISs. Cells in the distal IPL and GCL exhibited a moderate-to-high AGB-IR at PN0, PN2 and PN4. **(G-I)** In PN6, PN8 and PN10 controls, there were no AGB-IR cells in the ONL, however, the ISs exhibited moderate-to-high intensity AGB-IR and apparent photoreceptor processes in the ONL. Intense AGB-IR HCs, BCs, ACs and GCs were present at all ages and by PN10 there were distinct intense AGB-IR OSs. **(J-L)** In PN6 GLE retinas, there were small clusters of intense AGB-IR cells in the ONL, whereas in PN8 retinas there were dispersed intense AGB-IR cells in the ONL and by PN10 there were none. Similar to controls, in PN6, PN8 and PN10 GLE retinas there were moderate-to-high intensity AGB-IR localized to ISs, apparent photoreceptor processes in the ONL, the OPL, INL, IPL and GCL. Intense AGB-IR HCs were present at all ages. By PN10 there were distinct intense AGB-IR BCs and ACs, although the OSs were not yet AGB-IR. Scale bar = 40 µm.

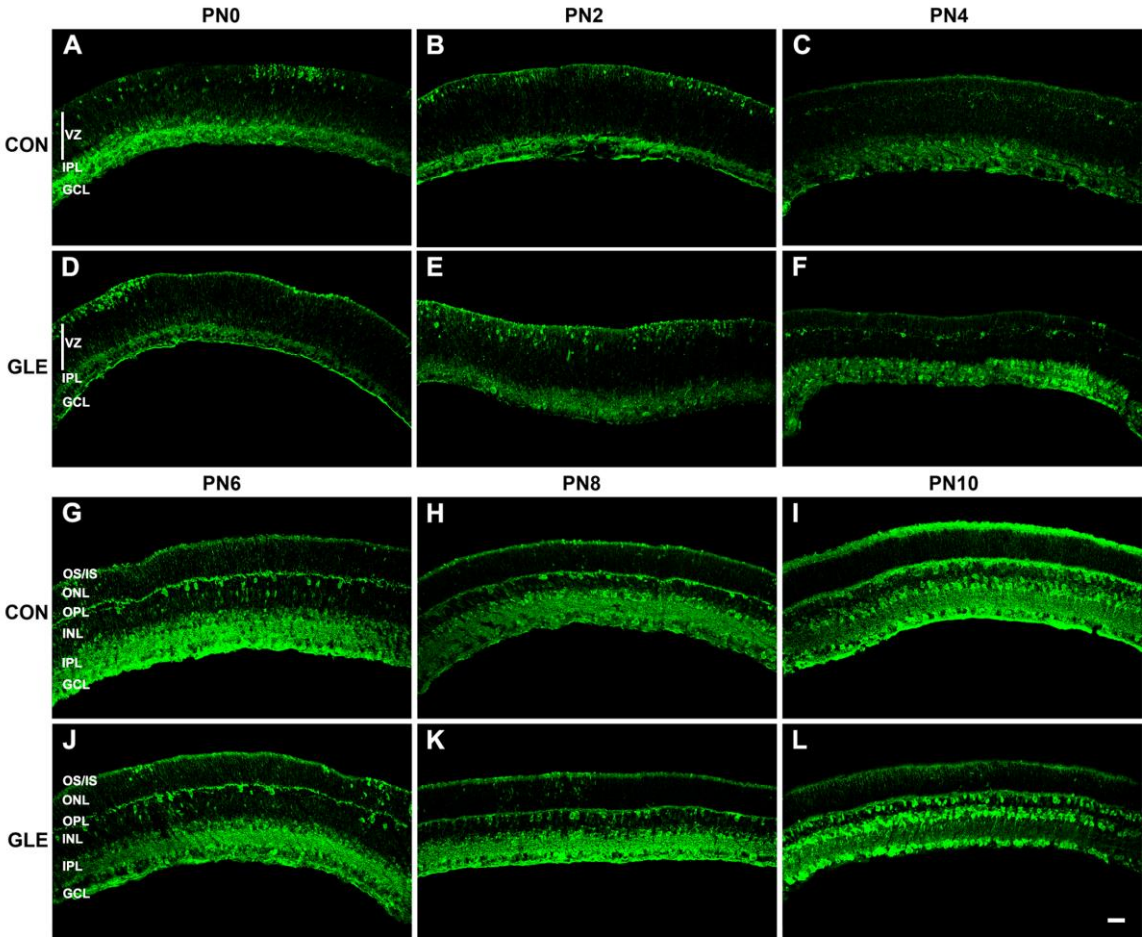
PN0
PN2
PN4
A
B
C
CON
VZ
IPL
GCL
D
E
F
GLE
VZ
IPL
GCL
PN6
PN8
PN10
G
H
I
CON
OS/IS
ONL
OPL
INL
IPL
GCL
J
K
L
GLE
OS/IS
ONL
OPL
INL
IPL
GCL

Figure 3.7 shows the spatiotemporal pattern of AGB-IR in developing control (Figures 3.7A-C and G-I) and GLE (Figures 3.7D-F and J-L) retinas following KA stimulation. As with AMPA, KA stimulation of developing retinas resulted in more intense AGB-IR than with glutamate stimulation. In control PN0 retinas, AGB entered a few cell clusters in the VZ, horizontal cells, amacrine cells, ganglion cells, and the developing IPL. At PN2, the number of AGB-IR cells in the distal VZ slightly increased, although there were no large clusters of AGB-IR cells. By PN4 in control retinas, the only AGB-IR cells in the VZ were associated with horizontal cells and the developing OPL. At this age, the amacrine and ganglion cells and the IPL labeled strongly with AGB. In control PN6 retinas, AGB strongly labeled a few cells in the ONL, both plexiform layers, horizontal cells, newly differentiated bipolar cells, amacrine cells and ganglion cells. A similar pattern persisted at PN8 in control retinas, except very few cells were AGB-IR in the ONL. By PN10, no AGB-IR cells were seen in the ONL and the intensity of AGB label in the IS, plexiform layers and INL and GCL increased.

In GLE retinas, the developmental pattern of KA-induced AGB-IR was different from controls at every age. At PN0, a cluster of AGB-IR cells was observed in the distal VZ, and unlike controls the horizontal cells, amacrine cells, and ganglion cells did not label as strongly for AGB. At PN2, GLE retinas exhibited more AGB-IR cells in the VZ. At PN4, both control and GLE retinas appeared relatively similar, although the inner retina in GLE retinas exhibited

more intense AGB-IR. At PN6, many of the newly differentiated bipolar cells observed in the INL control retinas were not present in GLE retinas. Unlike PN8 controls, GLE retinas had groups of lightly labeled AGB-IR clusters of cells in the ONL. By PN10, AGB-IR cells in the INL and GCL of GLE retinas labeled much more intensely that those in PN10 controls. Furthermore, the IS of PN10 GLE retinas were less developed than those of age-matched controls. In summary, these results reveal a delay in the functional development of the KA specific glutamatergic system in GLE retinas.

Figure 3.8 shows the developmental profile of AGB-IR in response to NMDA stimulation in control (Figures 3.8A-C and G-I) and GLE (Figures 3.8D-F and J-L) retinas. In control PN0 retinas, clusters of NMDA induced AGB-IR cells were in the VZ. By PN2 there was limited diffuse AGB label in the distal VZ. At PN4, AGB-IR in the VZ was associated only with horizontal cells and the developing OPL. The IPL, amacrine cells, and ganglion cells of control PN0, PN2, and PN4 all labeled with AGB after NMDA stimulation. At PN6, NMDA induced AGB labeling was strong in the developing IS, OPL, IPL, and GCL and light in the INL. By PN8 in control retinas, amacrine and ganglion cells were clearly defined by AGB-IR and this pattern intensified at PN10.

GLE PN0 retinas contained more AGB-IR clusters of cells in the distal VZ. Although control retinas did not have NMDA responsive cells in the distal VZ after PN0, GLE retinas continued to exhibit these cells at PN2, PN4, and to a lesser degree at PN6. As with KA and AMPA, the cells in the PN10 GLE retinas

that labeled with AGB in response to NMDA labeled more intensely than those of age-matched controls.

Figure 3.9 graphically summarizes the immunohistochemical data collected in the developmental profiles of AGB responses to glutamate, AMPA, KA, and NMDA in control and GLE retinas. To compare relative differences in the number of AGB-IR cells in the VZ (Figure 3.9A), ONL (Figure 3.9B), and the IPL and GCL (Figure 3.9C), two independent viewers scored and plotted the number of labeled cells on a relative scale of 0 – 4 (see METHODS). Relative changes in intensity within treatment groups are represented by grey/black and light blue/dark blue bar colors: lighter colors correspond to a less intense response. The graph shows that during development in control and GLE retinas, most of the AGB-IR occurred near the IPL. In the outer retina, the most AGB-IR occurred during the early postnatal ages (PN0, PN2, and PN4). Figure 3.9A shows that in the VZs of control retinas, the peak in the number of AGB-IR cells in response to all glutamate agonists occurred at PN2. With glutamate stimulation, approximately 75% of the cells in the distal VZ were AGB-IR. Both AMPA and KA stimulation resulted in approximately 50% of the distal VZ labeling with AGB-IR cells. This suggest that both AMPA and KA receptor types contribute to the overall glutamate signaling that occurred in the distal VZ of developing control retinas with some overlap. The peak intensity for AGB-IR in VZs of control retinas occurred at PN0 for glutamate, AMPA, and NMDA activation and at PN0-PN2 for KA stimulation.

Figure 3.8 Permeation of AGB after activation with 1 mM NMDA in control and GLE retinas. Control **(A-C; G-I)** and GLE **(D-F; J-L)** retinas from PN0, PN2, PN4, PN6, PN8 and PN10 mice were incubated in buffer containing 25 mM AGB plus 1 mM NMDA and processed as described in the Methods. **(A-C)** In control PN0 retinas, a cluster of moderate-to-high intensity AGB-IR cells were located in the distal VZ. At PN2 and PN4, there were no AGB-IR cells in the VZ. In control PN0, PN2 and PN4 retinas, there were very few low intensity AGB-IR ISs. The IPL and GCL exhibited a low-to-moderate intensity of AGB-IR on PN0 and PN2, and these increased to moderate-to-high intensity on PN4. **(D-F)** In GLE retinas from PN0 to PN4, there were an increasing number of moderate-to-high intensity clusters of AGB-IR cells in the distal VZ. The peak number and intensity of AGB-IR cells in the VZ was on PN4. Cells in the distal IPL and GCL exhibited a low intensity of AGB-IR at PN0 and PN2 and a moderate intensity of AGB-IR on PN4. **(G-I)** In PN6, PN8 and PN10 controls, there were no AGB-IR cells in the ONL, however, the ISs exhibited moderate-to-high intensity AGB-IR and apparent photoreceptor processes in the ONL. Intense AGB-IR HCs, BCs, ACs and GCs were present at all ages and by PN10 there were distinct intense AGB-IR OSs. **(J-L)** In PN6 GLE retinas, there was a cluster of moderately intense AGB-IR cells in the ONL, whereas in PN8 retinas there were just a few low intensity AGB-IR cells dispersed in the ONL and by PN10 there were none. At PN6, PN8 and PN10, there were low-to-moderate intensity AGB-IR localized to ISs, however, the OSs were not yet AGB-IR at PN10. At PN6 and PN8, there were low-to-moderate intensity AGB-IR apparent photoreceptor processes in the ONL and the OPL, INL, IPL and GCL exhibited low-to-moderate intensity AGB-IR. By PN10 there were distinct intense AGB-IR BCs and ACs. Scale bar = 40 µm.

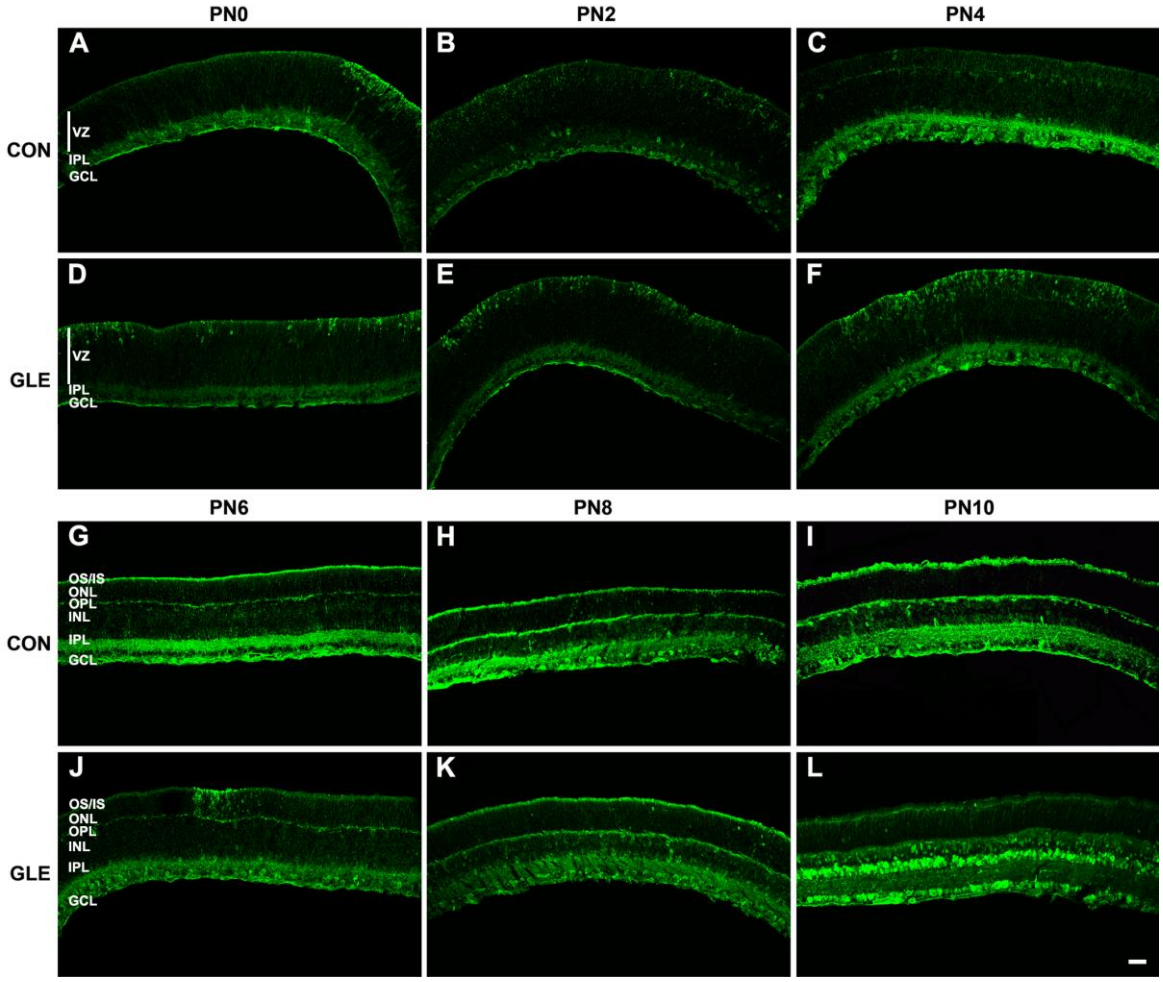
PN0
PN2
PN4
A
B
C
CON
VZ
IPL
GCL
D
E
F
GLE
VZ
IPL
GCL
PN6
PN8
PN10
G
H
I
CON
OS/IS
ONL
OPL
INL
IPL
GCL
J
K
L
GLE
OS/IS
ONL
OPL
INL
IPL
GCL

Figure 3.9. Quantitative summary of AGB permeation to glutamate receptor agonists during postnatal development in control and GLE retinas. The relative number and intensity of AGB-IR cells control and GLE retinas in response to glutamate (GLU), AMPA, KA and NMDA were analyzed, as described in the Methods, and plotted for the **(A)** VZ at PN0, PN2 and PN4, **(B)** ONL at PN6, PN8 and PN10 and **(C)** IPL and GCL at PN0, PN2, PN4, PN6, PN8 and PN10. The relative ranked number of AGB-IR cells is represented on a scale from 1 to 4. The color of each bar represents the relative intensity of AGB label for that age. Moderate-to-high intensity AGB-IR is plotted as black or dark blue bars in control and GLE retinas, respectively. Lower intensity AGB-IR is plotted as gray or light blue bars in control and GLE, respectively. The intensity comparisons were made within, but not between, treatment groups. In the developing VZ of control retinas, peak numbers of AGB-IR cells were consistently observed at PN2 for GLU, AMPA and KA, and at PN0 for NMDA. In GLE retinas, this peak was at PN2 for KA, but broadened to include PN2 and PN4 for GLU and NMDA and further broadened to include PN0, PN2 and PN4 for AMPA. In control retinas, the intensity of AGB-IR in the VZ decreased after the peak, whereas these decreases were not observed in GLE retinas. In the ONL of control retinas, the amount of AGB-IR peaked at PN6 and decreased to minimal levels at either PN8 or PN10. In the ONL of GLE retinas, the amount of AGB-IR peaked at PN6 and/or PN8 decreased to minimal levels at PN10. Moreover, in the ONL of GLE compared to age-matched controls, the number of AGB-IR cells was generally two-fold higher. The IPL and GCL of control and GLE retinas exhibited the highest amount and intensity of AGB-IR cells. The relative patterns were similar in control and GLE retinas for each agonist, although the initial increase in AGB-IR was delayed two to four days in GLE retinas. In summary, ionotropic activation of AGB permeation in developing control and GLE retinas VZ and ONL follows a coordinated spatiotemporal pattern that is agonist and age selective. Relative to age-matched controls, GLE retinas have an increased number and prolonged duration of AGB-IR cells in the VZ and ONL. This is consistent with the increased number of rods and bipolar cells in the GLE retinas (Giddabasappa et al. 2011).

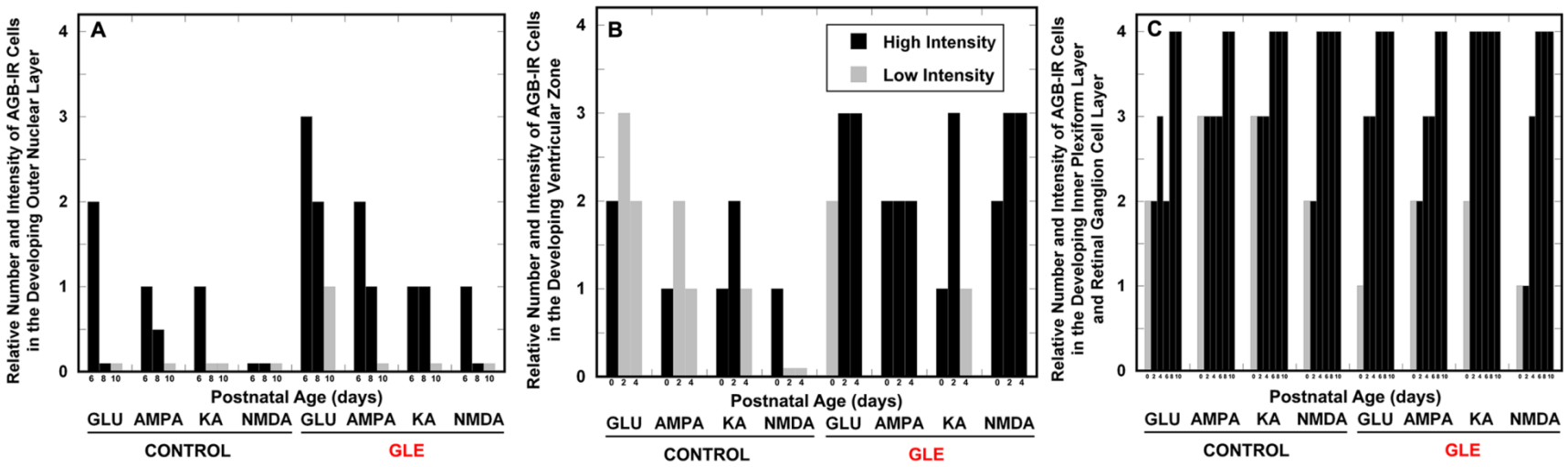
A
Relative Number and Intensity of AGB-IR Cells in the Developing Outer Nuclear Layer
Postnatal Age (days)
GLU AMPA KA NMDA GLU AMPA KA NMDA
CONTROL
GLE
B
High Intensity
Low Intensity
Relative Number and Intensity of AGB-IR Cells in the Developing Ventricular Zone
Postnatal Age (days)
GLU AMPA KA NMDA GLU AMPA KA NMDA
CONTROL
GLE
C
Relative Number and Intensity of AGB-IR Cells in the Developing Inner Plexiform Layer and Retinal Ganglion Cell Layer
Postnatal Age (days)
GLU AMPA KA NMDA GLU AMPA KA NMDA
CONTROL
GLE

In GLE retinas, KA was the only glutamate agonist that stimulated a peak number of AGB-IR cells at PN2. However, the number of AGB-IR cells at this age with KA stimulation was 50% more than that of age-matched controls. In GLE retinas, glutamate stimulation resulted in the highest number of AGB-IR cells in the VZ (approximately 75% of the cells) at PN4 and this peak continued with visible appearance of the ONL (Figure 3.9B). Likewise, the peak number of cells stimulated with AMPA in the VZs of GLE retinas (50% of cells in the VZ) was extended from PN2 to include PN0, PN4, and PN6 (Figure 3.9B). In control retinas, maturation of the ONL resulted in a decrease in the number of cells were AGB-IR (Figure 3.9B). The final age in which AGB-IR cells were detected in the ONL of control retinas was PN6 with glutamate stimulation and PN8 with AMPA and KA stimulation. NMDA no longer resulted in AGB entry into cells of the outer retina after PN2 (Figure 3.9A). In GLE retinas that were stimulated with glutamate, this endpoint was delayed such that a few lightly labeled cells were observed at PN10. The end for ONL stimulation was PN8 in GLE retinas for both AMPA and KA, similar to age-matched controls. NMDA stimulation resulted in AGB-IR cells in the ONLs of GLE retinas until PN6, long after the endpoint observed in control retinas.

The profile of AGB-IR after glutamate receptor agonist stimulation of the inner retina was similar in control and GLE retinas (Figure 3.9C). The initial peak of AGB-IR in the IPLs of control retinas occurred at PN8 with glutamate and APMA stimulation, PN0 with KA stimulation, and PN4 with NMDA stimulation. In

IPLs of GLE retinas, the peak of response was similar for glutamate but delayed to PN4 with AMPA, PN2 with KA, and PN6 with NMDA. Together this data shows that the glutamate response profile of GLE retinas differs from that of controls. GLE delayed peak response of the VZs of developing retinas to glutamate. Furthermore, the time frame in which glutamate elicited a maximum response in the VZs of GLE retinas increased when compared to controls.

3.3.3 Gene expression of AMPA, KA, and NMDA receptor subunits in developing control and GLE retinas

One possible reason for the changes in AGB-IR profiles of GLE mice in response to glutamate agonist is alterations in overall gene expression for the AMPA, KA, and/or NMDA receptor subunits. Therefore, I conducted RT-qPCR for: 1) the AMPA receptor subunits *AMPA1*, *AMPA2*, *AMPA3*, and *AMPA4* (Figure 3.10), 2) the KA subunits *KA1*, *KA2*, *GluR5*, *GluR6*, and *GluR7* (Figure 3.11), and 3) the NMDA subunits *NMDA1*, *NMDA2a*, and *NMDA2b* (Figure 3.12). The RT-qPCR results are presented as relative gene expression versus the ages E18.5, PN2, PN4, PN6, and PN10 in control and GLE retinas.

All AMPA receptor subunits showed an increasing trend in control and GLE retinas throughout development (Figure 3.10A-D, but only *AMPA2* showed a significant difference in expression at E18.5 and PN2 where GLE was lower than age-matched controls.

GluR5 expression showed the greatest increase over time for control and GLE retinas compared to the other KA receptor subunits (Figure 3.11A). The *GluR5* gene expression in GLE retinas was similar to controls at all ages. The *GluR6* and *GluR7* expression data was combined and showed no changes between control and GLE retinas (Figure 3.11B).

In control retinas, *KA1* receptor expression is similar at E18.5, PN2, and PN4 and then decreases to similar levels at PN6 and PN10; however, the total change in relative expression is less than one unit (Figure 3.11C and E). In GLE retinas, compared to controls, *KA1* expression was significantly decreased at PN2 and PN4, after which expression significantly increased at PN10. The relative gene expression of *KA2* in control retinas was relatively constant during development and did not change more than one unit in expression (Figure 3.11D and E). In GLE retinas, KA2 expression was significantly increased at PN10 relative to age-matched controls.

There are at least seven known NMDA receptor subunits (NMDA1, NMDA2a-NMDA2d, NMDA3a and NMDA3b) (Kew, 2005). *In situ* and protein data show that NMDA1 and NMDA2A-NMDA2D all are expressed in the developing rodent retina (Watanabe et al., 1994; Gründer et al., 2000). Since native NMDA receptors must contain NMDA1 in combination with one of or both NMDA2a and NMDA2b (Kew, 2005), the gene expression of these three subunits was analyzed. Figures 3.12A–C show that all three NMDA receptors increased

their expression slightly during development. At PN10, *NMDA1* and *NMDA2a* gene expression significantly increased in GLE retinas

The RT-qPCR data support the AGB-IR profiles at PN10 since the relative gene expressions of *KA1*, *KA2*, *NMDA1*, and *NMDA2a* and the KA and NMDA-induced AGB-IRs were increased at this age in GLE retinas. The RT-qPCR data for AMPA2, KA1, and NMDA2b, though, show decreases in relative expression during early developmental ages while the AGB-IR profiles show both increased number and intensity for these agonist during early retinal development in the VZ. It is likely that the decreases in gene expression of AMPA2, KA1, and NMDA2b during early retinal development reflects the decreases in IPL AGB labeling at these ages (Figure 3.9C) since: 1) the RT-qPCR data is representative of whole retina homogenate and 2) the AGB-IR cell clusters observed in the VZs of developing retinas only represent a small percentage of the total AGB-IR in the developing retina. Therefore, spatiotemporal resolution using RT-qPCR is rather poor and changes in the AGB-IR of the developing inner retina are consistent with the changes in relative gene expression while those in the developing VZ are not.

Figure 3.10. GLE selectively altered the relative gene expression of the glutamate receptor subunit *Ampa2 (Gria2)* during retinal development. RT-qPCR determined the relative gene expression of **(A)** *Ampa1 (Gria1),* **(B)** *Ampa2 (Gria2),* **(C)** *Ampa3 (Gria3) and* **(D)** *Ampa4 (Gria4)* in embryonic 18.5 (E18.5), PN2, PN4, PN6 and PN10 control and GLE retinas. All four subunits, which are plotted on the same relative axis for ease of comparison, increased relative expression from E18.5 to PN10. At E18.5 and PN2, the expression of *Ampa2* was significantly decreased in GLE retinas relative to age-matched controls. All values represent ΔCT ± SEM. Mean ± SEM values represent triplicate samples from four to five animals per treatment group per age. For each graph, values with an asterisk indicate $p<0.05$ compared to controls.

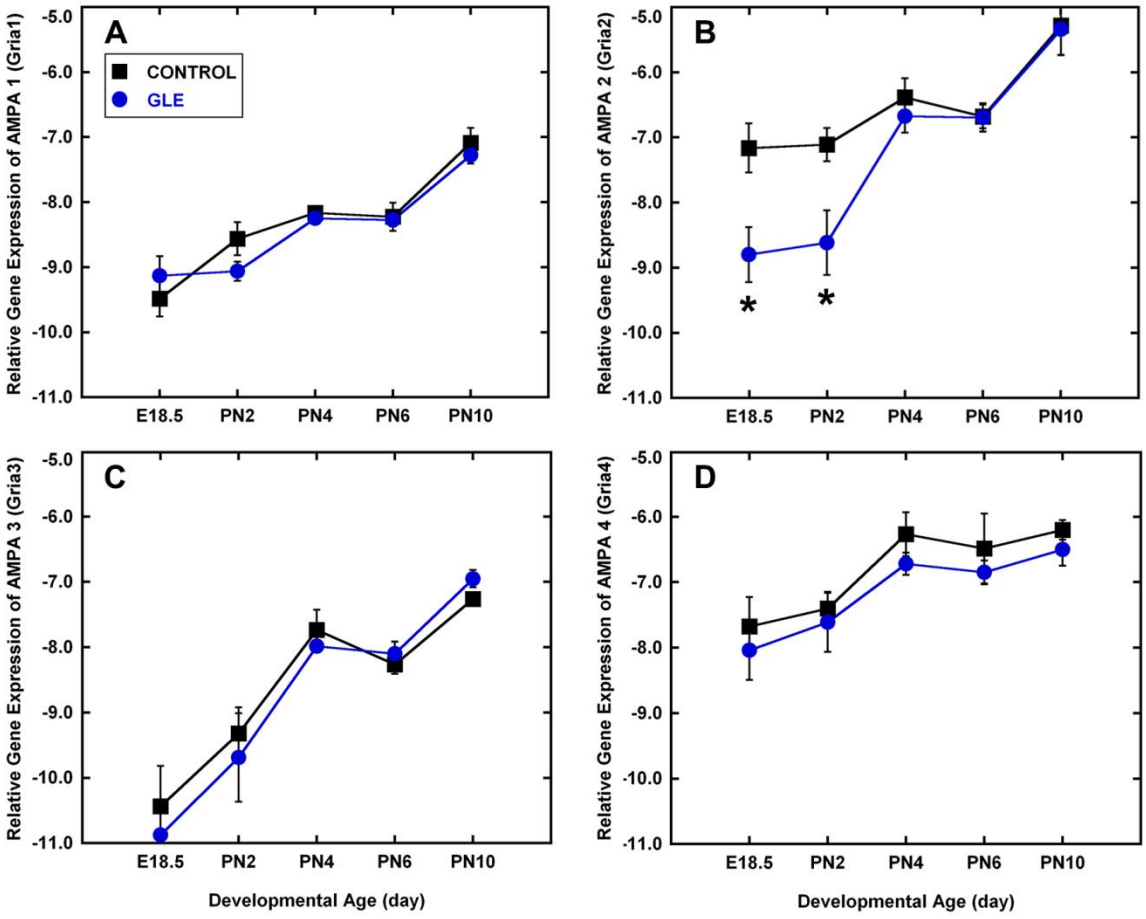

Figure 3.11. GLE selectively altered the relative gene expression of the glutamate receptor subunit *KA1 (Grik4)* and *KA2 (Grik5)* during retinal development. RT-qPCR determined the relative gene expression of **(A)** *Glur5 (Grik1),* **(B)** *Glur6+7 (Grik2+3)* **(C)** *KA1 (Grik4) and* **(D)** *KA2 (Grik5)* in embryonic 18.5 (E18.5), PN2, PN4, PN6 and PN10 control and GLE retinas. All four subunits are plotted on the same relative axis for ease of comparison **(A, B and E)**. From E18.5 to PN10, *GluR5, GluR6*+7 and KA2 increased relative expression in controls and GLE, whereas KA1 expression decreased in controls and increased in GLE. The expression of *KA1* significantly decreased in GLE retinas at PN2 and PN4, and increased in GLE retinas at PN10 relative to age-matched controls. The expression of *KA2* significantly increased in GLE retinas at PN10 relative to age-matched controls. All values represent ΔCT ± SEM. Mean ± SEM values represent triplicate samples from four to five animals per treatment group per age. For each graph, values with an asterisk indicate $p<0.05$ compared to controls

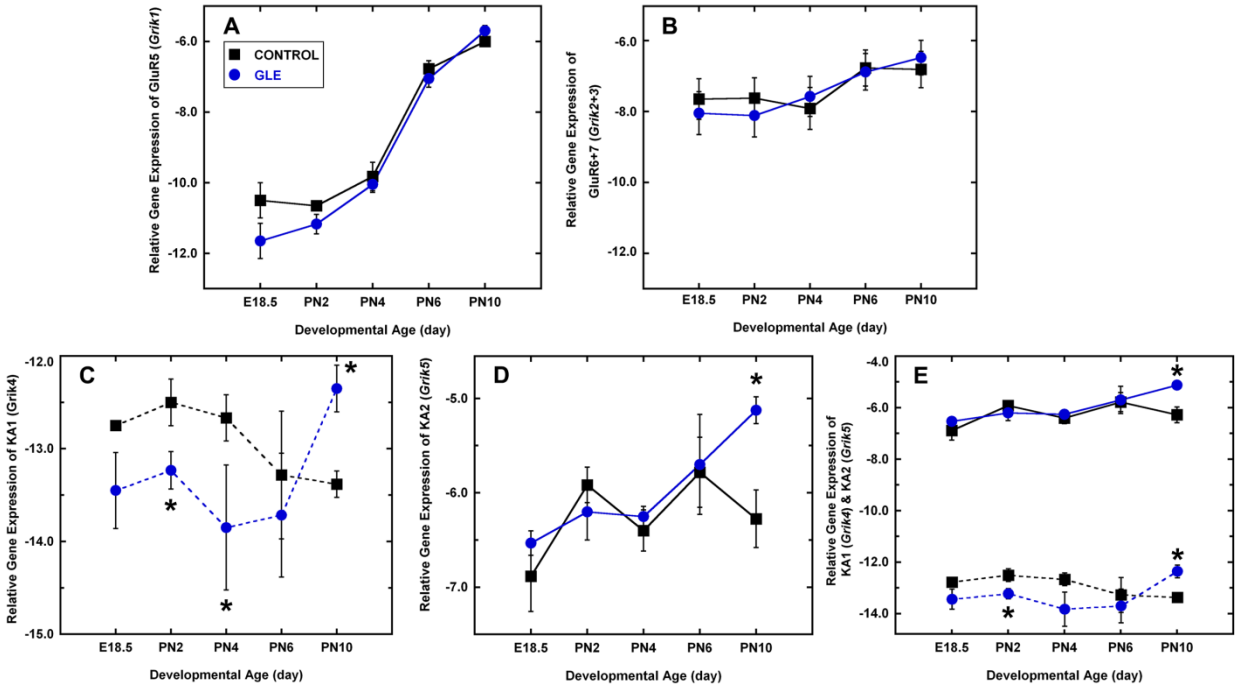
A
CONTROL
GLE
Relative Gene Expression of GluR5 (Grik1)
-6.0
-8.0
-10.0
-12.0
E18.5
PN2
PN4
PN6
PN10
Developmental Age (day)
B
Relative Gene Expression of GluR6+7 (Grik2+3)
-6.0
-8.0
-10.0
-12.0
E18.5
PN2
PN4
PN6
PN10
Developmental Age (day)
C
Relative Gene Expression of KA1 (Grik4)
-12.0
-13.0
-14.0
-15.0
*
*
*
E18.5
PN2
PN4
PN6
PN10
Developmental Age (day)
D
Relative Gene Expression of KA2 (Grik5)
-5.0
-6.0
-7.0
*
E18.5
PN2
PN4
PN6
PN10
Developmental Age (day)
E
Relative Gene Expression of KA1 (Grik4) & KA2 (Grik5)
-4.0
-6.0
-8.0
-10.0
-12.0
-14.0
*
*
*
E18.5
PN2
PN4
PN6
PN10
Developmental Age (day)

Figure 3.12 GLE increased the relative gene expression of the *NMDA1 (Grin1)* and *NMDA2a (Grin2a)* glutamate receptor subunits during retinal development. RT-qPCR determined the relative gene expression of **(A)** *NMDA1 (Grin1),* **(B)** *NMDA2a (Grin2a)* and **(C)** *NMDA2b (Grin2b)* in embryonic 18.5 (E18.5), PN2, PN4, PN6 and PN10 control and GLE retinas. All three subunits, which are plotted on the same relative axis for ease of comparison, increased relative expression from E18.5 to PN10. At PN10, the expression of NMDA1 and NMDA2a increased significantly in GLE retinas relative to age-matched controls. All values represent ΔCT ± SEM. Mean ± SEM values represent triplicate samples from four to five animals per treatment group per age.

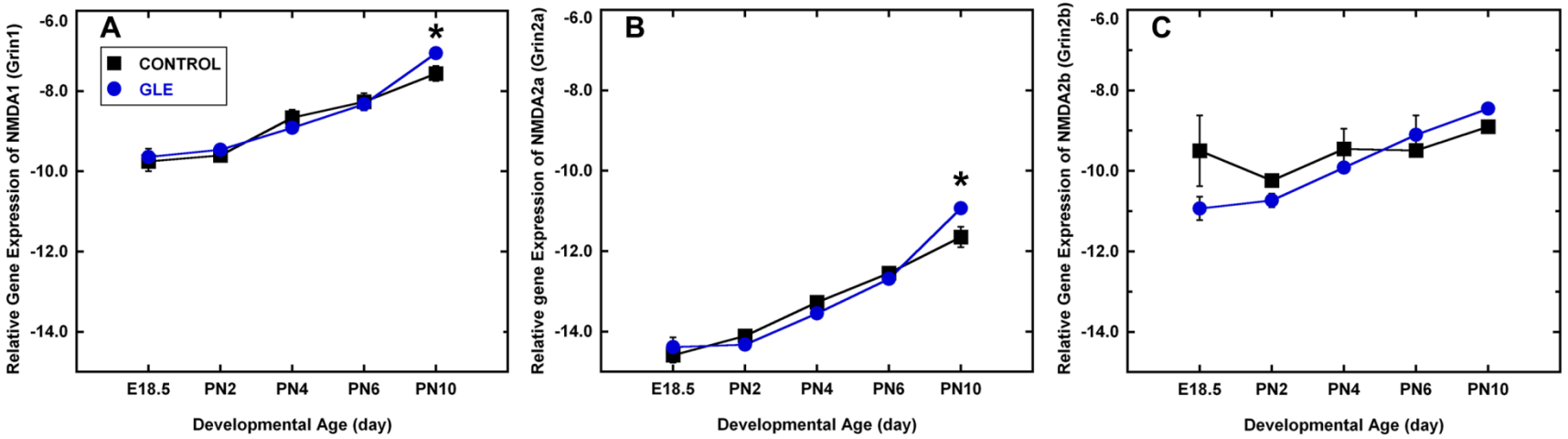

3.3.4 Identification of AGB-IR cells as rod photoreceptor and bipolar cell precursors

Other groups reported glutamate responsive cells in the developing outer retina (Acosta et al., 2007; Chang and Chiao, 2008), but the identity of the cells was not determined. Therefore, these glutamate responsive cells in control retinas were identified at PN2 using immunohistochemistry with AGB, well-characterized antibodies for proliferative cells, and the transgenic NRL (neural retina-specific leucine zipper)-GFP mouse. During the early stages of postnatal retinal development, a significant percentage of retinal cells are mitotic and the majority of retinal cells (i.e. rod photoreceptors and bipolar cells) are born (Young, 1985a, 1985b; Alexiades and Cepko, 1996; Rapaport et al., 2004). Hence, we first used antibodies against proliferating cell nuclear antigen (PCNA) and mini-chromosome maintenance 6 (MCM6) in KA stimulated PN2 retinas to determine whether AGB-IR cells in the VZ were proliferative or postmitotic. Both PCNA and MCM6 label RPCs, however, PCNA protein levels decrease quickly when RPCs exit cell cycle whereas MCM6 levels persist so that newly postmitotic cells are also MCM6-IR (Barton and Levine, 2008). Figures 3.13A-F show low and high magnification images of two independent AGB and PNCA double label experiments. Figures 3.13A and 3.13D show AGB-IR cells in the distal VZ and surrounding the IPL. Figure 3.13B and 3.13E show PCNA-IR cells throughout the VZ with a higher density of PCNA-IR cells in the proximal VZ. The overlay of

these markers showed that AGB-IR cells were not PCNA-IR (Figures 3.13C andF). Figures 3.13G-I show the single and double label images for AGB and MCM6. A characteristic cluster of AGB-IR reactive cells is observed in the distal VZ (Figure 3.13G). MCM6-IR cells span the VZ with many labeling in the distal VZ (Figure 3.13H). The overlay image (Figure 3.13I) shows that many of the AGB-IR cells in the cluster are also MCM6-IR. Taken together, these novel experiments show that the AGB-IR cells are newly postmitotic RPCs.

To determine whether these newly post mitotic AGB-IR cells would become rod photoreceptors and/or bipolar cells, two different experiments were designed. OTX2 is a homeobox transcription factor that labels neuronal precursors and differentiated rod photoreceptors and bipolar cells (Bass et al., 2000; Nishida et al., 2003; Das et al., 2009). Figure 3.14 shows KA stimulated PN2 control retinas labeled with antibodies against the AGB molecule and OTX2. Figures 3.14A and D show a cluster of AGB-IR cell in the distal VZ as described previously. Figure 3.14B and E reveal that OTX2 labeled cells throughout the VZ. An overlay of the images shows that many of the AGB-IR cells in the distal VZ are also OTX2-IR (Figure 3.14C and F) indicating that the newly postmitotic cells will become rod photoreceptors or bipolar cells.

To determine if the cells specifically became rods, NRL-GFP transgenic mice were used. NRL, a leucine zipper transcription factor, is one of the earliest rod-specific genes expressed in the retina (Akimoto et al., 2006). The NRL-GFP mouse expresses the green florescent protein behind the NRL promoter as early as E12 whereas rhodopsin expression does not begin until PN2 (Akimoto et al.,

2006; also see CHAPTER 2). Figure 3.15 shows two independent images of PN2 NRL retinas that were incubated in the presence of AGB and KA (Figures 3.15A and D). NRL-GFP was highly expressed in rod precursors in the most distal region of the VZ and weakly expressed in rod precursors in the deep VZ (Figure 3.15B and E). The KA-induced AGB-IR in the NRL-GFP mouse was very similar to that observed in other control retinas (Figures 3.2G and 3.7B). The overlays of the two labels (Figure 3.15C and F) show that many, but not all, of the AGB-IR cells were also GFP positive. These novel results, in conjunction with the OTX2 experiments indicate that AGB-IR cells are neural precursors, of both rod photoreceptors and bipolar cells during early postnatal ages.

Figure 3.13. AGB-IR cells are MCM6-IR, but not PCNA-IR. Retinas from PN2 control mice were incubated with AGB in the presence of 60 µM KA and single- or double-labeled with antibodies against the AGB molecule, and PCNA or MCM6. These two different cell cycle markers were chosen because MCM6-IR persists in retinal progenitor cells after the cell cycle compared to PCNA (Barton and Levine 2008). Low **(A-C)** and high **(D-I)** magnification images are presented. **(A, D and G)** The permeation of AGB with KA produced clusters of AGB-IR cells in the distal VZ, and labeled the amacrine cells, IPL and GCL. **(B and E)** PCNA labeled cells in the central and inner region of the VZ. **(C and F)** AGB and PCNA did not co-label. **(H)** MCM6-IR cells were located throughout the VZ and **(I)** most AGB-IR cells in the distal VZ co-labeled for MCM6. Scale bars = 40 µm.

A
AGB + KA
VZ
IPL
GCL
B
PCNA
C
AGB + KA & PCNA
D
AGB + KA
VZ
IPL
GCL
E
PCNA
F
AGB + KA & PCNA
G
AGB + KA
VZ
IPL
GCL
H
MCM6
I
AGB + KA & MCM6

Figure 3.14. AGB-IR cells in the distal VZ co-label with the rod and bipolar cell transcription factor OTX2. Retinas from PN2 control mice were incubated with AGB in the presence of 60 µM KA and single- or double-labeled with antibodies against the AGB molecule and OTX2. Low **(A-C)** and high **(D-F)** magnification images are presented. **(A and D)** The permeation of AGB with KA produced clusters of AGB-IR cells in the distal VZ. **(B and E)** OTX2 labeled retinal progenitor cells throughout the VZ. **(C and F)** OTX2 co-labeled almost all of the AGB-IR cells in the VZ. **(A-C)** Scale bar = 40 µm. **(D-F)** Scale bar = 50 µm.

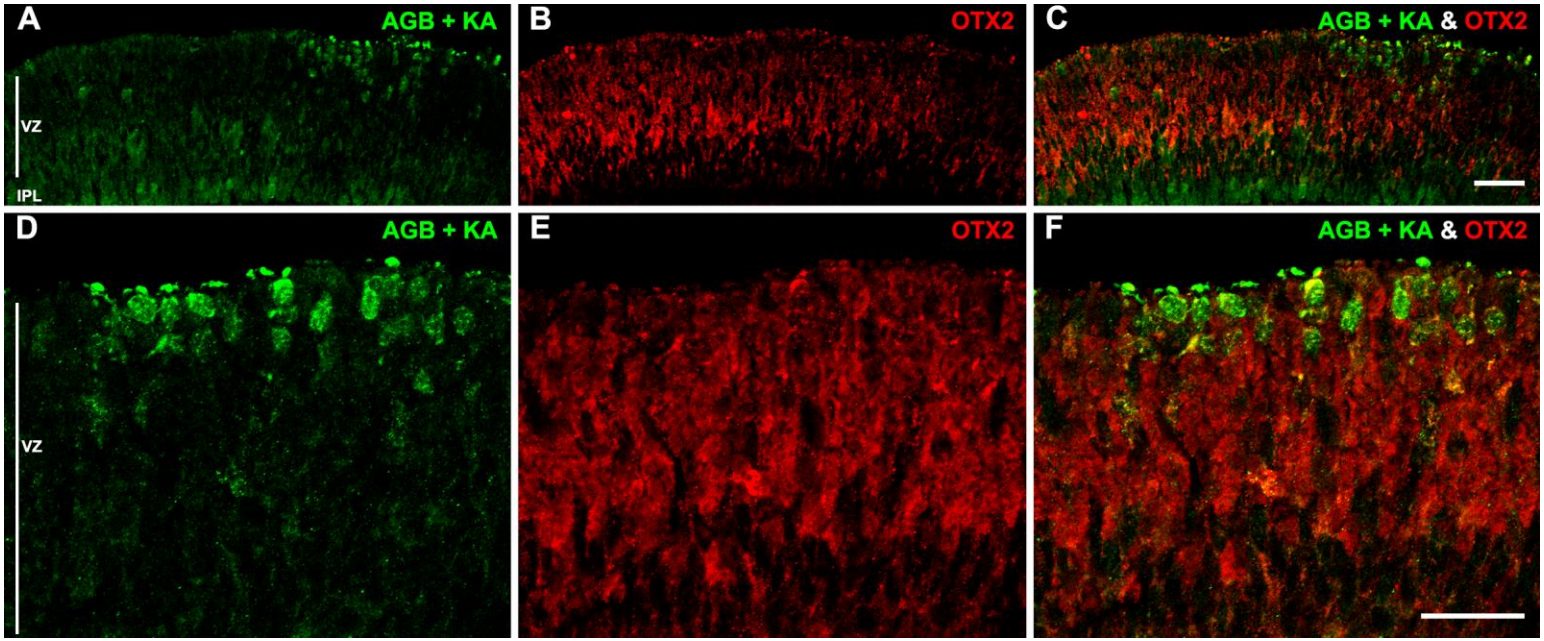

Figure 3.15. AGB-IR cells in the distal VZ co-label with the rod-specific transcription factor NRL. Retinas from PN2 NRL-GFP transgenic mice were incubated with AGB in the presence of 60 µM KA and single- or double-labeled with antibodies against the AGB molecule and GFP. In the NRL-GFP mouse, GFP is expressed in all differentiated and newly differentiated rod photoreceptors (Akimoto et al. 2006). Low **(A-C)** and high **(D-F)** magnification images are presented. **(A and D)** The permeation of AGB with KA produced clusters of AGB-IR cells in the distal VZ. **(B and E)** NRL-GFP labeled rod precursor and newly differentiated rods cells throughout the VZ as well as rod ISs. **(C and F)** AGB co-labeled a significant proportion the NRL-GFP cells in the VZ. Scale bars = 40 µm.

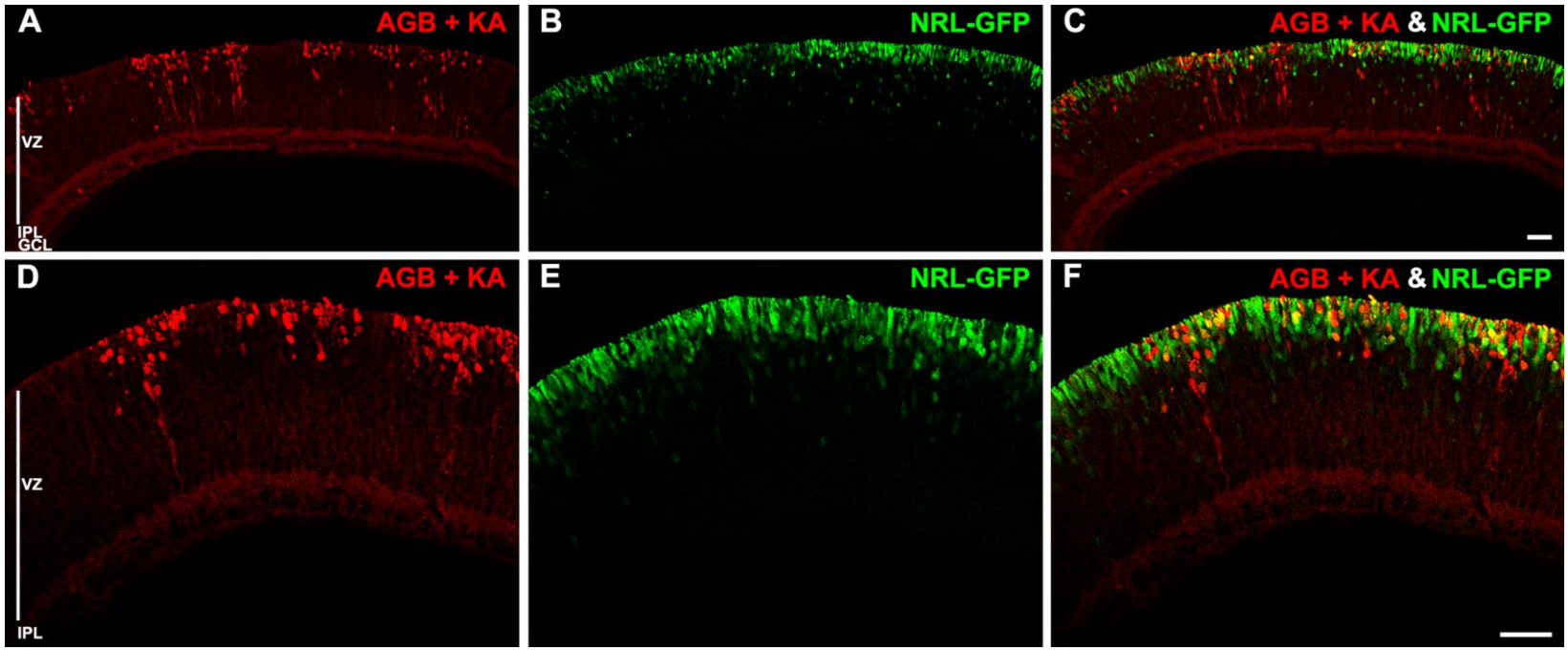

3.3.5. Pharmacological experiments to determine role of inner retinal contribution to AGB-IR in the VZ

In developing rabbits, spontaneous rhythmic calcium waves initiated by ganglion cells in the inner retina elicit similar propagating calcium waves in the VZ (Syed et al., 2004). Furthermore, the addition of the nicotinic agonist DMPP initiated calcium waves in the inner retina, whereas calcium waves in the VZ were sensitive to muscarinic agonists. Since the inner retina is specifically and independently stimulated by DMPP, I examined whether stimulation of the inner retina with a non-glutamate agonist would result in AGB-IR in the outer retina. Figure 3.16A-H shows the results from these experiments. PN2 control retinas were isolated and incubated in with (A) AGB only, (B) AGB and 1 mM ATP, (C) AGB and 50 mM KCL, (E) AGB and KA, (F) AGB, KA, and 50 µM hexamethomium (HM), (G) AGB and KA, and (H) AGB, KA and 100 µM 6,7-dinitroquinoxaline-2,3-dione (DNQX). Incubation of PN2 control retinas in the presence of AGB and the P2X agonist ATP resulted in a few clumps of brightly lit AGB-IR cells in the distal VZ. AGB and a depolarization concentration of KCL resulted in a brightly labeled AGB-IR IPL, however, the rest of the retina was non-specifically labeled such that the overall AGB-IR was slightly higher than what seen in AGB only PN2 tissue. The nicotinic agonist DMPP elicited a large increase in AGB permeation in the VZ resulting in a large number of AGB-IR clusters and it also increased AGB permeation in the INL, IPL, and GCL. KA induced AGB-IR as previously described (Figures 3.2G and 3.7B). KA in the

presence of the nicotinic receptor antagonist HM, showed very few dimly labeled AGB-IR cells in the distal VZ and IPL. The AMPA/KA antagonist DNQX blocked the KA-induced AGB permeation in the VZ as decreased AGB-IR in the inner retina. Together, this data shows that AGB permeation: 1) in the outer retina can be activated by ATP, 2) in the inner and outer retina is specific and cannot be achieved by global depolarization with KCl, 3) in the outer retina can be activated by a nicotinic agonist, and 4) induced by KA in the outer and inner retina can be blocked by a nicotinic antagonist and an AMPA/KA antagonist.

Figure 3.16. AGB entry is mediated by multiple mechanisms in PN2 control retinas. PN2 control retinas were incubated with AGB in the presence of **(A)** no agonist, **(B)** 1 mM ATP, **(C)** 50 mM KCl, **(D)** 50 µM 1,1-dimethyl-4-phenylpiperazinium (DMPP), **(E and G)** 60 µM KA, **(F)** 60 µM KA with 50 µM hexamethonium (HM), or **(H)** 60 µM KA with 100 µM 6,7-dinitroquinoxaline-2,3-dione (DNQX) and labeled with an antibody against the AGB molecule. **(A)** Basal permeation of AGB was minimal. Only a few cells in the most distal retina above the VZ, which are ISs, exhibited AGB-IR. **(B)** Activation with ATP increased AGB permeation in ISs, clusters of cells in the distal VZ, and in the IPL and GCL. **(C)** Incubation with KCl elicited a strong and specific AGB response in the ISs, IPL and GCL as well as a strong non-specific response throughout the rest of the retina. Noticeably, however, KCl did not increase AGB permeation into any neuronal precursor cells in the VZ. **(D)** Stimulation with the nicotinic agonist DMPP markedly increased AGB permeation in the VZ resulting in a large number of AGB-IR clusters. DMPP also increased AGB permeation into ACs in the distal INL, IPL and the GCL. **(E)** KA activation produced clusters of AGB-IR cells in the distal VZ, and in the IPL and GCL. **(F)** Pre-incubation with the nicotinic antagonist HM blocked most of the KA-induced AGB permeation in the VZ, IPL and GCL. **(A-F)** Scale bar = 20 µm. **(G)** Higher magnification image shows that KA activation produced clusters of AGB-IR cells in the distal VZ, and in the amacrine cells in IPL as well as all cells in the GCL. **(H)** Pre-incubation with the AMPA/KA antagonist DNQX blocked most of the KA-induced AGB permeation in the VZ, IPL and GCL. **(G-H)** Scale bar = 20 µm.

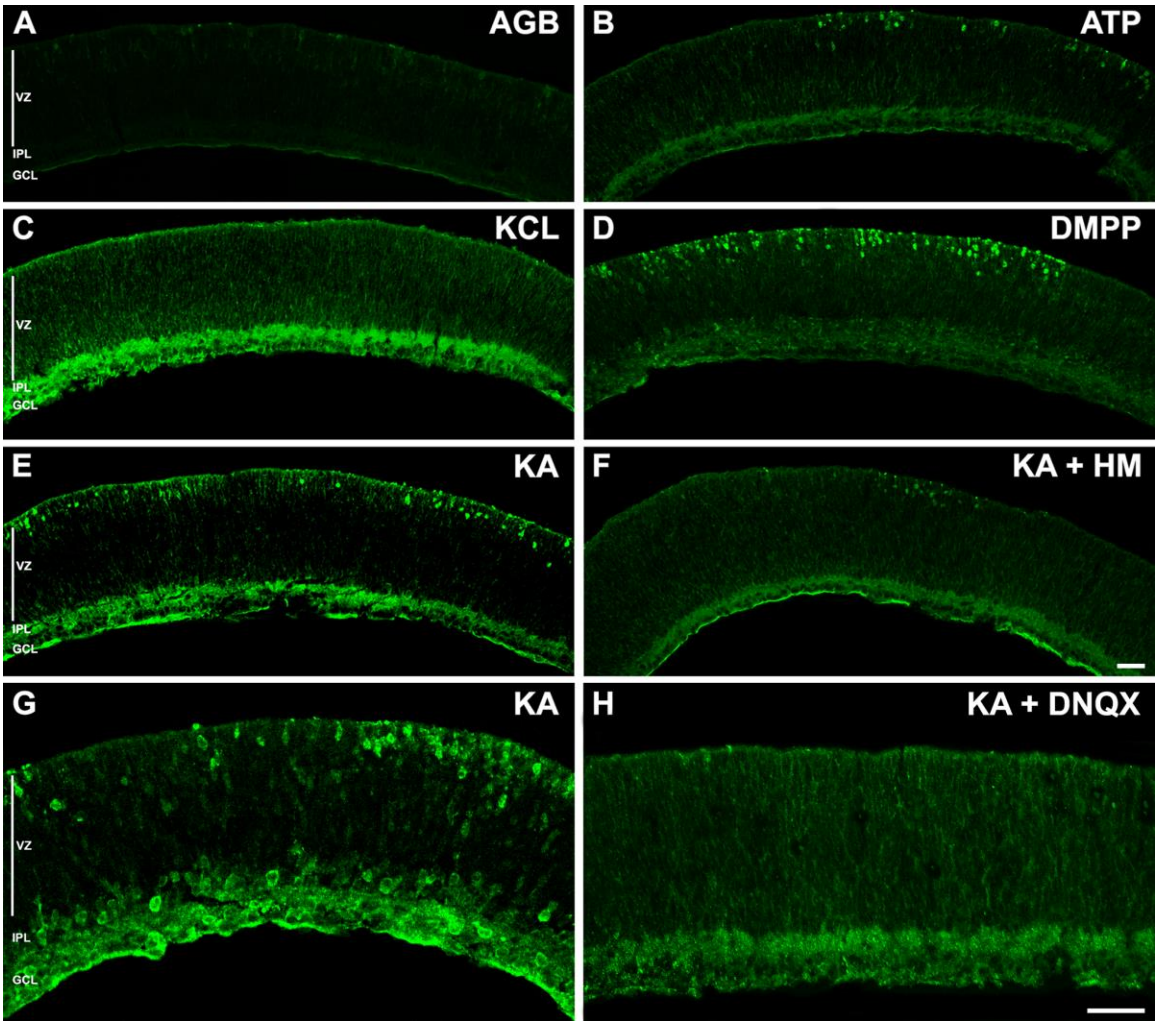
A
AGB
VZ
IPL
GCL
B
ATP
C
KCL
VZ
IPL
GCL
D
DMPP
E
KA
VZ
IPL
GCL
F
KA + HM
G
KA
VZ
IPL
GCL
H
KA + DNQX

3.3.6. *In vitro* lead exposure decreased AMPA and KA-induced AGB-IR

In GLE retinas, there is increased and prolonged RPC proliferation that results in a dose-dependent increase in rod photoreceptors and bipolar cells (Giddabasappa et al., 2011). We originally hypothesized that inorganic lead (Pb) inhibited the activation of glutamate receptors on RPCs in GLE retinas and delayed cell cycle exit in these cells thus enabling an extra round of cell cycle. Our *ex vivo* results with developing control and GLE retinas incubated in the presence of glutamate agonists and AGB, summarized in Figure 3.9, suggest that GLE retinas have increased sensitivity to glutamate agonists. Therefore, to determine the direct effect of lead, PN2 control retinas were incubated with Pb and two different glutamate agonists and the AGB-IR was examined. Figure 3.17 shows AGB-IR results for PN2 control retinas incubated with (A and E) AGB only, (B) AGB and 30 µM AMPA, (C) AGB, AMPA and 0.5 µM $PbCl_2$, (D) AGB, AMPA and 2 µM $PbCl_2$, (F) AGB and 60 µM KA, and (G) AGB, KA, and 0.5 µM $PbCl_2$, and (H) AGB, KA, and 2 µM $PbCl_2$. AMPA and KA both increased AGB-IR above basal levels in the distal VZ and IPL: consistent with earlier results (Figures 3.2E and G, 3.6B and 3.7B). Both concentrations of lead decreased most of the AMPA-induced AGB-IR in the VZ; however, AGB-IR in the IPL and GCL were slightly increased. Both concentration of lead decreased KA-induced AGB-IR in the VZ; however, AGB-IR in the IPL and GCL was slightly increased. These results in the VZ of the outer retina are opposite to those from GLE retinas

incubated with AMPA and KA. In contrast, it appears that lead activated AGB permeation in the inner retina, as discussed below.

Figure 3.17. Acute inorganic lead (Pb) exposure decreased and altered APMA-and KA-induced AGB permeation in PN2 control retinas. PN2 control retinas were incubated with AGB in the presence of **(A, E)** no agonist, **(B)** 30 µM AMPA, **(C)** 30 µM AMPA + 0.5 µM $PbCl_2$, **(D)** 30 µM AMPA + 2 µM $PbCl_2$, **(F)** 60 µM KA, **(G)** 60 µM KA + 0.5 µM $PbCl_2$ or **(F)** 60 µM KA + 2 µM $PbCl_2$ and labeled with an antibody against the AGB molecule. **(A, E)** Basal permeation of AGB was minimal. Only a few cells in the most distal retina above the VZ, which are ISs, exhibited AGB-IR. **(B)** Activation with AMPA increased AGB permeation in ISs, clusters of cells in the distal VZ, and in the IPL and GCL. **(C)** Incubation with 0.5 µM Pb or **(D)** 2 µM Pb blocked most of the AMPA-induced AGB permeation in the VZ, however, AGB permeation in the IPL and GCL slightly increased. **(F)** Activation with KA increased AGB permeation in ISs, clusters of cells in the distal VZ, ACs, and in the IPL and GCL. **(G)** Incubation with 0.5 µM Pb or **(H)** 2 µM Pb decreased KA-induced AGB permeation in the VZ, however, AGB permeation in the IPL and GCL slightly increased. Scale bar = 40 µm.

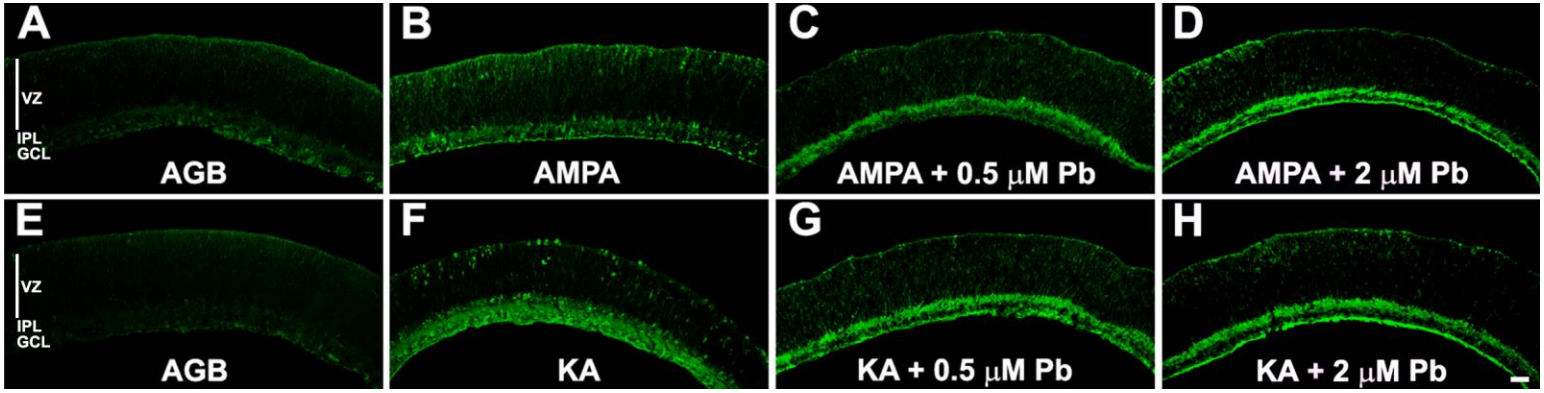

3.4 Discussion

The overall goals of this study were to determine the spatiotemporal immunocytochemical, functional, and molecular development of outer and inner retinal ionotropic glutamate receptors (iGluRs) in developing control and GLE mice during the stages of cell proliferation and late born neuronal differentiation. There were six major findings. First, I minimized artifacts and increased sensitivity for the functional mapping of AGB activation by developing new technical protocols for the whole isolated developing retinas incubated with glutamate, iGluR glutamate agonists, and other pharmacological agents. With these procedures, I characterized subsets of ionotropic glutamate responsive cells located in the distal VZ, ONL and inner retina (i.e., IPL and GCL) of PN0-PN10 retinas. Pharmacological experiments revealed that cells in these layers exhibited differentially sensitive agonist and age-dependent responses. Second, confocal experiments with two different RPC proliferation markers revealed that the glutamate receptor-activated AGB-IR cells were not proliferative RPCs, but rather postmitotic RPCs that differentiate into rods and/or bipolar cells. Third, using a model of GLE where there is an increased number and prolonged period of RPC proliferation that differentiate into an increased number of rods and BCs (Giddabasappa et al., 2011), we showed that the functional activation of iGluRs was increased and prolonged in the VZ and ONL compared to age-matched controls. Fourth, pharmacological experiments revealed that the AGB-IR cells in the VZ could be activated directly via various ligand-gated channels and indirectly by glutamate and acetylcholine released from the inner retina. Fifth,

RT-qPCR studies determined the relative gene expression of AMPA, KA and NMDA subunits during normal development and showed that GLE produced age- and subunit-dependent alterations. Sixth, and in contrast to the *in vivo* results, *in vitro* lead exposure decreased AMPA- and KA-induced AGB permeation in PN2 retina. Together, these findings in developing control mice provide new evidence that ligand-gated ion channel activation by glutamate, ATP and a cholinergic nicotinic analog in the developing retina plays an important role in differentiation of rods and bipolar cells in control retinas and that low level GLE prolongs and increases the activation period.

High levels of extracellular glutamate are present in the developing mammalian retina prior to the formation of phenotypic Müller glia cells (Redburn et al., 1992; Pow et al., 1994; Haberecht and Redburn, 1996; Fletcher and Kalloniatis, 1997). Although the sources of glutamate are unknown, a combination of RPCs, postmitotic cells, differentiated neurons, and the retinal pigment epithelium likely provide this glutamate (Haberecht and Redburn, 1996; Fletcher and Kalloniatis, 1997; Pearson et al., 2005). We introduced several procedural changes to the classical AGB functional mapping experiments (Marc, 1999; Acosta et al., 2007; Chang and Chiao, 2008). First, to lower background AGB-IR due to extracellular glutamate and glutamate released during/following dissection and thereby increase the sensitivity of the iGluRs, all dissected retinas from decapitated mice were free-floated in 10 ml of a glucose containing physiological buffer in a 25 ml Erlenmeyer flask for 5 min (37^0C in covered

shaking water bath) prior to any experimental studies. Second, to minimize cellular damage and artifacts all experiments were conducted at atmospheric oxygen levels (21%) since our preliminary results showed increased excitotoxic-induced retinal damage and cell death when the retinas were incubated with 95% O_2/5% CO_2. Third, a simplified glucose containing physiological buffer replaced the oxygenated Ames medium as previously described (Medrano and Fox, 1995; Shulman and Fox, 1996; He et al., 2000). Fourth, all experiments were performed with free-floating retinas incubated in 10 ml of glucose containing physiological buffer in the absence or presence of AGB with or without pharmacological agent for 5 min (37^{0}C in covered shaking water bath). Finally, after the retinas were placed in the Erlenmeyer flasks by plastic pipettes, all solution changes were made in these flasks with plastic pipettes until fixation was finished.

Wong (1995), using calcium imaging in isolated developing rabbit retina, first showed that approximately 50% of the cells in the VZ responded to glutamate, AMPA, and KA, although not NMDA. Furthermore, about 90% of the amacrine and ganglion cells in the developing rabbit retina increased their intracellular calcium concentration in response to glutamate, AMPA, and KA (Wong, 1995). Our results in the VZ and inner retina are consistent with these findings, but not with the two developmental AGB functional mapping studies (Acosta et al., 2007; Chang and Chiao, 2008). In control retinas, we found that glutamate, AMPA, KA, and NMDA produced agonist- and age-dependent

increases in the number and intensity of AGB-IR cells in the VZ that peaked at PN2, and in the IPL and GCL that peaked after PN6 (see Figure 3.9). The AGB-IR cells in the VZ of developing retinas mostly labeled as clone-like clusters of rod and bipolar cells, similar to those visualized in lineage tracing studies (Turner and Cepko, 1987; Turner et al., 1990). AMPA and KA produced larger numbers and more intense AGB-IR clusters in the VZ and more activation of horizontal cells in the OPL.

Previous AGB activation studies showed weak 20-30 μM AMPA-induced AGB-IR in the distal VZ and strong AGB-IR in the inner retina of developing mice (E18.5-PN6) and rabbit retina (E21-PN4), respectively (Acosta et al., 2007; Chang and Chiao, 2008). Stimulation with 50 μM KA, but not 1 mM NMDA produced similar results in the mouse (Acosta et al., 2007). The discrepancies with our results are likely due to different techniques for tissue dissection and incubation as well as data presentation. Both groups radially cut, flattened, mounted retinas to filter membranes, and then immediately incubated them in 95% 0_2/5% CO_2. We showed that any mechanical damage or trauma to the retina increases AGB permeation and that hyperoxia enhances excitotoxic injury (Fox, unpublished data). Furthermore, the retinal areas shown in the two AGB experiments were much smaller than those presented in the current study. Our AGB-IR cells generally labeled as patchy clusters throughout the VZ, rather than as a homogeneous population. Therefore, if only small retinal areas were

sampled or if possible areas of damage were avoided, they may have overlooked areas of genuine responsiveness.

Our second new finding was that the iGluR-activated AGB-IR cells in the distal VZ of PN2 retinas are newly postmitotic rod and/or bipolar cell precursors. Double-label confocal experiments with PCNA or MCM6 and AGB revealed that these cells were not proliferative RPCs, but rather early postmitotic RPCs. Furthermore, experiments with the OTX2 antibody and NRL-GFP mice established these cells were rod and/or bipolar cell precursors. These results are consistent with those of Maric et al. (2000) who found that functional iGluRs emerge during terminal cell division and early neuronal differentiation in the rat cortical neuroepithelium. Moreover, *in vitro* and *in vivo* brain studies reveal that different glutamate agonists differentially influence the proliferative state of progenitor cells in the neocortex, striatum, telencephalon, and retina depending upon the age of tissue at time of exposure, cellular location of the progenitor cell population, and subtype of glutamate agonist (LoTurco et al., 1995; Haydar et al 2000; Luk et al., 2003; Luk and Sadikot, 2004; Martins et al., 2006). For example, using dissociated E14.5 mouse retinas, exogenous glutamate decreased proliferative cells by reducing Cdk2 activity, however, the tissue localization of these cells was not assessed (Martins et al., 2006). Moreover, this explains the results in chick retina showing that interphase (defined to include postmitotic cells), but not mitotic cells, responded to glutamate (Pearson et al., 2002). Recent evidence suggests that RPCs commit to a neuronal fate during the last

round of cell cycle prior to cell cycle exit (Shibasaki et al., 2007; Hafler et al., 2012). Our iGluR-stimulated AGB-IR cells represent a snapshot of a population of closely related, newly postmitotic RPCs that commit to a late born neuronal cell fate. Therefore, responsiveness to iGluRs may constitute one of the first neuronal fate markers in postmitotic rod and bipolar cell precursors and consequently prevent these cells from re-entering cell cycle.

A third major finding was that PN0-PN10 retinas from mice with human equivalent GLE, as described (Leasure et al., 2008; Giddabasappa et al., 2011), exhibited an increased number and intensity of AGB-IR cells in the distal VZ and ONL compared to age-matched controls. Moreover, the period of functional activation of iGluRs was prolonged in the VZ and ONL in GLE retinas. However, the number, intensity and period of activation of the IPL were similar in control and GLE retinas as graphically summarized in Figure 3.9. The AGB-IR results in the outer retina recapitulate the findings that GLE increased the number of RPCs that differentiated into rods and bipolar cells (Giddabasappa et al., 2011). These results, in combination with those from other CNS tissues (LoTurco et al., 1995; Maric et al., 2000), suggest that the onset and degree of signaling efficiency by glutamate and likely other endogenous neurotransmitters activate ligand-activated receptors on early postmitotic RPCs and initiate neuronal differentiation.

Fourth, pharmacological experiments, conducted with control PN2 retinas, provided novel information about the mechanisms of functional activation of

AGB-IR cells in the developing VZ. ATP increased AGB-IR in the inner retina and induced cluster of AGB-IR cells in the VZ. AGB can permeate ligand-gated P2X receptor channels (Evans et al., 1996), although we found no published reports about these receptors in developing retina. However, several studies report that ATP acting on G-protein coupled P2Y1 receptors plays an important role in retinal proliferation (Martins and Pearson, 2008; Sholl-Franco et al., 2010). Since ATP is released from retinal pigment epithelium in developing retina (Pearson et al., 2005) and amacrine cells (Santos et al., 1999), it is possible that ATP acting on P2X receptors contributes to neuronal differentiation. The nicotinic acetylcholine agonist DMPP, which activates neuronal (Loring et al., 1989) and muscle (Cooper et al., 1996) type receptors, markedly increased the number of intense AGB-IR clusters in the VZ as well as increased inner retinal AGB-IR. The VZ, and inner retina of both E29-30 rabbit (equivalent to mouse PN2-3) and PN0-11 mice express functional nicotinic receptors that independently generate calcium waves (Bansal et al., 2000; Zhou and Zhao, 2000; Syed et al., 2004). Numerous nicotinic receptor subtypes are expressed throughout the outer and inner developing retina (Wong, 1995b; Keyser et al., 2000; Feller, 2002; Moretti et al., 2004), although subunit expression for muscle-specific receptors have not yet been examined. This latter caveat is important, since AGB acted as a mixed competitive and non-competitive inhibitor of DMPP on neuronal nicotinic receptors in chick retina (Loring, 1990). This raises the intriguing possibility that while activation of muscarinic acetylcholine receptors decreases RPC

proliferation (Wong, 1995b; Martins and Pearson, 2008), direct activation of unknown nicotinic receptors increases neuronal differentiation. Alternatively, DMPP could activate neuronal nicotinic receptors on amacrine and ganglion cells and increase their glutamate release (Wong, 1995b; Keyser et al., 2000; Feller, 2002; Moretti et al., 2004), that subsequently diffuses to the outer retina and activates iGluRs on early postmitotic RPCs. The experiments conducted with KA in the absence and presence of the non-competitive nicotinic antagonist hexamethonium suggest that KA increased acetylcholine release from starburst amacrine cells (Marc, 1999; Firth et al., 2003), which supports the idea of nicotinic receptors on early postmitotic RPCs in the VZ cells that regulate AGB permeation. The presence of KA receptors on early postmitotic RPCs in the VZ was demonstrated by KA plus DNQX experiments. In summary, we propose that activation of multiple ligand-activated ion channels, which are permeable to AGB, differentially initiates differentiation of late born neurons in the developing murine retina.

In situ hybridization and immunocytochemical studies reveal that AMPA, KA, and NMDA receptors are present in developing rodent retinas even prior to birth (Watanabe et al., 1994; Zhang et al., 1996; Gründer et al., 2000; Hack et al., 2002; Chang and Chiao, 2008; 2010). Our RT-qPCR studies using developing control retinas reveal that AMPA, KA and NMDA subunits exhibited differential patterns of gene expression from E18.5 to PN10. The four AMPA subunits (*Gria1, 2, 3, and 4*) increased expression during development and have the

highest relative expression among all iGluRs. The low affinity KA subunits (*Grik1, 2, and 3*) have markedly different developmental profiles, but reach the same relative high expression by PN10. In contrast, expression of the high affinity KA subunits (*Grik4 and 5*) is relatively unchanged during development, although their expression levels differ by six log units. The three NMDA subunits (*Grin1, 2a, and 2b*) increased expression by two log units during development, although their relative expression levels were different. In general, the relative expression levels in controls correlated with the age-dependent pharmacology and AGB-IR confocal results. In contrast, the significantly decreased expression of *Gria2* at E18.5 and PN2 and of *Grik4* at PN2 and PN4 as well as the increased expression of *Grik4*, *Grik5*, *Grin1*, *and Grin2a* at PN10 in GLE retinas do not correlate with the age-dependent pharmacology and AGB-IR confocal results. Instead, these measures obtained from whole homogenized retinas most likely reflect the prolonged RPC proliferation and subsequent increased neuronal differentiation that produced the adult retinal GLE phenotype (Giddabasappa et al., 2011).

The sixth major result demonstrates that micromolar concentrations of lead decreased AMPA- and KA-induced AGB permeation in the VZ of PN2 control retinas, although the AGB permeation in the inner retina slightly increased. Since lead acutely inhibits iGluRs (Heng-shan et al., 2002; Sadiq et al., 2012), we hypothesized that in vitro lead exposure would reduce the AMPA- and KA-induced increase in AGB permeation in both the outer and inner retina.

These results suggest that *in vitro* lead acted on different ligand-gated ion channels in the outer and inner retina. I infer that lead inhibited KA receptors located on RPCs in the VZ and thereby decreased AGB activation. In contrast, lead likely increased the nicotinic acetylcholine receptor-mediated inward current of amacrine and ganglion cells containing α3β2 subtypes (Keyser et al., 2000; Feller, 2002) and thus AGB-permeation, since micromolar lead selectively potentiates this inward nicotinic current (Zwart et al., 1995). Interestingly, these nicotinic receptors subtypes mediate the spontaneous calcium waves during retinal development (Bansal et al., 2000; Feller, 2002). The *in vitro* VZ results are markedly opposite to those observed in the VZ of PN2 GLE retinas treated with AMPA or KA, compared to age-matched controls. Since the free lead concentration in PN2 GLE retinas was <5 nM, as measured by a leadmium assay (Mukherjee and Fox, unpublished data), the GLE effects were most probably not directly due to lead. Together, these results will provide future insight into how iGluRs and other types of ligand-activated ion channels in developing outer and inner retina contribute to RPC proliferation and neuronal differentiation.

3.5 References

Acosta ML, Chua J, Kalloniatis M (2007) Functional activation of glutamate ionotropic receptors in the developing mouse retina. J Comp Neurol 500:923-941.

Agathocleous M, Harris WA (2009) From progenitor to differentiated cells in the vertebrate retina. Annu Rev Cell Dev Biol 25:45-69.

Akimoto M, Cheng H, Zhu D, Brzezinski JA, Khanna R, Filippova E, Oh EC, Jing Y, Linares JL, Brooks M, Zareparsi S, Mears AJ, Hero A, Glaser T, Swaroop A (2006) Targeting of GFP to newborn rods by Nrl promoter and temporal expression profiling of flow-sorted photoreceptors. Proc Natl Acad Sci 103: 3890–3895.

Alexiades MR, Cepko CL (1996) Quantitative analysis of proliferation and cell cycle length during development of the rat retina. Dev Dyn 205:293-307.

Alkondon M, Costa CA, Radhakrishnan V, Aronstam RS, Albuquerque EX (1990) Selective blockade of NMDA activated channel currents may be implicated in learning deficits caused by lead. FEBS Lett 261:124-130.

Baas D, Bumsted KM, Martinez JA, Vaccarino FM, Wikler CK, Barnstable CJ (2000) The subcellular localization of Otx2 is cell type specific and developmentally regulated in the mouse retina. Mol Brain Res 78:26-37.

Bansal A, Singer JH, Hwang BJ, Xu W, Beaudet A, Feller MB (2000) Mice lacking specific nicotinic acetylcholine receptor subunits exhibit dramatically altered spontaneous activity patterns and reveal a limited role for retinal

waves in forming ON and OFF circuits in the inner retina. J Neurosci 15:7672-7681.

Barton KM, Levine EM (2008) Expression patterns and cell cycle profiles of PCNA, MCM6, Cyclin D1, Cyclin A2, Cyclin B1, and phosphorylated Histone H3 in the developing mouse retina. Developmental Dynamics 237:672-682.

Baye LM, Link BA (2008) Nuclear migration during retinal development. Brain Res 1192:29-36.

Bleakman D, Lodge D (1998) Neuropharmacology of AMPA and kainate receptors. Neuropharmacology 37:1187-1204.

Bowie D (2012) Redefining the classification of AMPA selective ionotropic glutamate receptors. J Physiol 590:49-61.

Brandstatter JH, Koulen P, Wassle H (1998) Diversity of glutamate receptors in the mammalian retina. Vision Res 38:1385-1397.

Cepko CL (1993) Retinal cell fate determination. Prog Retin Eye Res 12:1-12.

Chang YC, Chiao CC (2008) Localization and functional mapping of AMPA receptor subunits in the developing rabbit retina. Invest Ophthalmol Vis Sci 49:5619-5628.

Chang YC, Chiao CC (2010) Visual experience-independent functional expression of NMDA receptors in the developing rabbit retina. Invest Ophthalmol Vis Sci 51:2744-2754.

Cooper JC, Gutbrod O, Witzemann V, Methfessel C (1996) Pharmacology of the nicotinic acetylcholine receptor from fetal rat muscle expressed in xenopus oocytes. Eur J Pharmacol 309:287-298.

Das G, Choi Y Sicinski P, Levine EM (2009) Cyclin D1 fine-tunes the neurogenic output of embryonic retinal progenitor cells. Neural Dev 4:15.

Demarque MA, Represa A, Becq H, Khalilov I, Ben-Ari Y, Aniksztein L (2002) Paracrine intercellular communication by a Ca2+- and SNARE-independent release of GABA and glutamate prior to synapse formation. Neuron 36:1051-1061.

Dyer MA, Cepko CL (2001) Regulating proliferation during retinal development. Nat Rev Neurosci 2:333-342.

Evans RJ, Lewis C, Virginio C, Lundstrom K, Buell G, Surprenant A, North RA (1996) Ionic permeability of, and divalent cation effects on, two ATP-gated cation channels (P2X receptors) expressed in mammalian cells. J Physiol 497:413-422.

Feller MB (2002) The role of nAChR-mediated spontaneous retinal activity in visual system development. J Neurobiol 53:556-567.

Firth SI, Li W, Massey SC, Marshak DW (2003) AMPA receptors mediate acetylcholine release from starburst amacrine cells in the rabbit retina. J Comp Neurol 466:80-90.

Fletcher EL, Kalloniatis M (1997) Localisation of amino acid neurotransmitters during postnatal development of the rat retina. J Comp Neurol 380:449-471.

Flores-Soto ME, Chaparro-Huerta V, Escoto-Delgadillo M, Vazquez-Valls E, Gonzales-Castañeda RE, Beas-Zarate C (2012) Structure and function of NMDA-type glutamate receptor subunits. Neurologia 27:301-310.

Fox DA, Kala SV, Hamilton WR, Johnson JE, O'Callaghan JP (2008) Low-level human equivalent gestational lead exposure produces supernormal scotopic electroretinograms, increased retinal neurogenesis, and decreased retinal dopamine utilization in rats. Environ Health Perspect 116:618-625.

Ghosh F, Taylor L, Arner K (2012) Exogenous glutamate modulates porcine retinal development in vitro. Dev Neurosci 34:428-439.

Giddabasappa A, Hamilton WR, Chaney S, Xiao W, Johnson JE, Mukherjee S, Fox DA (2011) Low-level gestational lead exposure increases retinal progenitor cell proliferation and rod photoreceptor and bipolar cell neurogenesis in mice. Environ Health Perspect 119:71-77.

Graham KJ, Holland MJ (2005) PrimerSelect: a transcriptome-wide oligonucleotide primer pair design program for kinetic RT-PCR-based transcript profiling. Methods Enzymol 395:544-553.

Gründer T, Kohler K, Kaletta A, Guenther E (2000) The distribution and developmental regulation of NMDA receptor subunit proteins in the outer and inner retina of the rat. J Neurobiol 44:333-342.

Guilarte TR, Miceli RC (1992) Age-dependent effects of lead on [3H]MK-801 binding to the NMDA receptor-gated ionophore: in vitro and in vivo studies. Neurosci Lett 148:27-30.

Haberecht M, Redburn DA (1996) High levels of extracellular glutamate are present in retina during neonatal development. Neurochem Res 21:285-291.

Hack I, Koulen P, Peichl L, Brandstatter JH (2002) Development of glutamatergic synapses in the rat retina: the postnatal expression of ionotropic glutamate receptors subunits. Vis Neurosci 19:1-13.

Hafler BP, Surzenko N, Beier KT, Punzo C, Trimarchi JM, Kong JH, Cepko CL (2012) Transcription factor Olig2 defines subpopulations of retinal progenitor cells biased toward specific cell fates. Proc Natl Acad Sci 109:7882-7887.

Haydar TF, Wang F, Schwartz ML, Rakic P (2000) Differential modulation of proliferation in the neocortical ventricular and subventricular zones. J Neurosci 20:5764-5774.

He L, Poblenz AT, Medrano CJ, Fox DA Lead and calcium produce rod photoreceptor cell apoptosis by opening the mitochondrial permeability transition pore. J Biol Chem 275:12175-12184.

Johnson JE, Perkins GA, Giddabasappa A, Chaney S, Xiao W, White AD, Brown JM, Waggoner J, Ellisman MH, Fox DA (2007) Spatiotemporal regulation of ATP and Ca2+ dynamics in vertebrate rod and cone photoreceptor ribbon synapses. Mol. Vision 13:887-919.

Kew JN, Kemp JA (2005) Ionotropic and metabotropic glutamate receptor structure and pharmacology. Psychopharmacology 179: 4-29.

Keyser KT, MacNeil MA, Dmitrieva N, Wang F, Masland RH, Lindstrom JM (2000) Amacrine, ganglion, and displaced amacrine cells in the rabbit retina express nicotinic acetylcholine receptors. Vis Neurosci 17:743-752.

Kurihara T, Kubota Y, Ozawa Y, Takubo K, Noda K, Simon MC, Johnson RS, Suematsu M, Tsubota K, Ishida S, Goda N, Suda T, Okano H (2010) Von Hippel-Lindau protein regulates transition from fetal to adult circulatory system in retina. Development 137:1563-1571.

Leasure JL, Giddabasappa A, Chaney S, Johnson JE, Pothakos K, Lau YS, Fox DA (2008) Low-level human equivalent gestational lead exposure produces sex-specific motor and coordination abnormalities and late–onset obesity in year-old mice. Environ Health Perspect 116:355-361.

Livesey FJ, Cepko CL (2001) Vertebrate neural cell-fate determination: lessons from the retina. Nat Neurosci 2:109-118.

LoTurco JJ, Owens DF, Heath MJS, Davis MBE, Kriegstein AR (1995) GABA and Glutamate depolarize cortical progenitor cells and inhibit DNA synthesis. Neuron 15:1287-1298.

Loring RH (1990) Agmatin acts as an antagonist of neuronal nicotinic receptors. J Pharmacol 99:207-211.

Loring RH, Zigmond RE (1990) Pharmacological and biochemical properties of nicotinic receptors from chick retina. Eur J Neurosci 2:863-872.

Luk KC, Kennedy TE, Sadikot AF (2003) Glutamate promotes proliferation of striatal neuronal progenitors by an NMDA receptor-mediated mechanism. J Neurosci 23:2239-2250.

Luk KC, Sadikot AF (2004) Glutamate and regulation of proliferation in the developing mammalian telencephalon. Dev Neurosci 26:218-228.

Marc RE (1999) Mapping glutamatergic drive in the vertebrate retina with a channel-permeant organic cation. J Comp Neurol 407:47-64.

Marc RE, Kalloniatis M, Jones BW (2005) Excitation mapping with the organic cation AGB2+. Vision Res 45: 3454-3468.

Maric D, Liu Q, Grant GM, Andreadis JD, Hu Q, Chang YH, Barker JL, Pancrazio JJ, Stenger DA, Ma W (2000) Functional ionotropic glutamate receptors emerge during terminal cell division and early neuronal differentiation of rat neuroepithelial cells. J Neurosci Res 61:652-662.

Marquardt T, Gruss P (2002) Generating neuronal diversity in the retina: one for nearly all. Trends Neurosci 25:32-38.

Martins RA, Linden R, Dyer MA (2006) Glutamate regulates retinal progenitors cells proliferation during development. Eur J Neurosci 24:969-980.

Martins RA, Pearson RA (2008) Control of cell proliferation by neurotransmitters in the developing vertebrate retina. Brain Res 1192:37-60.

Medrano CJ, Fox DA (1994) Substrate-dependent effect of calcium on rat retinal mitochondrial respiration: physiological and toxicological studies. Toxicol Appl Pharmacol 125:309-321.

Medrano CJ, Fox DA (1995) Oxygen consumption in the rat outer and inner retina: light and pharmacologically-induced inhibition. Exp Eye Res 61:273-284.

Moretti L, Pentikainen OT, Settimo L, Johnson MS (2004) Model structures of the N-methyl-D-aspartate receptor subunit NR1 explain the molecular recognition of agonist and antagonist ligands. J Struct Biol 145:205-215.

Neal AP, Worley PF, Guilarte TR (2011) Lead exposure during synaptogenesis alters NMDA receptors targeting via NMDA receptor inhibition. Neurotoxicology 32:281-289.

Nishida A, Furukawa A, Koike C, Tano Y, Aizawa S, Matsuo I, Furukawa T (2003) Otx2 homeobox gene controls retinal photoreceptor cell fate and pineal gland development. Nat Neurosci 6:1255-1263.

Pearson R, Casticas M, Becker D, Mobbs P (2002) Purinergic and muscarinic modulation of the cell cycle and calcium signaling in the chick retinal ventricular zone. J Neurosci 22:7569-7579.

Pearson RA, Dale N, Llaudet E, Mobbs P (2005) ATP released via GAP junction hemichannels from the pigmented epithelium regulates retinal progenitor proliferation. Neuron 46:731-744.

Pow DV, Robinson SR (1994) Glutamate in some retinal neurons is derived solely from glia. Neurosci 60:355-366.

Quraishi SJ, Gayet J, Morgans CW, Duvoisin RM (2007) Distribution of group-III metabotropic glutamate receptors in the retina. J Comp Neurol 501:931-943.

Rapaport DH, Wong LL, Wood ED, Yasumura D, LaVail MM, (2004) Timing and topography of cell genesis in the rat retina. J Comp Neurol 474:304-324.

Redburn DA, Agarwal SH, Messersmith EK, Mitchell CK (1992) Development of the glutamate system in rabbit retina. Neurochem Res 17:61-66.

Redburn DA Rowe-Rendleman C (1996) Developmental neurotransmitters signals for shaping neuronal circuitry. Invest Ophthalmol Vis Sci 37:1479-1482.

Rosenmund CY, Stern-Bach (1998) The tetrameric structure of a glutamate receptor channel. Science 280:1596-9.

Sadiq S, Ghazala Z, Chowdhury A, Busselberq D (2012) Metal toxicity at the synapse: presynaptic, postsynaptic and long-term effects. J Toxicol 132671:1-42.

Santos PF, Caramelo OL, Carvalho AP, Duarte CB (1999) Characterization of ATP release from cultures enriched in cholinergic amacrine–like neurons. J Neurobiol 41:340-348.

Shibasaki K, Takebayashi H, Ikenaka K, Feng L, Gan L (2007) Expression of the basic helix-loop-factor Olig2 in the developing retina: Olig2 as a new marker for retinal progenitors and late-born cells. Gene Expr Patterns 7:57-65.

Sholl-Franco A, Fragel-Madeira L, Macama Ada C, Linden R, Ventura AL (2010) ATP controls cell cycle and induces proliferation in the mouse developing retina. Int J Dev Neurosci 28:63-73.

Shulman L, Fox DA (1996) Dopamine inhibits mammalian photoreceptor Na+, K+-ATPase activity via a selective effect on the α3 isozyme. Proc Natl Acad Sci 93:8034-8039.

Silveira dos Santos BA, Hamassaki-Britto DE (2001) Ionotropic glutamate receptors during the development of the chick retina. J Comp Neurol 441:58-70.

Sucher NJ, Kohler K, Tenneti L, Wong H,Gründer T, Fauser S, Wheeler-Schilling T, Nakanishi N, Lipton SA, Guenther E (2003) N-Methyl-D-Aspartate receptor subunit NR3A in the retina: developmental expression, cellular localization, and functional aspects. Invest Ophthalmol Vis Sci 44:4451-4456.

Sui L, Ruan DY (2000) Impairment of the Ca2+-permeable AMPA/kainate receptors by lead exposure in organotypic rat hippocampal slice cultures. Pharmacol Toxicol 87:204-10.

Sun D, Kalloniatis M (2006) Mapping glutamate responses in immunocytochemically identidied neurons of the mouse retina. J Comp Neurol 494:686-703.

Syed MM, Lee S, Zheng J, He S, Zhou J (2004a) Spontaneous waves in the ventricular zone of developing mammalian retina. J Neurophysiol 91:1999-2009.

Syed MM, Lee S, Zheng J, Zhou J (2004b) Stage-dependent dynamics and modulation of spontaneous waves in the developing rabbit retina. J Physiol 560: 533-549.

Turner DL, Cepko CL (1987) A common progenitor for neurons and glia persists in rat retina late in development. Nature 328:131-136.

Turner DL, Snyder EY, Cepko CL(1990) Lineage independent determination of cell type in the embryonic mouse retina. Neuron 4:833-845.

Ujihara H, Albuquerque EX (1992) Developmental change of the inhibition by lead of NMDA-activated currents in cultured hippocampal neurons. J Pharmacol Exp Ther 263:868-75.

Watanabe M, Mishina M, Inoue Y (1994) Differential distributions of the NMDA receptor channel subunit mRNAs in the mouse retina. Brain Res 634:328-332.

Wong R (1995) Cholinergic regulation of Calcium during cell division and differentiation in the mammalian retina. J Neurosci 15:2696-2706.

Yang XL (2004) Characterization of receptors for glutamate and GABA in retinal neurons. Prog Neurobiol 73:127-50.

Young RW (1985) Cell differentiation in the retina of the mouse. Anat Rec 212:199-205.

Zhang C, Hammassaki-Britto DE, Britto LRG, Duvoisin RM (1996) Expression of glutamate receptor subunit genes during development of the mouse retina Neuroreport 8:335-340.

Zhou ZY, Zhao D (2000) Coordinated transitions in neurotransmitter systems for the initiation and propagation of spontaneous retinal waves. J Neurosci 20:6570-6577.

Zwart R, Van Kleef RG, Milikan JM, Oortqiesen M, Vijverberg HP (1995) Potentiation and inhibition of subtypes of neuronal nicotinic acetylcholine recepeotr by Pb2+. Eur J Pharmacol 291:399-406.

CHAPTER 4:

GESTATIONAL LEAD EXPOSURE ACCELERATED AND ENHANCED AGE-RELATED DEGENERATION

4.1 Introduction

Blood lead concentrations ([BPb]) at or below 10 µg/dL produce retinal, cognitive and visual-motor deficits in developing children. Postnatal only lead exposure produces rod-selective apoptosis, subnormal scotopic electroretinograms (ERGs) and scotopic vision deficits in man and experimental animals (Fox and Boyes, 2013). In contrast, children, monkeys, and rats with gestational lead exposure (GLE) have supernormal scotopic ERGs (Lilienthal et al., 1994; Rothenberg et al., 2002; Fox et al., 2008). Mice with gestational lead exposure (GLE) exhibit increased and prolonged retinal progenitor cell proliferation which results in a 20-30% increase in the number of late-born retinal neurons (rod photoreceptors and bipolar cells), but no change in the number of late-born Müller glial cells (Giddabasappa et al., 2011). While this novel phenotype has been characterized during development (Giddabasappa et al., 2011), little is known about the structure and function of the retina as these mice age. Interestingly, GLE produced late-onset obesity in year-old male mice (Leasure et al., 2008), revealing that GLE increased the susceptibility to disease later in life (Heindel, 2007). Since senescence adversely affects retinal function and cell number (Suzuki and Horiguchi, 1998; Gao and Hollyfield, 1992; Katz and Robison, 1986), it is possible that the retinas of mice with GLE are more susceptible to retinal degeneration. The goal of these experiments was to characterize the morphological and immunohistochemical changes in the retinas of control and GLE mice during aging.

Several eye well-known conditions pose a threat to proper vision as we age. These include cataract, age-related maculopathy (ARM), glaucoma, and diabetic retinopathy. The retina is often the site of action for age-related diseases associated with vision loss. In fact, age-related macular degeneration is the leading cause of legal blindness in people over 60. Excluding disease though, visual decline is often associated with normal aging. The photoreceptors of the retina are vulnerable to the aging and specifically, rod photoreceptors are more vulnerable than cones. In human retinas, equatorial rods decrease at a rate of 970/mm^2/year between the second and fourth decades and 570-330/mm^2/year thereafter resulting in a 15% decrease in rod density by the fourth decade, however, cones only decreased by 6.7% by the fourth decade (Gao and Hollyfield, 1992). Curcio et al (1993) reported that in the central retina rod density decreased by 30% between 34 to 90 years of age.

GLE increased and prolonged RPC proliferation during early retinal development resulting in a dose-dependent increase in the number of rod photoreceptors and bipolar cells in adult GLE mice. Since photoreceptors and bipolar cells compose the primary components of the vertical glutamatergic signaling pathway in the retina, the overall goal of my research was examine alterations in this pathway at several critical time points during the rodent's lifespan. The specific goals of my PhD research were to: 1) characterize the spatiotemporal and functional synaptic development of rod photoreceptors and bipolar cells in developing GLE retinas, 2) examine effect of GLE on proliferative

glutamate signaling prior to conventional synapse formation, and 3) examine the integrity of GLE retinas, especially rod photoreceptors and bipolar cells, during normal aging. This chapter addresses the third of these goals.

I hypothesized that GLE would enhance age-related degeneration of rod photoreceptors and bipolar cells. I based this hypothesis on the fact that the retina is a highly metabolic tissue in which rod photoreceptor experience oxidative stress with aging. An increase in these highly metabolic cells would likely overload the long-term energy producing capacity of the system. To test this hypothesis, I used commercially available and cell specific antibodies to characterize the morphology of photoreceptors and bipolar cell during aging in control and GLE retinas. I also examined the structure synapses made by these two types of neurons in aging control and GLE retinas.

In summary, I found that retinal thinning, loss of neurons, and synaptic disorganization occurred normally in aged control C57BL/6N mice. Although, GLE retinas were initially thicker than controls at 2 months of age, they became thinner than controls with aging. Measurements of each nuclear layer revealed that both the ONL and INL decreased in thickness in GLE retinas. Furthermore, immunohistochemical analysis showed that decreases in the number of rod photoreceptors and bipolar cells underlie the decreased retinal thickness in GLE retinas. Next, I found that GLE enhanced the age-related degeneration of synapses made between these two neurons. Finally, GLE increased the amount

of synaptic retraction and dendritic sprouting of rod photoreceptors and bipolar cells, respectively.

4.2 Materials and Methods

4.2.1 Mouse model of gestational lead exposure

All experimental and animal care procedures complied with the National Institutes of Health (NIH) Public Health Service Policy on Humane Care and Use of Laboratory Animals (NIH 2002) and were approved by the Institutional Animal Care and Use Committee of the University of Houston. All animals were treated humanely and with regard for alleviation of suffering. The protocol for housing, feeding, breeding, and lighting conditions were as previously described (Leasure et al., 2008; Giddabasappa et al., 2011). Briefly, naïve female were given either tap (control) or moderate-dose (55 ppm) lead acetate drinking water (GLE group) for two weeks before mating, during pregnancy, and until post-natal day 10, after which the lead was replaced with tap water. For embryonic-day 16.5 (E16.5) and E18.5 retinas, dams were mated overnight, checked for vaginal plugs in the morning and the pups were used for timed-pregnant experiments. Water, food, and weights were recorded throughout treatment. Mice were sacrificed by decapitation between 1000 and 1200 hours. Blood lead concentrations were measured as previously described for each pup to ensure relevant blood lead levels (Leasure et al., 2008). Pups in the control and GLE groups had peak blood lead concentration on PN0 and/or PN10 of 0.75 ± 0.06 and 22.11 ± 1.05 mg/dL, respectively. There were no statistical differences between control and GLE

groups on any dam measure, litter measure or body weight (Leasure et al., 2008).

4.2.2 Tissue processing and immunohistochemistry

All tissue processing and immunohistochemistry techniques were performed as described previously (Johnson et al., 2007; Fox et al., 2008; Giddabasappa et al., 2011). Briefly, adult or developing mice were decapitated and the eyes were quickly enucleated and place in ice-cold PBS where the corneas were gently punctured at the limbus. The eyes were then immersion fixed in room temperature, buffered 4% paraformaldehyde (Ladd Research, Williston VT) for 30 minutes, washed in PBS three times fro 10 minutes and cryoprotected in 30% w/v sucrose for 48 hours. Anterior segments were removed and the eyes were embedded in TissueTek OCT mounting medium (Electron Microscopy Services, Fort Washington, PA), flash frozen in liquid nitrogen and stored at -80°C. Three non-adjacent fixed-frozen transverse sections (10 µm) taken from the vertical meridian were mounted on Superfrost Plus glass slides (Thermo Fisher Scientific, Waltham, MA) and stored at -20°C.

All sections were taken from central retina: 200-400 µm from the optic nerve. The slides were thawed slowly, sections post-fixed with 4% paraformaldehyde, washed, and briefly immersed in a 1% sodium-borohydride (Sigma-Aldrich, St. Louis, MO) solution to reduce double bonds, allow proper epitope access for antibodies and decrease auto-fluorescence. Sections were washed with ddH_2O, then PBS and incubated for 2 hours with blocking buffer containing 10% normal

goat serum (Jackson ImmunoResearch Labs Inc.) and 0.3% Triton-X100 in PBS. Primary antibodies were applied for 2 days at 4°C after which slides were washed with PBS, blocked for 30 minutes, and secondary antibodies were applied. Table 4.1 lists the well-characterized and commercially available primary anitibodies that were used. For double-labeling experiments, primary antibodies from different host animals were applied simultaneously. Dilutions of Alexa 488, 555 and 647 (1:400) conjugated secondary antibodies were made in blocking buffer, applied to slides, and allowed to incubate in the dark at room temperature for one hour. Slides were washed with PBS, ddH_2O, dried, and mounted with Vectashield mounting medium (Vector Laboratories Inc. Burlinghame CA) and No.1 coverslip, and stored at 4°C. For experiments with DAPI labeling, sections were incubated with DAPI for one hour in the dark after secondary incubation. All antibodies were titrated through a broad range of working dilutions (3 orders of magnitude) to determine optimal working dilutions. Immunolabeling specificity was confirmed by processing retinal sections in the absence of primary anitibody.

Table 4.1
Cell Specific Primary Antibodies Used for Immunohistochemistry (IHC)

Primary Antigen	Imunogen	Source	Catalog. No.	Target	Host	Dilution	IHC or WB
CHX10	Recombinant amino acids 1-131 N-terminal of human protein	Exalpha Biologicals	X1180P	RPCs in development Bipolar cells in adult	Sheep	1:200	IHC
M- and S-Cone Opsin		Gift: Cheryl Craft		M- and S-Cone inner and outer segments	rabbit	1:1000	IHC
M- Cone Arrestin		Gift: Cheryl Craft		M- Cone pedicles	rabbit	1:1000	IHC
PKCa	Protein kinase C alpha	AbD Serotec	MCA1572	Rod bipolars	mouse	1:100	IHC
PMCA	Purified human erythrocyte ATPas	Affinity Bioreagents	MA3-914	OPL, IPL some amacrine and bipolar cells	Mouse	1:500	IHC
VGLUT1	Synthetic peptide from rat VGLUT1 protein	Chemicon	AB5905	Synaptic layers	Guinea Pig	1:1000	IHC

4.2.3 Statistical analyses

For all data, only one animal or one pooled group of animals from the same litter was used for each measure or sample. Data are presented as the mean ± SEM for four to nine animals per treatment group. Data were analyzed using an ANOVA followed by post-hoc analysis with Fisher's Least Significance Difference Test or the Student's T-test when only two means were compared. In all figures, values with $p<0.05$ were considered significantly different from controls and were noted where appropriate by asterisks. In the text, values noted as significantly different from controls had $p<0.05$. IHC images were compiled and presented with Adobe Photoshop CS (Adobe Systems Inc., Mountain View CA). Quantitative cell counts were conducted from three non-adjacent retinal sections using unbiased stereological procedures (He et al., 2003; Giddabasappa et al., 2011). Values from each retina were averaged to obtain one representative value. Graphs were generated with KaleidaGraph (Synergy Software, Reading PA).

4.3 Results

4.3.1 GLE increased age-related degeneration of rod photoreceptors and bipolar cells.

As previously observed, the two-month-old GLE retinas were thicker than age-matched controls (Giddabasappa et al., 2011). To test whether the increased thickness persisted with aging, I labeled 2-, 12-, and 15-month-old retinas with DAPI and examined them on an epifluorescent microscope. Figure 4.1 shows the DAPI images from these results. The 2-month-old GLE retinas were thicker than age-matched controls (Figures 4.1A and B). At 12 months the increased retinal thickness associated 2-month-old GLE retinas was no longer present (Figures 4.1C and D). At 15 months, the GLE retinas were slightly thinner than age-matched control retinas (Figures 4.1E and F).

To determine whether the decreased retinal thickness in aging GLE retinas was due to changes in the ONL and/or INL thicknesses, I measured the thicknesses of each nuclear layer independently and plotted the differences. Figure 4.2 shows the quantified data for these measurements. The thicknesses of control ONLs and INLs decreased with normal aging. The ONL and INL thicknesses of control retinas decreased 11-18% and 21-25%, respectively, from 2 to 12 months. There was no further decrease between 12 and 15 months in the control ONLs and INLs. At 2 months of age, the ONLs and INLs of GLE retinas

were 16% and 25% thicker than age matched controls, respectively. Degeneration in GLE retinas was accelerated such that the ONLs of 12-month-old GLE retinas were approximately 23% smaller than 2-month-old GLE retinas and similar in thickness to 12-month-old controls. The INLs of GLE retinas decreased by 44-46% when compared to 2-month-old GLE retinas: 2-fold more than controls. The increased loss of INL nuclei in aging GLE retinas resulted in INLs that were significantly thinner in 12 and 15 months in GLE mice compared to age-matched controls.

To determine which cell types were responsible for the decreased thicknesses of GLE ONLs, I first conducted immunohistochemical experiments with an antibody specific for cone photoreceptors. Figures 4.3 and 4.4 show the results from immunohistochemical experiments with M- and S-cone opsin (cone inner and outer segments), and M- and S- cone arrestin (M-CAR) (cone pedicles), respectively. Figure 4.3 shows no change in the number of M-cone opsin-IR cone outer segments in aging control or GLE. Similarly, Figure 4.4 shows no change in the number of M-CAR-IR cone pedicles in control and GLE retinas with aging. Together these results suggest that changes in the number of rod photoreceptors must be responsible for the decreased thickness of ONLs of GLE retinas. This is likely since: 1) rod and cone photoreceptors are the only cells that compose the ONL, 2) rods make-up about 95-97% of the cells in the rodent ONL, and 3) an increase in the number of rod photoreceptors are

responsible for thicker ONLs observed in 2-month-old GLE retinas (Giddabasappa et al., 2011).

Figure 4.1. Gestational Lead Exposure (GLE) increased retinal thickness at 2-months (2M) but not at 12 and 15M. Adult and aging **(A, C, and E)** control and **(B, D, and F)** GLE retinas were labeled with DAPI and imaged. **(A-B)** At 2M, GLE retinas were thicker than age-matched controls. **(C-D)** By 12M, the increased retinal thickness associated with 2M GLE retinas was no longer present. **(E-F)** At 15M GLE retinas appeared slightly thinner than age-matched controls. The ganglion cell layer showed no change. Scale bar = 40μm.

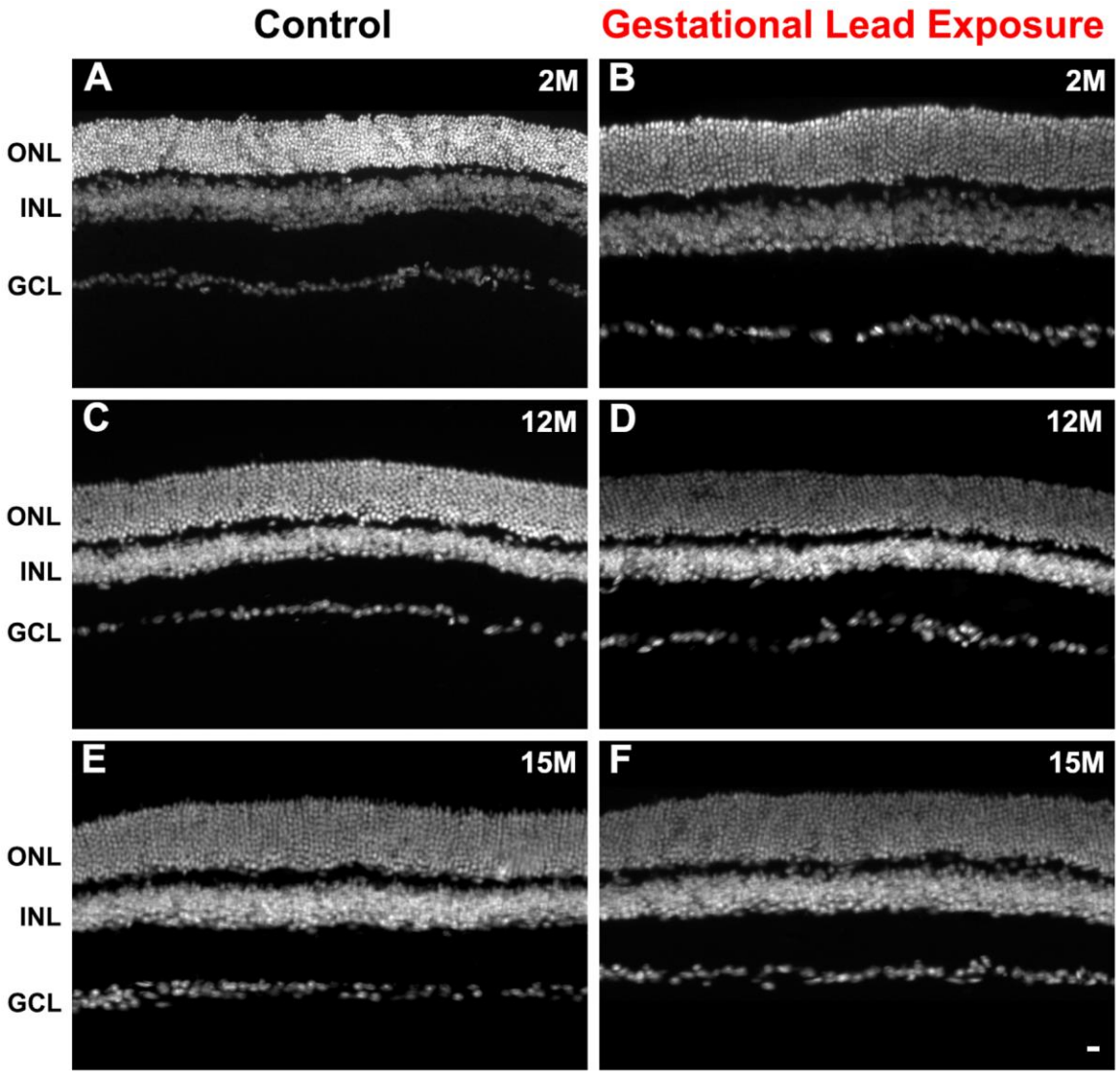

Figure 4.2. The ONLs and INLs of GLE retinas exhibited increased and accelerated degeneration. The ONL and INL thicknesses for 2, 12, and 15M control and GLE retinas were measured and quantified. There was a normal age-dependent decrease in the ONL and INL thickness in control retinas. In both the ONL and INL of control retinas, the thicknesses significantly decreased from 2 to 12M (11-18%) and from 2 to 15M (21-25%) but not from 12 to 15M. 2M GLE ONLs were thicker than age-matched controls by about 16%. In GLE mice at 12 and 15 months, the ONL thickness decreased 23-28% from 2M. 2M GLE INLs were approximately 25% thicker than age-matched controls. In GLE mice at 12 and 15 months, the INL thickness decreased 44-46% from 2M. The decrease observed in GLE INLs was approximately 2-fold more than controls. Matching letters above the bars represent statistically significant differences. Data is presented as mean ± SEM. Significance = $p<0.05$.

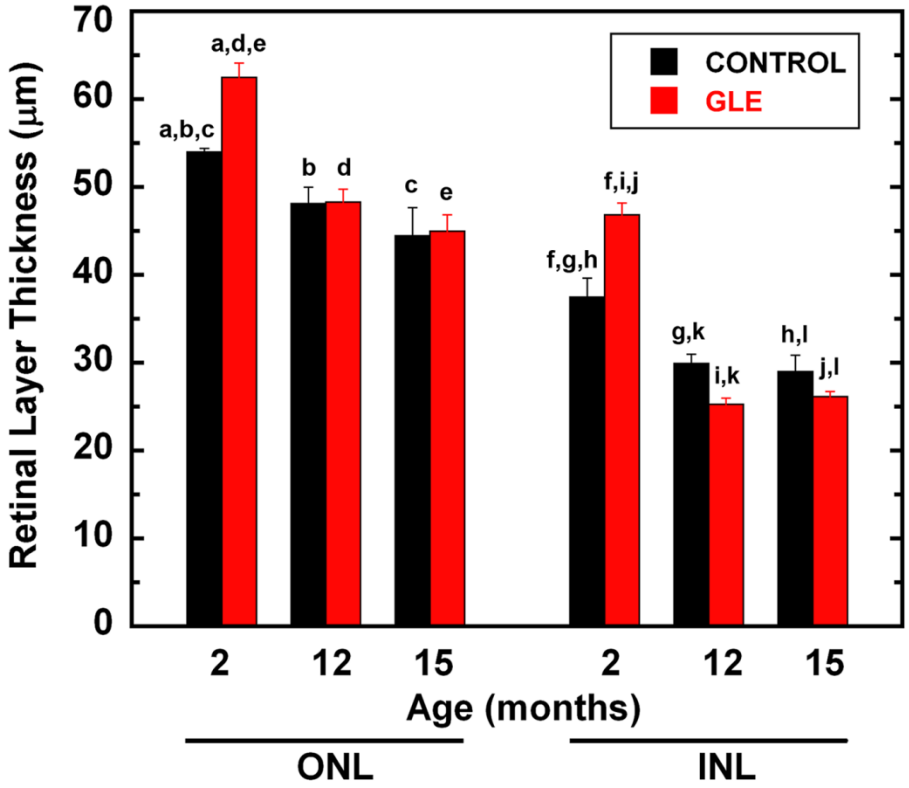

Since all types of bipolar cells were increased in PN60 GLE retinas (Giddabasappa et al., 2011), I labeled aging mouse retinas with the bipolar specific antibody CHX-10. Figures 4.5A-F show the immunohistochemical images from these experiments and Figure 4.6 shows the quantification of this data. In control retinas, the number of Chx10-IR bipolar cells did not significantly change between 2 and 12 months (Figures 4.5 A, C, and 4.6), however, they decreased by 10% at 15 months (Figures 4.6E and 4.6). In 2-month-old GLE retinas, there was a 30% increase in the number of Chx-10-IR bipolar cells when compare to age-matched controls (Figures 4.5B and 4.6). The number of Chx-10-IR bipolar cells decreased by approximately 40% at 12M (Figures 4.5D and 4.6) and 50% at 15 months (Figures 4.5F and 4.6). Together, these results show that in GLE retinas, rod photoreceptors and bipolar cells, the two cell types increased in PN60 GLE retinas, exhibited increased degeneration during aging.

Figure 4.3. GLE retinas showed no change in the number of M- and S-opsin-IR cones with aging. (A, C, and E) Control and **(B, D, and F)** GLE aging retinas were labeled with antibodies against M- and S-cone opsins. M- and S-cone opsins labeled inner and outer segments of M- and S- cone photoreceptors at all ages. There were no significant differences in the number of M- and S-opsin immunoreactive inner and outer segments between 2, 12, and 15M control and GLE retinas. Scale bar = 40µm

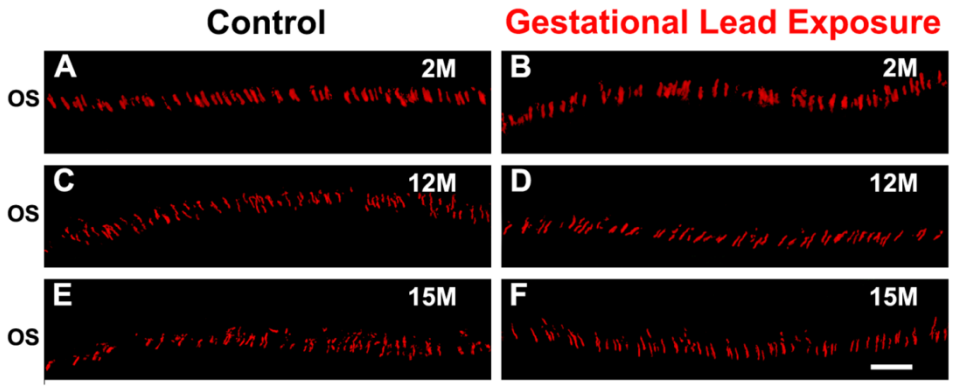

Figure 4.4. GLE retina showed no change in the number of VGluT1 and M-CAr cone pedicles. (A-C and G-I) Control and **(D-F and J-L)** GLE aging retinas were labeled with antibodies against VGluT and M-CAr. **(A, D, G, and J)** VGluT1 labeled the synapses of both rod and cone photoreceptor terminals at all ages. **(B, E, H, and K)** M-CAr labeled only cone pedicles. **(C, F, I, and L)** Double label panels show that M-CAr-IR cone pedicles label in the proximal OPL. There were no changes in the number of M-CAr-IR cone pedicles in aging control or GLE retinas. Scale bar = 40μm

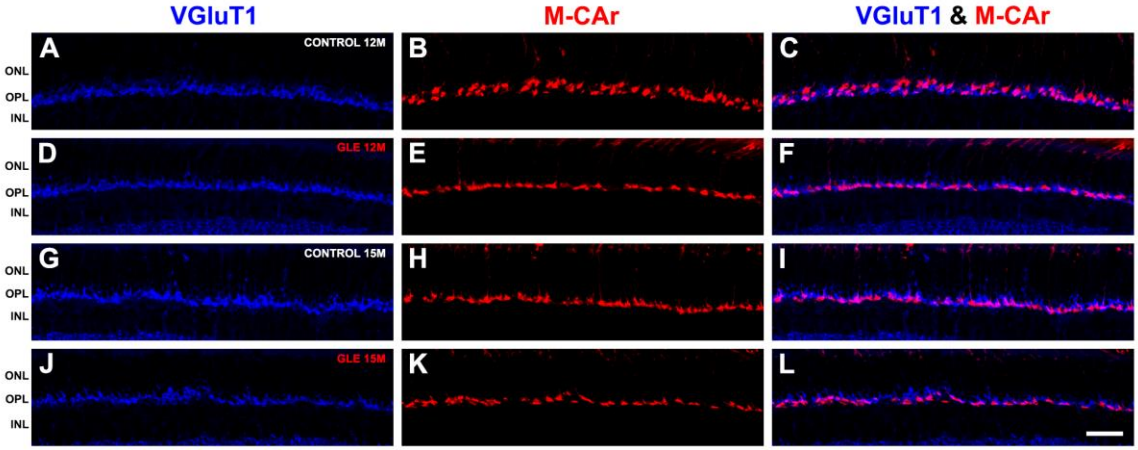

Figure 4.5. Chx10-IR cells decreased in GLE retinas with age when compared to controls. Retinas of aging **(A, C,** and **E)** control and **(B, D,** and **F)** GLE retinas were labeled with an antibody against the CHX10 protein. **(A, C,** and **E)** In control retinas, the number of Chx10-IR nuclei decreased from 2 to 15M with normal aging. **(B)** At 2M, GLE retinas showed more Chx10-IR cells than control. **(D)** The number Chx10-IR cells was similar to controls at 12M and **(F)** less than controls at 15M. Scale bar = 40μm

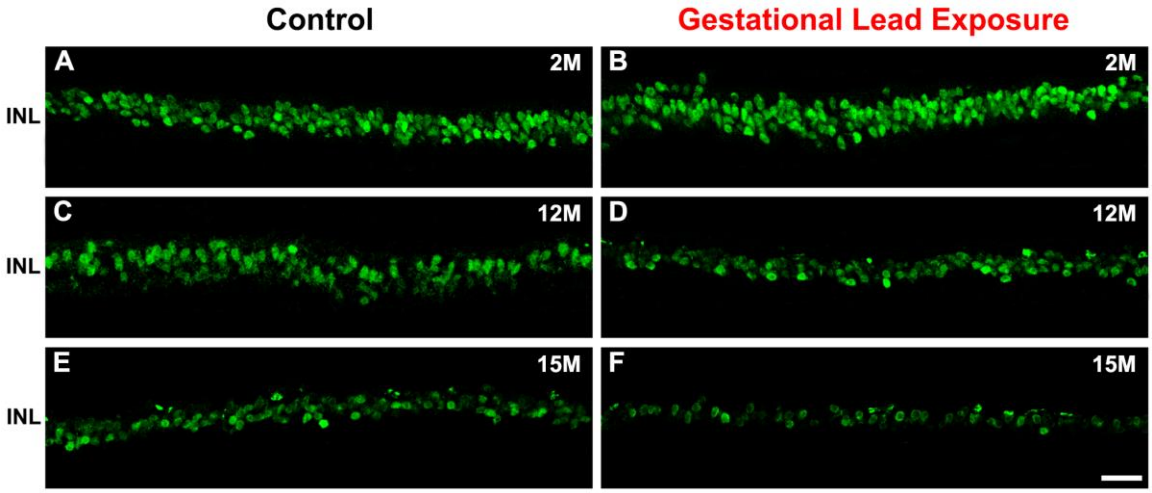

Figure 4.6. Quantification of the decrease in Chx10-IR cells in aging control and GLE retinas. The number of Chx10-IR cells at each age were counted and quantified as the number of cells per 350 µM of central retina in control and GLE retina. In control retinas, the number of Chx10-IR cells in the INL did not change between 2 and 12M, however, 10% were lost between 2 and 15M. 2M GLE retinas had about 25% more Chx10-IR cells in the INL when compared to age-matched controls. At 12M, the number of Chx10-IR cells in GLE INLs decreased such that there were significantly less (40%) cells when compared to 2M GLE retinas, but not to age matched controls. At 15M, the INLs of GLE retinas had approximately 50% fewer Chx10-IR cells when compared to 2M GLE retinas. Matching letters above the bars denote statistically significant differences. Data is presented as mean ± SEM. Significance = $p<0.05$

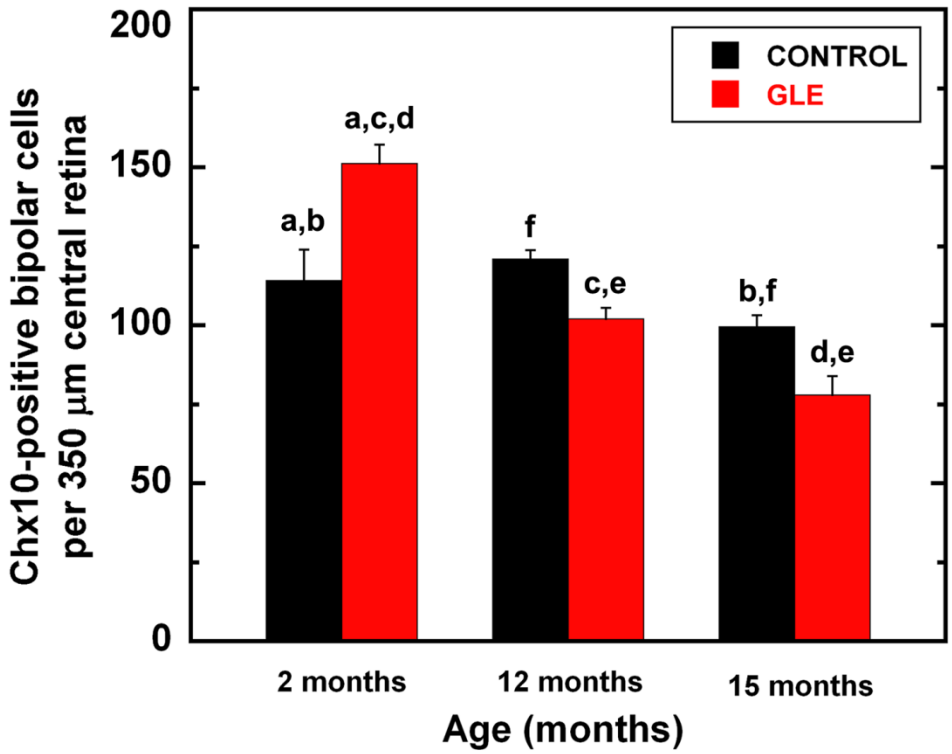

4.3.2 GLE increased disorganization and bipolar cell dendritic sprouting

Since the two of the major populations of cells in the adult retina, rod photoreceptors and bipolar cells, exhibited increased degeneration in aging GLE retinas, I examined the structural integrity of synapses in the OPL (rod photoreceptors and bipolar cells) and IPL (bipolar cells). Figure 4.7 shows the immunohistochemical images for aging control (Figures 4.7A-C, G-I, and M-O) and GLE (Figures 4.7D-F, J-L, and P-R) retinas labeled with antibodies against pan-plasma membrane calcium ATPase (PMCA) and vesicular glutamate transporter 1 (VGluT1). Neurons, especially rod bipolar cells, use PMCA to return to or maintain basal levels of intracellular calcium after activation of the voltage operated calcium channel and subsequent neurotransmitter release (Garcia et al., 1999; Johnson et al., 2007). I used the commercial pan-PMCA antibody that recognizes all four known PMCA isoforms. In control 2-month-old retinas, PMCA selectively labeled rod spherules and the apical portion of cone pedicles in the OPL, some bipolar cells in the INL, and the IPL, consistent with data from other groups (Figure 4.7A) (Krizaj et al., 2002; Johnson et al., 2007). VGluT1, a protein that uses a proton electrochemical gradient to load glutamate into vesicles for synaptic release and is the primary isoform associated with synaptic release in mouse and rat retina (Sherry et al., 2003; Shigeri et al., 2004; Stella et al., 2008), labeled synapses in the OPL and IPL in the 2-month-old control retinas (Figure 4.7B). Furthermore, VGluT1 showed differential label in the ON sublamina of the

IPL (IPLb) where it strongly labeled the large axon terminals of rod bipolar cells (Figure 4.7B). The overlay of PMCA and VGluT1 in 2-month-old control retinas revealed a significant amount of co-label in the OPL, but minimal co-label in the IPL (Figure 4.7C). In control retinas at 12 months (Figure 4.7G), PMCA-IR showed that the OPL was not as compact as in 2-month-old control retinas and at 15 months (Figure 4.7M), it was noticeably disorganized with ectopic PMCA-IR puncta in the ONL. Furthermore, the PMCA-IR IPLs of 15-month-old control retinas (Figure 4.7M) were thinner than at 2 months. VGluT1-IR in 12- and 15-month-old control retinas showed similar changes in the OPL (Figures 4.7H and N). VGluT1-IR in 12- and 15-month-old control retinas (Figures 4.7H and N) also revealed that in the most proximal sublamina of IPLb, the axon terminals of the rod bipolar cells were larger than in 2-month-old control. Double-labeling with PMCA and VGluT1 in 12- and 15-month-old control (Figures 4.7I and O) retinas showed that the OPLs of aging control retinas were thicker and less compact than at 2 months. Furthermore, the IPLs of 12- and 15-month-old (Figures 4.7I and O) controls had significantly increased co-labeling when compared with 2-month-old control retinas. Thus, these results show altered expression of functional synaptic proteins during normal aging and suggest that some degeneration normally occurs in the OPL and IPLs of aging control C57BL/6N mice retinas.

Figure 4.7. GLE retinas enhanced age-dependent thinning and disorganization of the OPL and IPL. Retinas from **(A-C, G-I,** and **M-N)** control and **(D-F, J-L,** and **P-R)** GLE retinas were labeled with antibodies against PMCA and VGluT1 at 2, 12, and 15M. In both control and GLE retinas, PMCA labeled rod spherules in the OPL, cell somas in the INL, and the IPL. VGluT1 strongly labeled the inner and outer plexiform layers in control and GLE retinas. **(A)** In control retinas at 2M, PMCA-IR was intense in both plexiform layers. **(B)** VGluT1-IR was intense in the OPL of 2M control retinas, whereas the IPL showed differential VGluT1-IR. Rod axon terminals in proximal (ON) layer of the IPL labeling more intensely with VGluT1. **(C)** In 2M control OPLs, PMCA and VGluT1 strongly co-labeled, while little to no co-label occurred in the IPL. **(D)** PMCA-IR in GLE retinas at 2M revealed a thicker OPL when compared to controls and consistent with the GLE model (Giddabasappa et al., 2011). **(E)** In GLE retina at 2M, VGluT1-IR showed an increase in the number of rod bipolar cell axon terminals in the proximal IPL. **(F)** The pattern of PMCA and VGluT1 co-label in GLE retinas was similar to controls. **(G)** In control 12M retinas, PMCA-IR revealed OPL spreading, **(H)** while VGluT1-IR in the IPL revealed enlarged bipolar cell axon terminals in the proximal IPL. **(I)** In control 15M retinas, both the OPL and IPL showed strong co-label with PMCA and VGluT1 unlike PN60 controls where only the OPL showed co-labeling. **(J)** In GLE 12M retinas, the PMCA-IR OPL was thinner than in age-matched controls and **(K)** VGluT1-IR showed enlarged rod bipolar cell axons as in 12M controls. **(L)** The uncharacteristic co-label of PMCA and VGluT1 was also observed in the IPL of 12M GLE retinas. **(M)** By 15M in control retinas, PMCA-IR puncta were observed in the ONL and the IPL had thinned. **(N)** VGluT1-IR puncta were also observed in the ONL and rod bipolar cell axon terminals were further enlarged in 15M controls. **(O)** PMCA and VGluT1 co-labeled in ONL and intensified in the IPL in 15M controls. **(P)** In GLE 15M retinas, the PMCA-IR OPL appeared more dispersed than age-matched controls. **(Q)** The enlarged VGluT1-IR bipolar cell axons were larger and **(R)** VGluT1-IR in relation to PMCA-IR labeled higher in the OPL when compared to age-matched controls. Scale bar = 40μm

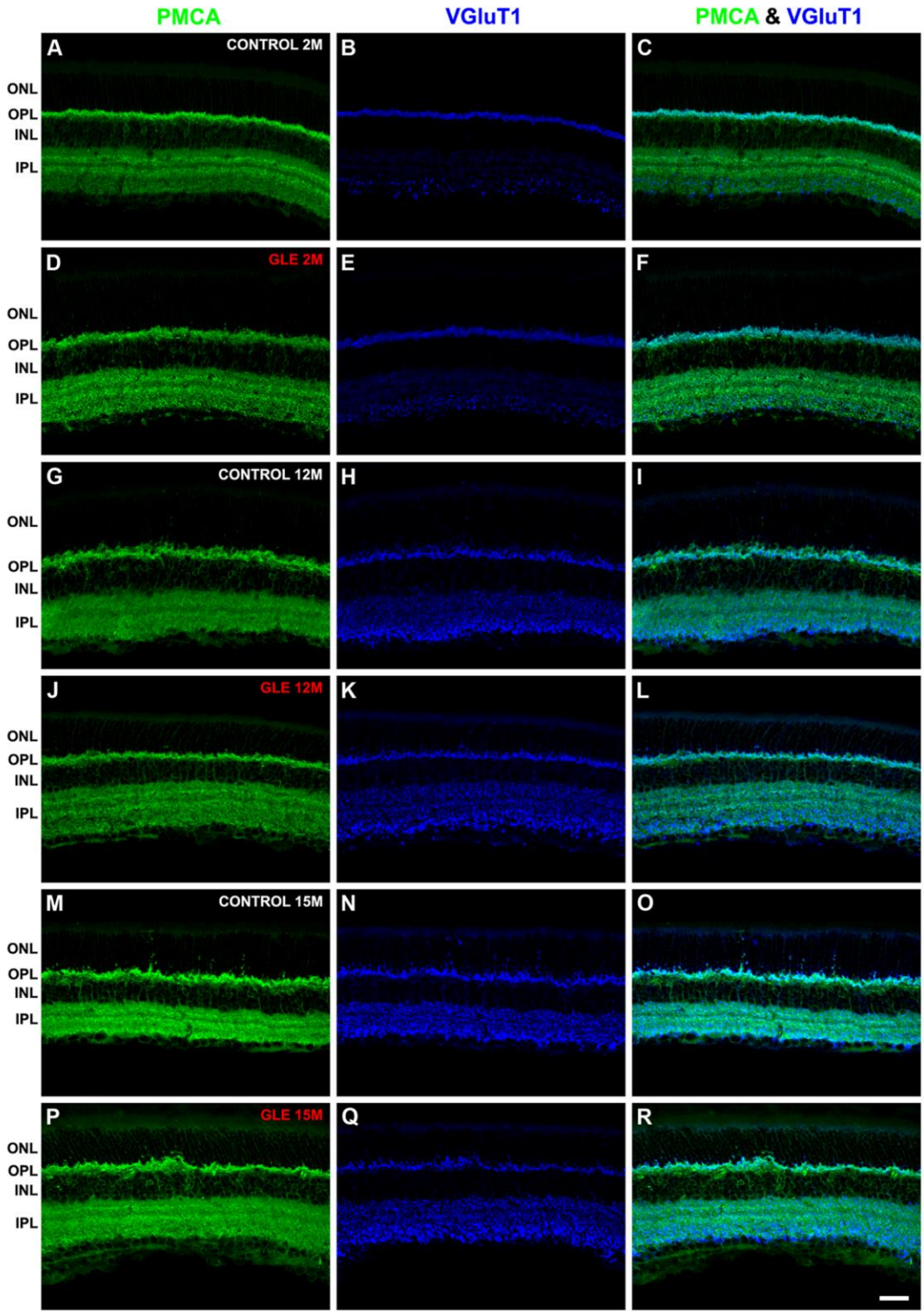
PMCA
VGluT1
PMCA & VGluT1
A
CONTROL 2M
B
C
ONL
OPL
INL
IPL
D
GLE 2M
E
F
G
CONTROL 12M
H
I
J
GLE 12M
K
L
M
CONTROL 15M
N
O
P
GLE 15M
Q
R

In GLE retinas at 2 months, PMCA-IR revealed a thicker OPL, consistent with synapses made between an increased number of rod photoreceptors and bipolar cells (Figure 4.7D) (Giddabasappa et al., 2011). VGluT1-IR in 2-month-old GLE retinas additionally showed an increase in the number of rod bipolar cell axon terminals in the ON sublamina of the IPL (Figure 4.7E). Double-labeling with PMCA and VGluT1 in 2-month-old GLE retinas showed strong co-labeling in the OPL, but little co-labeling in the IPL, comparable to control retinas (Figure 4.7F). In GLE 12-month-old retinas, the PMCA-IR OPLs were slightly thinner than age-matched controls (Figure 4.7J). VGluT1-IR in the IPL of 12-month-old GLE retinas revealed swollen rod bipolar cell axon terminals, similar to age-matched controls (Figure 4.7K). Furthermore, as in age-matched controls, double-labeling with PMCA and VGluT1 In 12-month-old GLE retinas showed a significant increase in co-labeling in the IPL. In 15-month-old GLE retinas, PMCA-IR showed that the OPL was more dispersed when compared to age-matched controls (Figure 4.7P). VGluT1-IR in 15-month-old GLE retinas showed that rod bipolar cell axon terminals were larger than 15 month controls (Figure 4.7Q). In 15-month-old GLE retinas, the PMCA and VGluT1 double-label experiment (Figure 4.7R) revealed the VGluT1 labeled more proximally in relation to PMCA in the OPL compared to age-matched controls. This data revealed advanced age-related synaptic degeneration and disorganization in GLE retinas compared to aged-matched controls.

One additional observation in the PMCA and VGluT1 experiments was that there were PMCA and VGluT1-IR puncta in the ONLs of 15-month-old control and GLE mice (Figures 4.7M-R) that was not observed in 2-month-old mice (Figure 4.7A and B). We hypothesized that these were points of synaptic retraction and dendritic sprouting of rod photoreceptors and bipolar cells, respectively, and that GLE retinas would exhibit more of these points since there was increased degeneration of these cells. Figure 4.8 shows a high magnification image of a dendritic sprout. PMCA and VGluT1-IR rod spherules normally localize in the OPL where they contact PKCα-IR rod bipolar cell dendrites (Figure 4.7A-C). However, Figure 4.8 reveals several PMCA and VGluT1-IR rod spherules that make contact with an ectopic PKCα-IR bipolar cell dendrite in the ONL. Therefore, we used PKCα as a marker to count the number of dendritic sprouts in control and GLE retinas. A dendrite was counted as a sprout if its length exceeded double the thickness of the OPL (Terzibasi et al., 2009). Figures 4.9 and 4.10 show the immunohistochemistry and counts from aging retina labeled with PKCα. In control and GLE 2-month-old retinas (Figure 4.9A and B), PKCα-IR bipolar cell dendrites were restricted to the OPL. In 12- and 15-month-old control retinas, PKCα-IR bipolar cell dendrites began to sprout in the ONL with an average of two to four dendritic sprouts per 350 μm of central retina, respectively (Figures 4.9A, C, E, and 4.10). In GLE retinas, the number of PKCα-IR dendritic sprouts were significantly increased (approximately doubled) relative to controls at both 12 and 15 months (Figures 4.9B, D, F, and 4.10). Together,

these results demonstrate that GLE retinas had increased bipolar dendritic sprouting, which accompanied photoreceptor retraction and disorganization of the OPL.

Figure 4.8. A sprouting PKC-IR rod-bipolar dendrite associates with the retracting axon of PMCA and VGluT1 rod spherules. An aged 12M control retina was labeled with antibodies against PMCA (green), PKC (red), and VGluT1 (blue). This figure shows a high magnification example of the dendritic sprout of an ON-rod bipolar cell. PKC labeled all ON-rod bipolar cell somas and their dendrites in the INL and OPL, respectively. One PKC-IR dendrite uncharacteristically extended up into the ONL. PMCA and VGluT1 labeled components of the pre-synaptic rod spherule associated with the sprouting dendrite. Scale bar = 40 µM

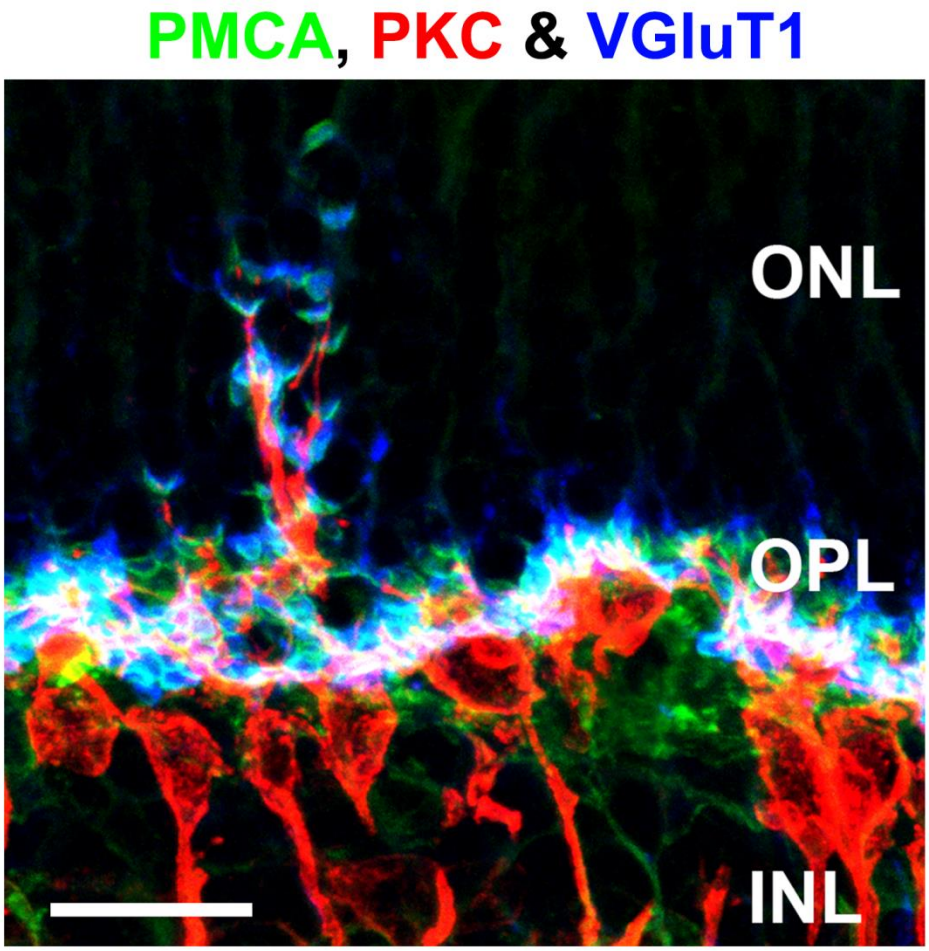

Figure 4.9. GLE increased the amount of dendritic sprouting in the OPL. Retinas from **(A, C, and E)** control and **(B, D, and F)** GLE retinas were labeled with an antibody against PKCα at 2, 12, and 15M. **(A-B)** At 2M, GLE retinas contained more PKCα-IR somas in the INL and all PKCα-IR dendrites were restricted to the OPL in control and GLE retinas. **(C)** By 12 months in the control, a few PKCα –IR dendrites extended into the ONL. **(E)** At 15 months, the number of the PKCα-IR sprouts doubled in the OPLs of control retinas. **(D and F)** At 12 and 15M, GLE retinas exhibited twice the number of dendritic sprouts when compared to age-matched controls. Scale bar = 40 µM.

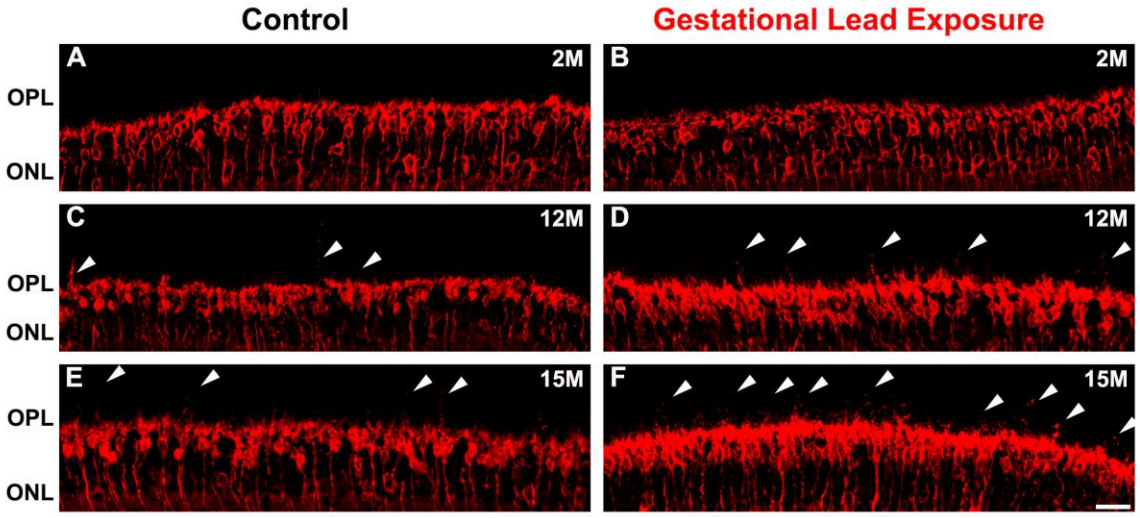

Figure 4.10. Quantification of PKCα-IR dendritic sprouts in aging control and GLE retinas. The number of PKC-α-IR dendritic sprouts were counted and plotted as total number per 350 µM of central retina. In control and GLE retinas, there were no dendritic sprouts at 2M. Approximately 2 to 4 dendritic sprouts were observed in central control retina at 12 and 15M. In GLE retinas, dendritic sprouts significantly increased 2 and 2.6 fold at 12 at and 15M, respectively. Matching letters denote statistically significant difference. Data is presented as mean ± SEM. Significance = $p<0.05$

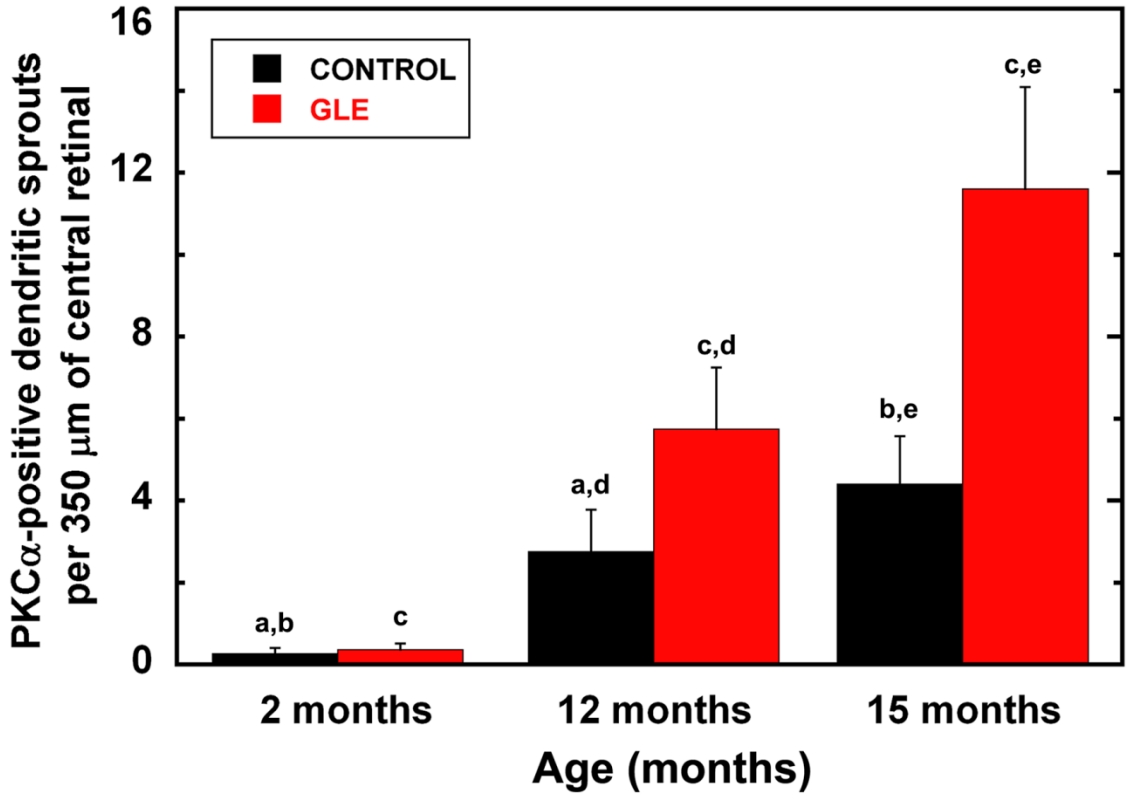

4.4 Discussion

Human equivalent GLE results in increased and prolonged RPC proliferation and ultimately the differentiation of an increased number of rod photoreceptors and bipolar cells in mouse retinas (Giddabasappa et al., 2011). The main goal of this study was to examine the structural integrity, specifically, the number of and synaptic connectivity between rod photoreceptors and bipolar cells of these GLE retinas as they age. There were four main findings in this study. First, DAPI and immunohistochemical experiments showed that control C57/BL6N mouse retinas degenerated during normal aging. This was supported by observed ONL and INL thinning, loss of CHX10-IR bipolar cells, increased OPL and IPL disorganization, and increased dendritic sprouting. Second, although 2-month-old GLE retinas were thicker than age-matched control retinas, this increased thickness was not seen at 12 months. The decrease in overall retinal thickness of GLE retinas was due to increased thinning of both the ONL and INL. In GLE retinas, the INL became thinner than in controls, whereas the ONL thinned to levels equal to that in controls. Third, the thinning of the ONL and INL resulted from the loss of both rod photoreceptors and bipolar cells. Fourth, both the OPL and IPL of GLE retina exhibited increased degeneration and disorganization compared to aging controls. Furthermore, increased dendritic sprouting of bipolar cells accompanied the increased disorganization observed in GLE OPLs.

The data presented here suggest that retinal thinning, neuronal death, and synaptic degeneration occur with normal aging in C57BL/6N mouse retinas. GLE accelerates and increased these age-related changes, especially in the case of rod photoreceptor and bipolar cell degeneration. Rod photoreceptors degenerate prior to cones in most models of retinal degeneration. In the human disease retinitis pigmentosa, genetic mutations occur only in rods, which subsequently die before cones (Cideciyan et al., 1998; Hicks and Sahel, 1999; Curcio et al., 2000). The consensus is that rod photoreceptors are more susceptible than cones to most insults including genetic alterations and aging. In human donor retinas, the number of rod photoreceptors starts to decrease during the second decade and continues until the ninth decade resulting in a 30% total decrease (Gao and Hollyfield, 1992). Furthermore, rod loss in humans is region specific (Curcio et al., 1993; 1996). The morphological changes observed in aging human retina could be the reason that loss in scotopic sensitivity and dark adaptation occurs in aging patients without ocular disease (Jackson et al., 1998; 1999).

The majority of published aging data in non-diseased rodent retina confirms what is observed in humans. Early studies in pigmented rats showed that between 4 and 30 months of age, the nuclear densities of the ONL, INL, and GCL decreased by 32-41%, 25-34%, and 25-28%, respectively (Katz and Robison, 1985). These changes in nuclear densities were attributed partially to increased eye size, but mostly to cell loss: especially of rod photoreceptors (Katz and Robison, 1985). Rod outer segments also decrease in number, length, and

morphology in aging rat (Fox and Rubinstein, 1989; Li et al., 2003; Cunea and Jeffery, 2007). Similar results also occur in other mice strains (Gresh et al., 2003; Kolesnikov et al. (2010). Conversely, others show no loss in rod photoreceptors with aging in control retinas, and suggest that retinal layers thin due to retinal expansion and consequently retinal neurons become less densely packed (Liets et al., 2006; Feng et al., 2007; Samuel et al., 2011). While density measurements are not comparable to cell counts, whole retinal cell counts do not take into account localized changes in photoreceptor number. Therefore, it is probable that both components, eye growth and photoreceptor degeneration, contribute to decreased retinal thickness in aged retinas. My data supports the former since the GLE retinas exhibited major differences in rod photoreceptor and bipolar cell populations prior to terminal differentiation and through adulthood. However, more work must be done to determine whether the eyes of GLE mice expand more than control eye during aging.

The retina has one of the highest rates of oxygen consumption of any tissue (Graymore, 1969). Furthermore, the outer retina consumes ~90% of the total oxygen consumed in the adult retina (Medrano and Fox, 1995). A 20% increase of the rods would result a high metabolic load on the system. The retinal pigmented epithelium (RPE), which is proximally located to the retina, contacts photoreceptor outer segments and is responsible for absorbing light energy, providing nutrients and antioxidants (i.e., vitamin A) and eliminating waste (i.e., reactive oxygen species [ROS]) (Strauss, 2004). Oxidative stress plays a major

role in age-related retinal degeneration. This is supported by the finding that caloric restriction slows age-related degeneration in rat retinas (Li et al, 2003). It is unknown whether the RPE functionally and/or structurally accommodates the increase in rod photoreceptor outer segments, but accommodative failure would likely result in deficiencies in photoreceptor longevity due to increased ROS and decreased nutrient delivery. Therefore, a possibility in the aging GLE retina is that the significantly increased number of rod photoreceptors overloads the supportive system resulting in increased oxidative stress and loss of rod photoreceptors. This is supported by the fact the thickness of GLE ONLs, when compared to controls, thinned to similar rather than lower levels. Genes associated with oxidative phosphorylation, DNA stability and modification, and inflammatory responses are significantly altered in aging rod photoreceptors (Parapuram et al., 2010). These changes began in mouse rods as early as 5-months-old: prior to any observable morphological changes (Parapurm et al., 2010). Therefore, the photoreceptor loss observed in GLE retinas is likely the outcome of a process of metabolic events initiated earlier in the mouse.

Here, I report two phenomenon associated with bipolar cells in aging GLE retinas. First, bipolar cells decreased in density in GLE retinas as characterized by CHX10-IR. Second, bipolar cells exhibited twice the amount of dendritic sprouting when compared to aging control retinas. Although there is only one published report of bipolar cell loss with age in human donor retinas (Aggarwal el al., 2007), several studies report bipolar cell dendritic sprouting with age (Liets et

al., 2006; Terzibasi et al., 2009). The age-induced changes in bipolar cells in GLE retinas may represent two independent consequences of the GLE phenotype: 1) an unmet increase in energy demand of the inner retina and 2) the statistical possibility of having more dendritic sprouting because there are more bipolar cells. Unlike the outer retina, the inner retina of the rodent consumes 35-40% of the total oxygen consumed in the retina (Medrano and Fox, 1995). In the GLE model, there is likely a conflict between the increased energy demands of the outer and inner retina. Bipolar cells in the inner retina have a smaller percentage of available oxygen to use compared to the outer retina and, therefore, may be more sensitive to energy deficits in the GLE. This may explain why CHX10-IR bipolar cells decrease to numbers below, rather than equal to, that of controls.

Finally, I found advanced synaptic disorganization of both plexiform layers of aging GLE retinas. VGluT1 and PMCA-IR rod spherules were ectopically expressed in the ONLs of aging control and GLE retinas (Figure 4.7) whereas M-CAR was not (Figure 4.4). This suggests that synaptic retraction may be a step in the process of photoreceptor degeneration: rods are more prone than cones. A single mitochondrion supplies the calcium and energy demands of rod spherules, whereas cone pedicles contain five to six mitochondria (Johnson et al., 2007). Mitochondrial DNA damage increases with age in rodent retina, especially in photoreceptors (Wang et al., 2010) and mitochondria lose their ability to repair oxidative DNA damage with age (Mandavilli et al., 2002). Therefore, rod

synapses are likely more sensitive to oxidative stress in the synaptic layer than cones. Interestingly, the mitochondrial damage caused by light-induced damage and postnatal lead exposure localizes to the photoreceptor synaptic layer, although most of the mitochondria in photoreceptors are confined to the inner segments (Perkins et al., 2003; Cortina et al., 2005; Johnson et al., 2007; Perkins et al., 2012). In control and GLE retinas, synaptic retraction is likely the first morphological symptom of age-related degeneration.

This study has implications for a broad range of age-related retinopathies. Specifically these results suggest that energy demand and oxidative stress play major roles in the structural integrity of the aging retina. Furthermore, the data shows that early exposure to environmental toxicants, even if short-term, can have major adverse consequences later in life. Compelling epidemiological and toxicological evidence shows that there are several critical/vulnerable periods of growth and development during which environmental interactions with the immune system and genome increase susceptibility to diseases later in life (Cameron and Demerath 2002; Gluckman et al. 2007; Heindel 2008; Bilbo and Schwartz 2009). This also appears to be the case with aging. Age-related retinal degeneration and vision loss adversely affect 10 million Americans, and their prevalence and socioeconomic cost will increase 50% by 2020 (Gupta et al., 2007). Therefore, early detection of risk factors that can induce age-related changes represents a cost effective and medically beneficial way to combat such degeneration.

4.5 References

Aggarwal P, Naq TC, Wadhwa S (2007) Age-related decrease in rod bipolar cell density of the human retina: an immunohistochemical study. J Biosci 32:293-298.

Bilbo SD, Schwarz JM (2009) Early-life programming of later-life brain and behavior: a critical role for the immune system. Front Behav Neurosci 3:14.

Cameron N, Demerath EW (2002) Critical periods in human growth and their relationship to diseases of aging. Am J Phys Anthropol 35:159-184.

Cideciyan AV, Jacobson SG (1996) An alternative phototransduction model for human rod and cone ERG a-waves: normal parameters and variation with age. Vision Res 36:2609-2621.

Cortina MS, Gordon WC, Lukiw WJ, Bazan NG (2005) Oxidative stress-induced retinal damage up-regulates DNA polymerase gamma and 8-oxoguanine-DNA-glycosylate in photoreceptor synaptic mitochondria. Exp Eye Res 81:742-750.

Cunea A, Jeffery G (2007) The ageing photoreceptors. Vis Neurosci 24:151-155.

Curcio CA, Medeiros NE, Millican CL (1996) Photoreceptor loss in age-related macular degeneration. Invest Ophthalmol Vis Sci 37:1236-1249.

Curcio CA, Millican CL, Allen KA, Kalina RE (1993) Aging of the human photoreceptor mosaic: evidence for selective vulnerability of rods in central retina. Investigative Ophthalmology and Visual Science 34:3278-3296.

Curcio CA, Owsley C, Jackson GR (2000) Spare the rods, save the cones in aging and age-related maculopathy. Invest Ophthalmol Vis Sci 41:2015-2018.

Feng L, Sun Z, Han H, Zhou Y, Zhang M (2007) No age-related cell loss in three retinal nuclear layers of the Long-Evans rat. Vis Neurosci 24:799-803.

Fox DA, Boyes WK (2013) Toxic responses of the ocular and visual system, In: Casarett and Doull's Toxicology: The Science of Poisons (Klaassen CD, ed) 8th ed. New York:McGraw-Hill, 767-798.

Fox DA, Kala SV, Hamilton WR, Johnson JE, O'callaghan JP (2008) Low-level human equivalent gestational lead exposure produces supernormal scotopic electroretinograms, increased retinal neurogenesis, and decreased retinal dopamine utilization in rats. Environ Health Perspect 116:618-625.

Fox DA, Rubinstein SD (1989) Age-related changes in retinal sensitivity, rhodopsin content and rod outer segment length in hooded rats following low-level lead exposure during development. Exp Eye Res 48:237-249.

Garcia ML, Strehler EE (1999) Plasma membrane calcium ATPases as critical regulators of calcium homeostasis during neuronal cell function. Front Biosci 4:D869-882.

Gao H and Hollyfield (1992) Aging of the human retina. Investigative Ophthalmology and Visual Science 33:1-17.

Giddabasappa A, Hamilton WR, Chaney S, Xiao W, Johnson JE, Mukherjee S, Fox DA (2011) Low-level gestational lead exposure increases retinal progenitor cell proliferation and rod photoreceptor and bipolar cell neurogenesis in mice. Environ Health Perspect 119: 71-77.

Gluckman PD, Lillycrop KA, Vickers MH, Pleasants AB, Phillips ES, Beedle AS, Burdge GC, Hanson MA (2007) Metabolic plasticity during mammalian development is directionally dependent on early nutritional status. Proc Natl Acad Asci 104:12796-12800.

Graymore CN (1970) Metabolic survival of the isolated retina. Br Med Bull 26:130-133.

Gresh J, Goletz PW, Crouch RK, Rohrer B (2003) Structure-function analysis of rods and cones in juvenile, adult, and aged C57bl/6 and Balb/c mice.Vis Neurosci 20:211-220.

Gupta N, Yucel YH (2007) What can we expect in the brain of glaucoma patients. Surv Ophthalmol 2:S122-126.

Heindel JJ (2007) Role of exposure to environmental chemicals in the developmental basis of disease and dysfunction. Reprod Toxicol 23:257-257.

Heindel JJ (2008) Animal models for probing the developmental basis of diseases and dysfunction paradigm. Basic Clin Pharmacol Toxicol 102:76-81.

Hicks D, Sahel J (1999) The implications of rod-dependent cone survival for basic and clinical research. Invest Ophthalmol Vis Sci 40:3071-3074.

Jackson GR, Owsley C, Cordle EP, Finley CD (1998) Aging and scotopic sensitivity. Vision Res 38:3655-3662.

Jackson GR, Owsley C, McGwin G (1999) Aging and dark adaptation. Vision Res 39:3975-3982.

Johnson JE, Perkins GA, Giddabasappa A, Chaney S, Xiao W, White AD, Brown JM, Waggoner J, Ellisman MH, Fox DA (2007) Spatiotemporal regulation of ATP and Ca^{2+} dynamics in vertebrate rod and cone photoreceptor ribbon synapses. Mol. Vision 13:887-919.

Katz M and Robison WG (1986) Evidence of cell loss from the rat retina during senescence. Exp Eye Res 42:293-304.

Kolesnikov AV, Fan J, Crouch RK, Kefalov VJ (2010) Age-related deterioration of rod vision in mice. J Neurosci 30:11222-11231.

Krizaj D, Demarco SJ, Johnson J, Strehler EE, Copenhagen DR (2002) Cell-specific expression of plasma membrane calcium ATPase isoforms in retinal neurons. J Comp Neurol 451:1-21.

Leasure JL, Giddabasappa A, Chaney S, Johnson JE Jr, Pothakos K, Lau YS, Fox DA (2008) Low-level human equivalent gestational lead exposure

produces sex-specific motor and coordination abnormalities and late-onset obesity in year-old mice. Environ Health Perspect 115:355-361.

Li D, Sun F, Wanq K (2003) Caloric restriction retards age-related changes in rat retina. Biochem Biophys Res Commun 309:457-463.

Liets LC, Eliasieh K, Van der List DA, Chalupa LM (2006) Dendrites of rod bipolar cells sprout in normal aging retina. Proc Natl Acad Sci 103:12156-12160.

Lilienthal H, Kohler K, Turfeld M, Winneke G (1994) Persistent increases in scotopic B-wave amplitudes after lead exposure in monkeys. Exp Eye Res 59:203-209.

Mandavilli BS, Santos JH, Van Houten B (2002) Mitochondrial DNA repair and aging. Mutat Res 509:127-151.

Medrano CJ, Fox DA (1995) Oxygen consumption in the rat outer and inner retina: light and pharmacologically-induced inhibition. Exp Eye Res 61:273-284.

Parapuram SK, Cojocaru RI, Chang JR, Khanna R, Brooks M, Othman M, Zareparsi S, Khan NW, Gotoh N, Coqliati T, Swaroop A (2010) Distinct signature of altered homeostasis in aging rod photoreceptors: implications for retinal diseases. PLoS One 5:e13885.

Perkins GA, Ellisman MH, Fox DA (2003) Three-dimensional analysis of mouse rod and cone mitochondrial cristae architecture: bioenergetic and functional implications. Mol Vis 9:60-73.

Perkins GA, Scott R, Perez A, Ellisman MH, Johnson JE, Fox DA (2012) Bcl-xL-mediated remodeling of rod and cone synaptic mitochondria after postnatal lead exposure: electron microscopy, tomography and oxygen consumption. Mol Vis 18:3029-3048.

Rothenberg SJ, Schnaas L, Salgado-Valladares M, Casanueva E, Geller AM, Hudnell HK, Fox DA (2002) Increased ERG a- and b-wave amplitudes in 7- to 10-year-old children resulting from prenatal lead exposure. Invest Ophthalmol Vis Sci 43-2036-2044.

Samuel MA, Zhang Y, Meister M, Sanes JR (2011) Age-related alterations in neurons of the mouse retina. J Neurosci 31:16033-16044.

Sherry DM, Wang MM, Bates J, Frishman LJ (2003) Expression of vesicular glutamate transporter 1 in the mouse retina revels temporal ordering in development of rods vs. cone and ON vs OFF circuits. J Comp Neurology 465:480-498.

Shigeri Y, Seal RP, Shimamoto K (2004) Molecular pharmacology of glutamate transporters, EAATs and VGLUTs. Brain Res Rev 45:250-265.

Stella SL, Li S, Sabatini A, Vila A, Brecha NC (2008) Comparison of the ontogeny of the vesicular glutamate transporter 3 (VGLUT3) with VGLUT1 and VGLUT2 in the rat retina. Brain Res 1215:20-29.

Strauss O (2005) The retinal pigment epithelium in visual function. Physiol Rev 85:845-881.

Suzuki S, Horiguchi M, Tanikawa A, Miyake Y, Kondo M (1998) Effect of age on short-wavelength sensitive cone electroretinogram and long- and middle-wavelength sensitive cone electroretinogram. Jpn J Ophthalmol 42:424-430.

Terzibasi E, Calamusa M, Novelli E, Domenici L, Strettoi E, Cellerino A (2009) Age-dependent remodeling of retinal circuitry. Neurobiol Aging 30:819-828.

Wang X, Michaelis EK (2010) Selective neuronal vulnerability to oxidative stress in the brain. Front Aging Neurosci 2:12.

CHAPTER 5 OVERALL CONCLUSIONS AND FUTURE DIRECTIONS

5.1 Conclusions and future directions

In this Ph.D. dissertation, I examined the effects of GLE on developing and aging retina. Mice with GLE showed a 20% increase in the number of retinal progenitor cells, which resulted in 20-30% more rod photoreceptors and bipolar cells (Giddabasappa et al., 2011). Since these studies stem from observations that children with GLE exhibited supernormal electroretinogram activity (Rothenberg et al., 2002), my findings have increased significance when applied to clinical manifestations and/or consequences of GLE in developing children and aging humans.

My first finding was that GLE delayed the differentiation and functional development of late-born neurons in developing mouse retina by two to three days. PN2 was the first age to show a developmental delay in murine GLE retinas. This age correlates to approximately 15 weeks, or the end of the first trimester in humans (Martins and Pearson, 2008), and marks the developmental period for various brain regions, including the cerebellum, mesencephalic tectum, striatum, amygdala, neocortex, and the dentate gyrus of the hippocampus (Rice and Barone, 2000). Therefore, the age in which I first observed delayed differentiation in GLE mice directly parallels a time of increased susceptibility to neurotoxicants in humans. One conclusion from this dissertation work is that alterations to the initial events of neurogenesis (i.e. proliferation and differentiation), will alter subsequent events such as synaptogenesis.

Unpublished data from our laboratory shows that the murine brain, specifically the hippocampus, exhibits a phenotype similar to that of the retina: increased neurogenesis. Therefore, it is likely that the brain also exhibits a delay in differentiation and/or synaptic development. More work is required to determine if delays in differentiation and synaptic development occurs in the brains of GLE mice and, by extension, children with GLE.

Increases in brain size, neuronal number and alterations in synaptic development have been implicated in autism spectrum disorders (Courchesne et al., 2003; 2011). Interestingly, blood and urine lead concetrations are also linked to autisitic disorders (El-Ansary et al., 2011; Lakshmi and Geetha, 2011; Yorbik et al., 2010; Soden et al., 2007). Therefore, the retinal phenotype associated with GLE is indicative of what likely occurs on a larger scale throughout the CNS and these developmental studies suggest a link and possible mechanism for GLE and neurodevelopmental disorders such as autism in children.

An increase in the number of rod bipolar cells in GLE retinas accommodates the increased number of rod photoreceptors (Giddabasappa et al., 2011). Although there is an increase in the number of cone-bipolar cells in GLE retinas, there is no increase in the number of cone photoreceptors. In normal retina, the rod photoreceptor to rod bipolar cell connection ratio is 1:1 whereas one cone photoreceptor communicates with many cone bipolar cells. It is unkown whether the cone photoreceptor to cone bipolar cell connections are altered in GLE retinas. Therefore, further studies should examine whether the

number of synaptic connections between cone phototreceptor and cone-bipolar cells increase or if there is an increase in the number of atypical synapses between rod photorreceptors and cone bipolar cells.

A second finding of my research was that GLE altered glutamatergic signaling in the developing retina prior to the formation of functional glutamatergic synapses. The work presented here is novel as it is the first to show that late-born neurons (rod photoreceptors and bipolar cells) express functional glutamate receptors prior to the expression of known differentiation markers. Furthermore, I showed that inner retinal activity might influence early postnatal glutamate signaling through an acetylcholine dependent mechanism. However, my study focused on postnatal ages since this is when rod photoreceptors and bipolar cells (the two neurons affected in the GLE model) are born. It would be interesting to determine whether early born retinal neurons (cone photoreceptors, ganglion, amacrine, or horizontal cells) also express glutamate or other neurotransmitter receptors before expression other differentiation markers.

I also showed that while acute *in vitro,* lead exposure alters glutmamatergic receptor activity during early postnatal retinal development, the change is opposite to what occurs *in vivo*. Since free Pb^{2+} <5 nM in GLE retinas it is likely that acute Pb^{2+} acts through a different mechanism. However, since glutamate and other neurotransmitters influence calcium waves during

development, it would be interesting to determine, through live tissue calcium imaging, whether GLE alters the basal activity of calcium waves.

Finally, I found that GLE enhanced and accelerated are-related degeneration in the retinas of aging mice. My conclusion was that increased oxidative stress brought about by a 20-30% increase in rod photoreceptors was not sustainable during aging. Future studies in aging GLE retinas should determine whether the RPE accommodates the GLE phenotype and if an increase in reactive oxygen species causes photoreceptor death in aging GLE retinas. Since mitochondrial damage is one of the nine known hallmarks of aging (Lopez-Otin et al., 2013), and each rod spherule contains only one mitochondria (Johnson et al., 2007), further studies in normal and aging GLE retinas should examine whether mitochondrial damage in the OPL initiates the synaptic retraction of rod photoreceptors and dendritic sprouting in bipolar cells. Taken together, my aging studies indicate the children with GLE should be monitored for increased and/or accelerated retinal degeneration as they age.

5.2 References

Courchesne E, Carper R, Akshoomoff, N (2003) Evidence of brain overgrowth in the first year of life in autism. J Am Med Assoc 290: 337-344.

Courchesne E, Mouton PR, Calhoun ME, Semendeferi K., Ahrens-Barbeau C, Hallet MJ, Barnes CC, Pierce K, (2011) Neuron number and size in prefrontal cortex of children with autism. J Am Med Assoc 306: 2001-2010.

El-Ansary AK, Bacha AB, Ayahdi LY (2011) Relationship between chronic lead toxicity and plasma neurotransmitters in autistic patients from Saudi Arabia. Clin Biochem 44:1116-1120.

Giddabasappa A, Hamilton WR, Chaney S, Xiao W, Johnson JE, Mukherjee S, Fox DA (2011) Low-Level Gestational lead exposure increases retinal progenitor cell proliferation and rod photoreceptor and bipolar cell neurogenesis in mice. Environ Health Perspect 119: 71-77.

Johnson JE, Perkins GA, Giddabasappa A, Chaney S, Xiao W, White AD, Brown JM, Waggoner J, Ellisman MH, Fox DA (2007) Spatiotemporal regulation of ATP and Ca^{2+} dynamics in vertebrate rod and cone photoreceptor ribbon synapses. Mol. Vision 13:887-919.

Lakshmi P, Geetha A (2011) Level of trace elements (copper zinc, magnesium and selenium) and toxic elements (lead and mercury) in the hair and nail of children with autism. Biol Trace Elem Res 142:148-158.

Lopez-Otin C, Blasco MA, Partridge L, Serrano M, Kroemer G (2013) The hallmarks of aging. Cell 153:1194-1217.

Martins RA, Pearson RA (2008) Control of cell proliferation by neurotransmitters in the developing vertebrate retina. Brain Res 1192:37-60.

Rice D, Barone S (2000) Critical periods of vulnerability for the developing nervous system: evidence from humans and animal models. Environ Health Perspect 108 Suppl 3:511-533.

Rothenberg SJ, Schnaas L, Salgado-Valladares M, Casanueva E, Geller AM, Hudnell HK, Fox DA (2002) Increased ERG a- and b-wave amplitudes in 7- to 10-year-old children resulting from prenatal lead exposure. Invest Ophthalmol Vis Sci 43-2036-2044.

Soden SE, Lowry JA, Garrison CB, Wasserman GS (2007) 24-hour provoked urine excretion test for heavy metals in children with autism and typically developing controls, a pilot study. Clin Toxicol (Phila) 45:479-481.

Yorbik O, Kurt I, Oztürk O (2010) Chromium, cadmium, and lead levels in urine of children with autism and typically developing controls. Biol Trace Elem Res 135:1-3.